Characterisation of Chitosan/PVA/PVP Crossed-linked Nanofibrous Scaffolds for the Potential Application in Dermal Tissue Engineering

Bhavini Patel

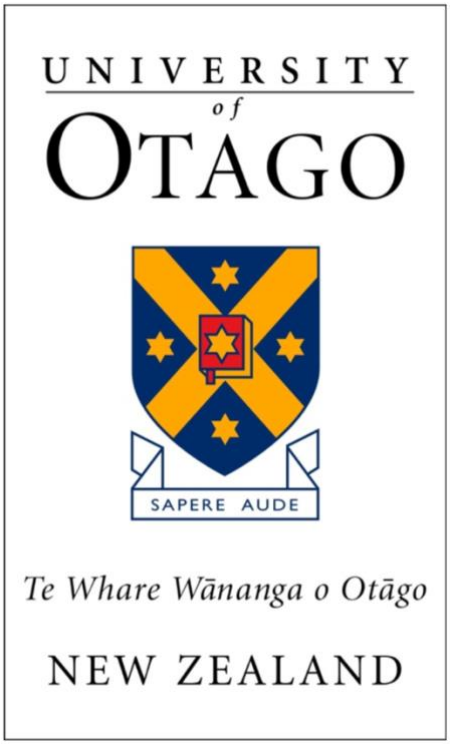

A thesis submitted for the degree of Master of Science

Centre for Bioengineering and Nanomedicine

University of Otago, Dunedin

New Zealand

February 2020

Table of Contents

List of Tables

List of Figures

Abstract

Severe burn injuries lead to significant morbidity and mortality as they are traumatic and affect nearly every organ system. Commonly used clinical practices are early burn lesion removal and skin grafting which have improved outcomes for patients with severe burns by lessening mortality rate and length of hospitalisation (Wood 2014). However, the challenges of sourcing donor site tissue especially as in the case of large burn wounds, and poor healing outcomes, for example, scarring, still remain.

Tissue engineering combines science and engineering to create functional tissue and organs to maintain, restore or replace diseased parts of the body (Peltola et al. 2008). The applications of tissue engineering are broad; from aiding the growth of new skin, to the delivery of biologically active molecules such as stem cells and growth factors in order to enhance wound healing and regeneration of skin tissue (Kang et al. 2018). The fundamental goal of dermal tissue engineering is to create new fully functional skin including all skin appendages such as blood vessels, nerves, and sweat glands (Wang et al. 2018). This tool not only aids in healing and regeneration, but also to reduce scarring and the long-term consequences associated with having scarred tissue (Chua et al. 2016).

The electrospinning technology is a popular choice when it comes to producing nanofibers with large surface area to volume ratios and structural architecture similar to the extracellular matrix (ECM) found in skin tissue. Chitosan is the second most abundant natural biomaterial after cellulose (Schiffman and Schauer 2007) and possesses enticing advantages for use in tissue engineering are due to: its intrinsic biocompatibility, biodegradability and high-water adsorption capability.

Chitosan based composite nanofibers, blended with carrier polymers polyvinyl alcohol (PVA) and polyvinyl pyyrolidone (PVP) were prepared by the electrospinning method. The blend solutions were characterised before electrospinning using rheology. The synthesised three-dimensional electrospun nanofibrous scaffolds (3DENS) were characterised by SEM, FTIR, degradation, and swelling studies. The biological compatibly of the 3DENS were characterised by MTT and live-dead cell assay using cultured human keratinocytes (HaCaT) and normal human dermal fibroblasts (NHDF) cells lines.

The dry weight ratio of materials influences the viscosity and spinnability of the material. 3DENS were successfully fabricated using chitosan, PVA and PVP. The 3DENS mechanical

and chemical properties were affected by the varying concentrations of materials. Crosslinking the 3DENS using heat increased the water adsorption capability by increasing the number of functional hydrophilic groups in the 3DENS. Crosslinked 3DENS resisted degradation compared to uncrosslinked 3DENS. The addition of chitosan to PVA/PVP increased the rate of degradation for uncrosslinked and crosslinked scaffolds. All the fabricated 3DENS displayed excellent biocompatibility. Uncrosslinked 3DENS showed better NHDF cell viability than crosslinked 3DENS. However, all 3DENS provided a favourable environment for cell viability and growth for HaCaT and NHDF cells.

Acknowledgements

Firstly, I would like to thank my supervisor Azam Ali for giving me the opportunity to do my research project in such an interesting area. Your enthusiasm towards the topic and your interest in my career goals have been motivational and inspiring.

I would like to give special thanks to Maree Gould. You have been heaven sent, especially during the last few months of my Masters. I cannot thank you enough for the support and kindness you have shown. From being in the lab with me and giving me writing advice to mental health checks and keeping me in check, you always went above and beyond to help in any way that you could! You have been my Uni mum and I am so grateful to you.

Ian Ross, you always made things so easy for me. You always come through with anything that I asked without hesitation. Thank you, Liz Girvan for helping me with microscopy. Many thanks to Stephen Giteru for his input on rheology. Special acknowledgement to Shelly and Kazima, you both always did your best to find out answers to all my difficult questions with a smile on your face. I would like to acknowledge the Department of Food Science; your morning teas have been amazing and it's lovely to see friendly faces every day.

Thank you to Tajul Islam for being a mentor and good friend during your time here. Time is the greatest gift someone can give you and I am so grateful for all the hours you spent explaining things to me and helping me with experiments. I miss our conversations about books and philosophies of life and late-night cooking in the tea room with whatever items were available. I'm coming to Bangladesh someday to get the lamb and goat curry that you still have to make me! Mozammel Adib, you and your Farjana have treated me like family. Thank you for always welcoming me into your home and being there for me, listening to me and for feeding me yummy curries! I'm going to miss hanging out at our secret bridge.

Christina, some days I came to the office just chat with you. You've been a trusted friend and so easy to talk to. Christina, Minami and Sonali, we've been on this journey together and I'm so pleased to have gotten to know such intelligent and wonderful women. I love our cultural diversity- we had the best chats and I've gained so much perspective from talking to you ladies. Our little support group has helped me stay focuses and work harder. My tea room friends Jano, Sahar, Mina, and Nimesh, lunch time with you all never failed to lift my spirits. Thank you to all my Dunedin friends for making my time here a memorable one; especially Ashly, for your unwavering faith in me and keeping me fed.

Most importantly, I would like to thank my family for their faith and investment in me. I would especially like to thank my father, Hasmukh Lal, without your support and encouragement, I wouldn't be where I am today. Thank you, mum, Mina Patel, for calling me every other day and checking up on me and for sending me endless parcels of food from Fiji. Dharma, missing your teenage years has been the hardest part of this journey. I'm so grateful for snapchat and video calls which allowed me to be a part of your life.

To my best friends and sisters, Poonam and Aline, thank you so much for that constant supply of memes, late night video calls, pep talks, and encouragements. You have been my biggest cheerleaders and have gotten me through the toughest days, so much love for you both.

Abbreviations

2D	Two-Dimensional
3D	Three-Dimensional
3DENS	Three Dimensional Electrospun Nanofibrous Scaffold
CAD	Computer Aided Design
cDMEM	Complete DMEM
CL	Crosslinked
cm	Centimetres
DMEM	Dulbecco's Modified Eagle Medium
DSC	Differential Scanning Calorimetry
ECM	Extracellular Matrix
FGF	Fibroblast Growth Factor
FTIR	Fourier-Transform Infrared Spectroscopy
GA	Glutaraldehyde
GAGs	Glycosaminoglycans
h	Hour(s)
HA	Hyaluronic Acid
HaCaT	Cultured Human Keratinocytes
HCl	Hydrochloric Acid
kDa	Kilodalton
kV	Kilovolts
LVR	Linear Viscoelastic Range
ml	Millilitres
MSC	Mesenchymal Stem Cells

MTT	Methylthiazolyldiphenyl-Tetrazolium Bromide
Mw	Molecular Weight
n.s	Not Specified
NHDF	Normal Human Dermal Fibroblasts
PDGF	Platelet-Derived Growth Factor
PEO	Poly (Ethylene Oxide)
PGA	poly (Glycolic Acid)
PI	Propidium Iodide
PLA	Poly (Lactic Acid)
PVA	Polyvinyl Alcohol
PVP	Polyvinyl Pyrrolidone
RP	Rapid Prototyping
SDS	Sodium Dodecyl Sulphate
SEM	Scanning Electron Microscopy
TBSA	Total Body Surface Area
UCL	Uncrosslinked
VEGF	Vascular Endothelial Growth Factor
WHO	World Health Organisation
XRD	X-ray Powder Diffraction

1.0 Literature Review

1.1 Introduction

The World Health Organisation (WHO) reported that burn injuries are the direct cause of over 265 000 deaths per year with most of these cases occurring in the low- to middle-income countries (WHO 2019). In New Zealand, burn injuries are the seventh leading cause of non-fatal injuries in children age 0 to 14 years (Aotearoa 2015). In Australia, severe burn or scald injuries are responsible for approximately 10,000 hospitalisations each year (Wang et al. 2018).

The financial burden worldwide warrants for novel strategies to achieve effective wound healing (Boateng and Catanzano 2015). While a combination of established prevention strategies and developments in the care of burn patients have made a considerable impact in reducing the rate of burn related deaths, these efforts have not been completely translated to low- and middle-income countries. Doing so would significantly reduce the global rates of burn-related death and disability. With this in mind, solution strategies should consider cost-effectiveness, ease of fabrication, use of readily obtainable material and the environmental impact.

In order to design an effective treatment option, it is important to understand the structure and function of the skin and burn wound pathology. The present thesis is organised as follows: firstly, there will be a review of literature which discusses the function and architecture of the skin, pathology of dermal burn wounds, outline the current treatments available and their limitations, and finally provide an overview of tissue engineering as a solution.

1.1 The Skin: Structure and Function

The skin is not only the largest but also the most active immune organ in our body (Salmon, Armstrong, and Ansel 1994). It is vital in thermoregulation, maintaining body fluid homeostasis, regulating many metabolic processes and serving as the first line of defence from external environments. In general, three distinct layers make up the skin; the epidermis, dermis and hypodermis (Figure 1).

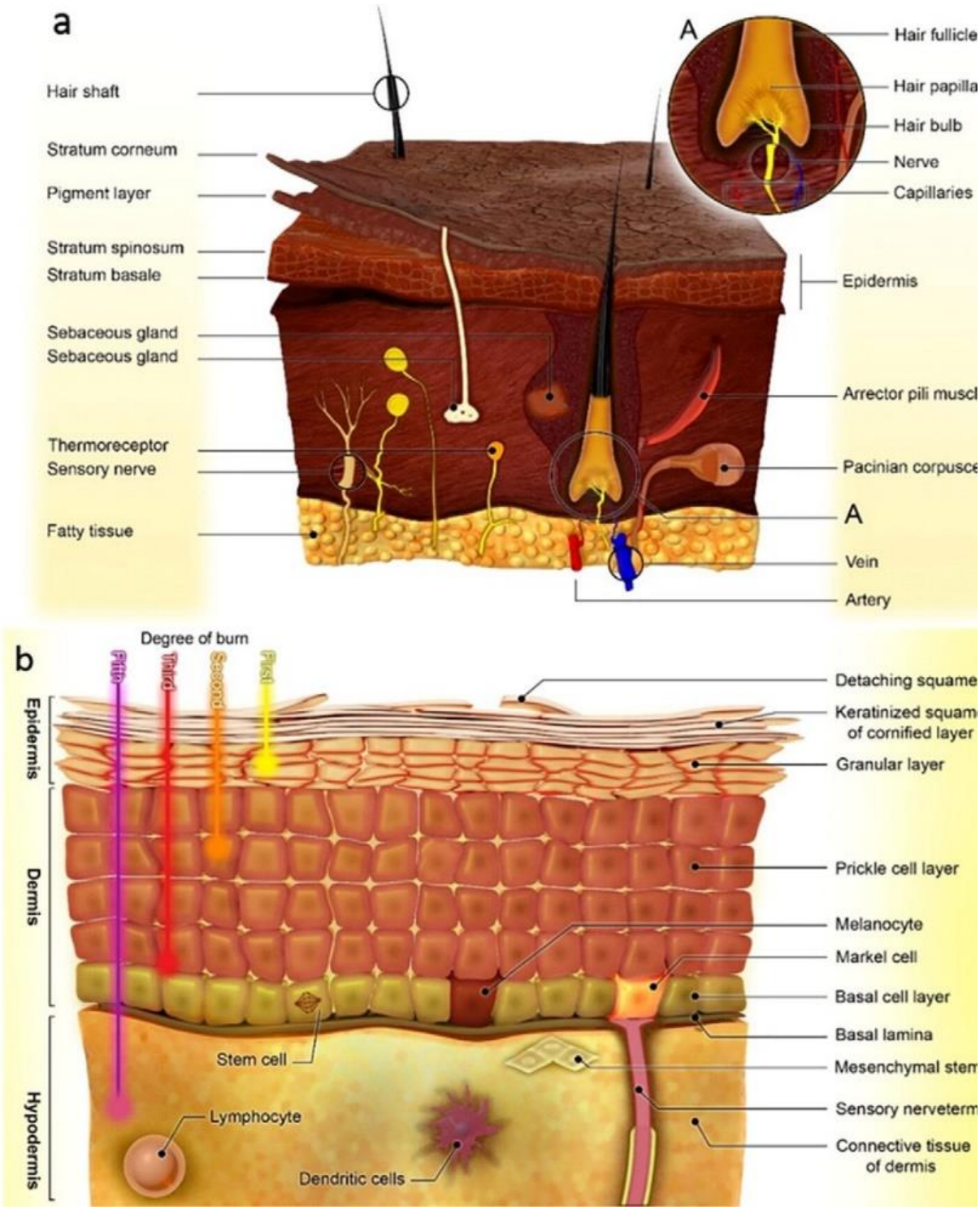

Figure 1. Structure of the skin

The figure shows the structure of skin (a), and layers of skin including epidermis, dermis, and hypodermis and their constituent cells and sub-layers (b). Taken from (Jahromi, Zangabad et al. 2018).

The epidermis, which is the top layer of the skin, is formed primarily of keratinocytes (95%) and provides a barrier from exogenous chemicals, pathogens and substances, and also regulates fluid in order to prevent dehydration (Chua et al. 2016). The epidermis is attached to the underlying dermis layer by a specialised basement membrane zone consisting of different types of collagen fibre. Next is the dermis which is the layer between the epidermis and hypodermis, composed of a thicker layer of connective tissue consisting mainly of the extracellular matrix (ECM). ECM is the structural component of skin which provides mechanical strength and elasticity. Spread throughout the ECM are cells such as fibroblast, endothelial cells, smooth muscle cells, and mast cells (Chua et al. 2016). Glycosaminoglycans (GAGs) are a key organic constituent of the ECM (Salbach et al. 2012). The two main types of GAGs are non-sulphated GAGs such as hyaluronic acid, and, sulphated GAGs, such as chondroitin sulphate (Gandhi and Mancera 2008). Various types of GAGs make up 0.1% - 0.3% weight of the epidermis and dermis of skin tissue (Bernstein et al. 1996). Despite their small amount, they have a large water retaining capability and thus define skin volume and elasticity (Bernstein et al. 1996).

Also present in this layer is collagen protein, hair roots, sweat glands, blood vessels, lymphatic vessels, nerve cells, and mesenchymal stem cells (MSC) (Gurtner et al. 2008). The inner most layer, the hypodermis or subcutaneous fat, functions to support and anchor the dermal and epidermal layer and is comprised of vasculature, fibroblasts, adipocytes, macrophages and nerves, (Bellas et al. 2012). The epidermis and dermis communicate in order to maintain homeostasis via distinct glycoprotein and proteoglycans in the ECM structure of the epidermis and protein in the basement membrane of the epidermis.

1.2 Dermal wounds

Since the skin is the outer most part of the body, it is the most exposed to external factors making it prone to damage. Types of trauma to the skin includes surgery, injury, abrasions, and burns. A dermal wound can be described as a disruption to the anatomical structure and function of the skin. It can extend to deeper structures like the hypodermis, muscles, tendons, vessels, nerves, and even bone (Boateng and Catanzano 2015).

Dermal wounds can be characterised according to the number of layers that are affected as follows: 1) superficial wound where only the dermal layer is affected, 2) partial thickness wound where both epidermis and dermis layers are affected including appendages such as blood vessels, hair follicles and sweat glands, 3) full thickness wound where subcutaneous

fat/deeper tissues are damaged in addition to the epidermis and dermis (Boateng and Catanzano 2015).

Based on their repair process, wounds can be further classified as either acute or chronic. The first type usually heals completely within 8-12 weeks with minimal scarring (Percival 2002). They are primarily caused by external factors for example, knife, gunshots, and surgical incisions. Chronic wounds such as burns are in a prolonged state of inflammation (Salbach et al. 2012). Here, persistent release of proteases including matrix metalloproteinases (MMPS) and reactive oxygen species (ROS), damage surrounding tissue (Salbach et al. 2012). This is not ideal as the ECM, growth factors and their receptors are needed for the healing process.

In the event of a wound, the normal physiological conditions are disrupted. Slow and incorrect repair can cause things such as loss of skin, hair, onset of infection or skin disease, injury to the circulatory system and in severe cases, necrosis of the tissue (Boateng and Catanzano 2015). Several inter-related biological activities at molecular level are involved for wound healing. In general, wound healing occurs in five highly integrated and overlapping physiological phases: inflammation, cell recruitment, matrix deposition, epithelialization and tissue remodelling (Wang et al. 2018).

1.3 Burns

Usually two criteria are used to classify the severity of burns (Jahromi et al. 2018). In the first method, the depth of the thermal damage is assessed and further categorised into four degrees. In the first degree, the burn wound comprises of only the epidermis. The site of damage exhibitions redness, dryness and pain. Second degree burns can affect the upper or deeper dermis and usually presents with blistering of the skin, with a yellow or white colour and moist appearance. Third degree burns involve full thickness damage to both the epidermis and dermis. It has a stiff or leathery consistency and scarring, and contractures will form after healing. In fourth degree burns, fatal damage is cause in the underlying tissues, tendons, ligaments, muscles and even bone (Jahromi et al. 2018).

In the second method, the percentage of total body surface area (TBSA) affected by the injury is estimated. When burns are assessed in terms of percentage of TBSA, a precise assessment can be evaluated by the criteria set by Lund Browder charts where a range of proportions of body parts in adults and children are accounted for e.g. burn wound >10% in children have the same severity as 15% for adults. Hypovolemic shock can be potentially life threating and is therefore an important measure. Loss of fluid from damaged micro vessels

produces oedema and hypoproteinaemia in burns where about 25% of the body is affected (Jahromi et al. 2018).

1.3.1 Burn Wound Healing

1.3.1.1 Homeostasis Phase

This initial phase occurs approximately 10 minutes after the thermal insult has occurred. The autonomic response tries to keep the damage to a minimum. During this phase, several events occur including platelet aggregations, immune activation, blood clotting and complement system activation. The blood clot is composed of vitronectin, fibrin, fibronectin and thrombospondins, which provides a scaffold-like matrix for the migration of keratinocytes, fibroblasts, leukocytes and endothelial cells along with causing an accumulation of growth factors (Gurtner et al. 2008).

1.3.1.2 Inflammatory Phase

This phase occurs 1-3 days after infliction of the wound. In the early phase neutrophils arrive and produce factors that start the inflammatory response and trigger other factors including vascular endothelial growth factor (VEGF) to repair blood vessels. In the late phase, monocytes transform into macrophages that produce more growth factors including fibroblast growth factor (FGF), platelet-derived growth factor (PDGF) and VEGF, in order to encourage cell expansion and migration, and generation of ECM by native skin cells. After about four days, adaptive immunity takes place which mainly involves lymphocytes (Li, Chen, and Kirsner 2007, Strbo, Yin, and Stojadinovic 2014).

1.3.1.3 Proliferation Phase

The proliferation phase includes three steps and occurs 3-10 days after injury. In the first phase, cytokines and growth factors cause increase in epithelial cells, keratinocytes, fibroblasts and stem cells causing reepithelialisation. Some fibroblast cells differentiate into myofibroblasts that construct ECM which offers a suitable structure for cell adhesion and organises the growth and differentiation of the cells including fibroblasts. The second step in the proliferation phase is new blood vessel formation (angiogenesis). The production of granulation tissue makes up the final stages of this phase. Fibroblasts are the key cells driving the granulation phase as they produce collagen and other ECM molecules. In the end, fibroblasts differentiate into myofibroblasts, forming a scar, or undergo apoptosis. In particular, the collagen that is responsible for producing a mature scar (Jahromi et al. 2018).

1.3.1.4 Remodelling Phase

This is the final step of wound healing process and initiates 2-3 weeks after the burn has occurred and continues for as long as a year or more. More collagen and elastin are produced by the wound scar and the fibroblasts mature into myofibroblasts. Apoptosis of keratinocytes and inflammatory cells, like T cells and macrophages, also plays an important role in ending the response to injury (Jahromi et al. 2018).

1.3.2 Overview of Current Treatments for Burn Injuries

In cases of burns that are partial or full thickness wounds, the primary healing process or suturing are not enough to close the wound and surgical procedures are required. This is due to the prolonged inflammation occurring which ultimately leads to destruction of the surrounding tissue including ECM, growth factors and receptors needed for the healing process (Salbach et al. 2012).

Autologous skin grafting remains to be the gold standard treatment for full and partial thickness burns. Skin grafting involves taking a piece of skin from an unburnt part of the body and grafting it onto the wound. In practice, donor site is limited when the burn is extremely large (>50% total body surface area) (Wang et al. 2018). Repeated harvesting of donor tissue can address this however, pain, slow healing of donor site, scarring and possible discoloration of the skin can be a problem (Wang et al. 2018). Meshing the donor tissue increases the graft site by up to four times and is a technique used in clinical practice. While this practice reduces the need for the amount of harvesting required, it also reduces the quality of the original tissue and results in the patient skin healing with mesh patterns and severe scarring (Wang et al. 2018).

Several acellular and cellular skin substitutes exist on the market as an alternative to skin grafting. Acellular substitutes may contain combinations of natural and synthetic polymers, and organic molecules like proteins and fats but do not contain any living material. On the other hand, cellular substitutes, as the name suggests, contain living cells or are from living origin. Cellular skin substitutes can be distinguished by their origin: autologous (from the patient themselves), syngeneic grafts (from genetically identical individual e.g. monozygotic twin), allogenic (another human individual) or xenogeneic (from a different species) (Barbosa et al. 2016). The limitation of the use of allogenic grafts includes the availability of skin banks, safety for patient, denial of use based on religious beliefs, and the risk of viral disease transition (Shevchenko, James, and James 2009). The transfer of porcine retrovirus

and prion diseases are a major concern when it comes to grafts engineering from xenogeneic origins (Barbosa et al. 2016). Skin substitutes available on the market for the treatment of burn injuries and their constituents are listed in Table 1.

Table 1. Existing skin substitutes for the treatment of burns

Skin Substitute	Composition	Reference
Acellular		
Integra ®	Bovine collagen, GAG, silicone	(Dantzer and Braye 2001)
Renoskin	Bovine collagen 1, GAG	(Fabienne et al. 2007)
Terudermis	Polyester mesh, collagen, silicone	(Shahrokhi, Arno, and Jeschke 2014)
Matriderm®	bovine type I, II and V collagen covered with bovine elastin hydrolysate	(Min et al. 2014)
Hyalograft 3D™	Membrane incorporating benzyl-esterified derivatives of hyaluronic acid	(Dieckmann et al. 2010)
Oasis™	Porcine small intestine submucosa acellular collagen matrix	(Shahrokhi, Arno, and Jeschke 2014)
Suprathel®	DL-lactidetrimethytencarbonate, trimethylencarbonate and ε-caprolactone	(Schwarze et al. 2008)
Epigard®	Teflon	(Dieckmann et al. 2010)
Syspurderm®	Polyurethane (PUR)	(Dieckmann et al. 2010)

Biobrane®	Silicone bonded to woven nylon containing peptides from type 1 porcine collagen	(Farroha et al. 2013)
XenoDerm	Acellular lyophilised porcine dermis	(Hosseini, Mousavinasab, and Fallahnezhat 2007)
GraftJacket®	Acellular, meshed human dermis	(Nathoo, Howe, and Cohen 2014)
Permacol™	Acellular porcine-derived matrix	(MacLeod et al. 2008)
GlyaDerm®	Derived from glycerol-preserved human allogeneic skin, containing collagen and elastin	(Pirayesh et al. 2015)
TissueTech Autograft System	Hyaluronic acid membrane	(Shevchenko, James, and James 2009)
Pelnac®	atelocollagen type I derived from porcine tendon, sponge layer with silicone film	(Widjaja and Maitz 2016)
Cellular		
Transcyte	Nylon mesh with collagen and fibroblast, silicone	(Noordenbos, Doré, and Hansbrough 1999)

Hyalomatrix	Hyaluronan matrix with fibroblasts	(Shahrokhi, Arno, and Jeschke 2014)
Laserskin ®	Membrane incorporating hyaluronic acid, autologous keratinocytes and fibroblasts	(Lam et al. 1999)
Dermagraft®	Polyglycolic acid, fibroblasts	(Hansbrough, Doré, and Hansbrough 1992)
TransCyte®	Nylon mesh coated with collagen, human fibroblasts, silicone	(Dieckmann et al. 2010)
Apligraf®	Bilayered substitute of bovine type 1 collagen matrix with fibroblast, and epidermal sheet derived from keratinocytes	(Barbosa et al. 2016)
Epicel®	Epidermal autograft made of autologous keratinocytes grown *in vitro* in the presence of fibroblasts.	(Dieckmann et al. 2010)
PermaDerm®	Collagen, type 1 bovine collagen, fibroblasts, keratinocytes	(Varkey, Ding, and Tredget 2015)
Karoskin	Allogenic graft containing dermal and epidermal cells	(Shevchenko, James, and James 2009)
StrataGraft®	Dermis and fully stratified epidermis generated from Neonatal Immortalized KeratinocyteS (NIKS)	(Schurr et al. 2009)

OrCel®	Bilayered type 1 collagen matrix, keratinocyte, fibroblasts	(Still et al. 2003)
MySkin™	Silicone membrane, autologous keratinocytes	(Shevchenko, James, and James 2009)

Mortality following a burn injury is most commonly due to wound infection (Wang et al. 2018). Worldwide, most infections are caused by gram negative bacteria: *Pseudomonas aeruginosa*, *Klebsiella pneumonia* and *Escherichia coli* (Azzopardi et al. 2014, Issler-Fisher et al. 2016). The presence of gram-negative bacteria and the gram-positive *Staphylococcus aureus* independently predict mortality (D'Avignon et al. 2010). Some antimicrobial agents such as silver sulfadiazine, have been reported to show poor healing outcomes with little evidence of preventing wound infections compared to alternate dressings (Aziz, Abu, and Chong 2012). This prompts investigation into alternate antimicrobial agents that do not compromise wound healing. The role that naturally antibacterial biomaterials can play to help address this problem is discussed later in this review.

1.4 Tissue Engineering – Dermal

Tissue engineered dermal substitutes provide a suitable alternative to harvesting and using skin grafts, thereby eliminating the need to create a wound elsewhere in the body in order to obtain healthy tissue. Moreover, harvesting skin tissue to be used as a graft is a painful process that results in further scar tissue. The engineered scaffold should take into account the patient's safety, clinical efficacy and ease of use and the materials used should be practical so that it may achieve clinical acceptance (MacNeil 2007).

Tissue engineering is an approach in regenerative medicine that focusses on the regeneration and restoration of functional cells, tissue, and organs (Dieckmann et al. 2010). In this approach, a three-dimensional (3D) material is created and referred to as a matrix or scaffold that is gelatinous or porous in nature. As in the case of severe burns where native tissue is destroyed, the scaffold provides guidance and mechanical support for the growth of fully functional skin including all skin appendages (Yeong et al. 2004). The 3D nature of the scaffold should encourage the migration, proliferation, and differentiation of incorporated cells within the structure and not only on the surface (Landers et al. 2002).

The ideal tissue engineered substitute should protect the injury from protein loss, inhibit exogenous microorganism invasion, mimic the natural skin functions and improve the aesthetic appearance of the wound site (Wu et al. 2016). It should adhere to the wound bed, allow vascularisation and must not illicit an immune response from the body in order to effectively heal the wound (MacNeil 2007). In order for new tissue to form, the originally implanted scaffold matrix needs to be broken down and cleared therefore, materials used to fabricate the scaffold must be entirely biodegradable with nontoxic by-products. The scaffold

material should eventually degrade within the body and leave behind a matrix of connective tissue that resembles structural and mechanical properties of the native skin.

It is a well-known fact that nanostructures are the most ideal choice for the fabrication of tissue regeneration scaffolds due to their large surface area and small pore size. Nanofibrous scaffolds have shown positive outcomes in enhancing cell attachment, stimulating cell proliferation, protein adsorption and assisting in cell differentiation (Tysseling-Mattiace et al. 2008, Woo, Chen, and Ma 2003).

Over 30 new skin substitutes have been tested or used in the treatment of burn injuries since 2000 (Table 1**)** and these can be categorised into biological substitutes, synthetic substitutes or a combination of both. Various biomaterials and fabrications techniques have been used over the years to engineer tissue scaffolds. Fabrication methods for scaffolds include techniques such as solvent casting and particulate leaching, phase separation, solution casting, freeze-drying, melt moulding and gas foaming. The above listed methods are not precise at controlling pore architecture; such as size, geometry, interconnectivity, and spatial distribution (Peltola et al. 2008). Moreover, many of these techniques utilise organic solvents to dissolve synthetic polymers which leaves behind residues that are toxic and carcinogenic to cells (Peltola et al. 2008).

Advanced methods of scaffold fabrication that attracts a lot of attention nowadays include rapid prototyping (RP), hydrogels and electrospinning. RP techniques uses computer-aided design (CAD) data to print a series of cross-sectional layers using bio-inks and polymer solutions. However, based on the results of our literature search, very few RP techniques are suitable for fabricating soft tissue such as skin. Busaina et al. used stereolithography to entrap cells in a PEO hydrogel scaffold (Dhariwala, Hunt, and Boland 2004). The resulting hydrogel had desired shape but did not have pore structure or display high mechanical properties which can be attributed to the use of PEO alone. Another limitation of the study was the use of photo initiator which is toxic to cells (Dhariwala, Hunt, and Boland 2004)

1.5 Electrospinning Nanofibrous Scaffold: Theory and Set Up

The electrospinning method relies on the stretching of a charged polymer solution jet (Haider, Haider et al. 2018). It is dependent on the coulomb forces between surface charges of the fluid and the applied force of the external electric field. The electrospinning set up consists of four main parts: (1) a syringe containing the polymer solution that is to be electrospun, (2) a metallic needle and (3) a metallic collector (which can be of varying morphology), and (4) a power supply. The polymer solution is fed through the needle at a constant flow rate. The needle is connected to a power supply and the induced charge moves into the polymer solution via the needle causing instability within the polymer droplet (Haider, Haider, and Kang 2018). On the other end, the collector is oppositely charged creating an electric potential that opposes the surface tension of the polymer solution droplet. The electric potential created between the needle and collector causes the polymer solution to be drawn in the direction of the electric field (towards the collector) (Haider, Haider, and Kang 2018). Increasing the electric field will result in a Taylor cone being formed; this is conical shaped, from which nanofibers emerge and get collected on the collector plate at an optimised distance (Haider, Haider, and Kang 2018). The nanofibers are formed as a result of the whipping motion that occurs due to the electric field in the chamber, allowing the polymer chains within the solution to stretch and slide past each other (Bae et al. 2013, Haider et al. 2013). In order for a stable jet to form, the solution must have sufficient cohesive force (Haider, Haider, and Kang 2018).

Electrospun mats have been utilised for several different biomedical applications including pharmaceutical repositories, drug-loaded carriers for medical therapy, nucleic acid delivery for gene therapy, tissue engineering, filtration material, among others (Ding et al. 2019). They mimic diversified hierarchical structures found in the natural ECM with regard to structure and composition depending on the materials chosen (Mahoney et al. 2012). The simple technology allows the fabrication of ultra-fine solid and continuous fibres of polymers with diameters ranging from 1-1000 nm (Subramanian et al. 2014). Moreover, is a relatively cost-effective and easy technique. Its ability to spin versatile materials, both natural and synthetic polymers, is a major advantage.

Interconnected pores in electrospun scaffolds allow for new vessels to grow. Moreover, it can play a role in directing the growth by the size of the porous channel. The small pore size means the polymeric nanofibers have a large surface area allowing more sites for cell adhesion and proliferation. However, too small pores can pose the limitation of reduced cell

infiltration to deeper layers of the scaffold. Therefore, pore size should be adequate to allow a 3D infiltration within the scaffold rather than two dimensional (2D), where cells only populate the surface of the scaffold (Haider, Haider, and Kang 2018).

A number of factors affect the electrospinning process which can be classified as electrospinning, solution, or environmental parameters. The effects of each are explained below and summarised in Table 2.

1.5.1 Electrospinning Parameters

Electrospinning parameters include the voltage applied in the chamber, the distance between the tip of the needle and the collector, the rate at which the solution is delivered in the chamber (flow rate), and the collector type. The minimum voltage required to deform the spherical droplet into a Taylor cone and form nanofibers is the critical voltage (Laudenslager and Sigmund 2012). The critical voltage varies between different polymers and combinations of polymers, as does the flow rate. Critical flow rate for a polymeric solution ensures the formation of uniform beadless nanofibers. Using flow rates beyond critical value leads to increase in fibre diameter and pore size due to incomplete drying of the polymer solution between the needle tip and collector, and therefore less stretching (Megelski et al. 2002). The non-evaporation of the solvent and low stretching can result in ribbon-like structures (Li and Wang 2013). Because flow rate affects fibre formation and size, the minimum flow rate required to maintain a balance between the leaving polymeric solution and the replacement of that solution at the tip of the needle during jet formation, thereby producing a stable jet is preferred (Megelski et al. 2002). A receded jet can also form where no obvious droplet or cone is formed at the tip of the needle and the polymer jet arises from inside the needle (Haider, Haider, and Kang 2018). This type of jet produces scaffold with a range of fibre diameters because is not a stable jet, due to the receded jet frequently being replaced by a cone jet (Haider, Haider, and Kang 2018).

Surface charge density is another important factor that affects the morphology of the nanofiber. Flow rate and electric current have been found to be directly related (Theron, Zussman, and Yarin 2004). In his study of PEO, Theron et al., observed a decrease in surface charge density with an increase in flow rate and a simultaneous increase in the electric current (2004). The needle to collector distance also affects the morphology as it relies on the deposition time, evaporation rate of solvent and the period of whipping motion (Matabola and Moutloali 2013).

Table 2. Parameters that influence fibre morphology in the electrospinning setup

Parameters	Effects on Fibre Morphology		References
Electrospinning Parameters			
	Increase	Decrease	
Applied voltage	Decrease in fibre diameter attributed to the stretching of polymer solution associated with the charge repulsion within polymer jet, an increase beyond the critical voltage will result in the formation of beads.	Increase in fibre diameter	(Sill and von Recum 2008, Topuz and Uyar 2017)
Distance between tip and collector1	Formation of beads with too large distance, minimum distance required for uniform fibres	Formation of beads with too small distance, minimum distance required for uniform fibres	(Ki et al. 2005)
Flow rate	Increase in fibre diameter and pore size generation of bead with too high flow rate, possible formation of ribbon-like structures.	Decrease in fibre diameter,	(Haider, Haider, and Kang 2018, Megelski et al. 2002, Nadri, Nasehi, and Barati 2017)

Collector type	Influence structural morphology of electrospun fibres. A non-conductive collector creates a porous structure with circular pores on the fibre surface		(Sill and von Recum 2008)
Solution Parameters			
	Increase	Decrease	
Viscosity	Increased fibre diameter and disappearance of beads	Bead generation	(Ramakrishna et al. 2006)
Polymer concentration	Increase in fibre diameter	Decrease in fibre diameter	(Megelski et al. 2002)
Molecular weight of polymer	Reduction in the number of bead and droplets	Increase in the number of bead and droplets	(Malik et al. 2015)
Conductivity	Decrease in fibre diameter, if conductivity is too high results in negative effect on Taylor cone	Increase in fibre diameter, if conductivity is too low, Taylor cone cannot form	(Haider, Haider, and Kang 2018, Lee et al. 2015)
Surface tension	High surface tension results in instability of jets, no conclusive link with fibre morphology	No conclusive link with fibre morphology	(Khalil et al. 2015)

Environmental parameters			
	Increase	Decrease	
Humidity	High humidity results in circular pores on the fibres	-	(Bedane et al. 2016, Park and Lee 2010, Pelipenko et al. 2013)
Temperature	Decrease in fibre diameter	Increase in fibre diameter	(Liu et al. 2016)

1cases where no effect was seen (Zhang et al. 2005).

1.5.2 Solution Parameters

The solution parameters include viscosity, polymer concentration, molecular weight of the polymer, conductivity of the solution, and surface tension. The solvent used to make the solution should completely dissolve the polymer. Generally, higher volatile solvents are preferred as they have lower boiling points and thus high evaporation rates which encourages solvent evaporation from the nanofiber during flight from the needle to the collector (Haider, Haider, and Kang 2018). However, they can also dry too quickly and cause drying and subsequent blocking of the needle. Comparably, less volatile substances may prevent solvent evaporation during flight time due to low boiling points (Haider, Haider, and Kang 2018). The use of two solvents, one solvent and one non-solvent, with different evaporation rates will lead to phase separation and result in a highly porous scaffold (Sill and von Recum 2008).

Since electrospinning relies on the stretching of charged jet, it is also affected by polymer concentration. In instances where the polymer concentrations in the solution are low, the entangle polymer chains to break in the electric field before they reach the collector (Haider et al. 2013, Pillay et al. 2013). The fragments then lead to the formation of beads. By increasing the polymer concentration in the solutions, and thereby increasing its viscosity, we can increase the number of chain entanglements and overcome the surface tension; resulting in bead-free, uniform fibres (Haider, Haider, and Kang 2018).

On the other hand, increasing polymer concentration beyond the concentration at which uniform fibres can be obtained, leads to defective nanofibers as the flow of solution is hindered due to drying of the solution at the tip of the needle (Haider et al. 2013). Doshi et al. reported that the optimum viscosity for the generation of electrospun fibres is 800-4000cp.

A conductive solution has enough free charges to move onto the surface of the solution droplet (electrostatic force of surface charges) and form a Taylor cone in the presence of the external applied electric field (Haider, Haider, and Kang 2018). Without conductivity or with lower conductivity, the droplet will not have sufficient surface charge to form a Taylor cone. Not only does the solution conductivity affect formation of the Taylor cone, but it also controls the diameter of the nanofiber (Haider, Haider, and Kang 2018). The addition of salts to increase polymer solution conductivity is a common practice as it increases the number of ions in the solution, thereby increasing the surface charge on the droplet, and increases the conductivity of the polymer solutions (Haider, Haider, and Kang 2018).

1.5.3 Environmental Parameters

Environmental parameters include humidity and temperature. Humidity can affect the solidification process of the charged jet and change fibre morphology. Studies have shown that in general, fibre diameter decreases with an increase in humidity (Park and Lee 2010, Pelipenko et al. 2013). Binary solvent systems are also affected by humidity as they rely on different evaporation rates of the two solvents; a technique which can be used to create porous nanofibers (Bae et al. 2013). Increasing temperatures lead to an increase in the evaporation rate of the solvent and a decrease in the solution viscosity. Both of which result in smaller fibre diameter (Haider, Haider, and Kang 2018). Environmental parameters may be an important consideration when fabricating electrospun scaffolds on a large scale in tropical countries.

1.6 Biomaterials for Skin Tissue Engineering

Biomaterials can be distinguished by their ability to degrade or be incorporated in by biological host (Banyard et al. 2015). They are often used for creating the structure of skin substitutes and should be evaluated to determine the presence of any toxic effects to the body, taking into account the inflammation, wound healing and immunological responses they elicit (Anderson 2019, Dieckmann et al. 2010). They can be of synthetic or natural origin and are acellular.

1.6.1 Synthetic Polymers in Dermal Tissue Engineering

Most synthetic polymers are degraded via chemical hydrolysis and insensitive to enzymatic processes so that their degradation does not vary from patient to patient (Yang 2001). Poly (ethylene oxide) (PEO) is one of the few polymers approved for internal use in cosmetics, food and pharmaceuticals. It is easy to process and therefore utilised for many biomedical applications (Mahoney et al. 2012). Poly (lactic acid) (PLA), and poly (glycolic acid) (PGA), are thermoplastic polymers characterized by polyesters links of, respectively, lactic or glycolic acid have an extensive U.S. Food and Drug Administration (FDA) approval history. They are both biodegradable and can be absorbed *in vivo*. They have been applied in the fabrication of absorbable suture material and wound healing grafts (Chong et al. 2007, Lou et al. 2008). However, it should be pointed out that all polyesters release acidic degradation products that can adversely affect biocompatibility (Yang 2001). The concern is regarding toxic residual monomers from incomplete polymerisation as well as degradation products and plasticisers and therefore, require extensive and comprehensive testing prior to clinical translation. Moreover, these polyesters tend to be relatively stiff materials. While this may be an advantage in load-bearing applications, it becomes a disadvantage when mechanical compliance for soft tissue application (Yang 2001).

Polyvinyl alcohol (PVA) is the largest volume synthetic resin produced in the world. It is hydrophilic in nature and displays bioadhesive properties. It is biocompatible and degrades into water and carbon dioxide and hence has been widely used for a variety of biomedical applications owing to its non-toxic and non-carcinogenic nature (Subramanian et al. 2014). PVA has become a popular synthetic blending polymer for use with natural polymers to facilitate their electrospinning due to its superior rheological and fibre forming properties (Jia et al. 2007).

Polyvinylpyrrolidone (PVP) is a water-soluble polymer that is chemically inert and biocompatible. It is a viscosity enhancer, lubricator and an important precursor polymer (Gökmeşe, Uslu, and Aytimur 2013). Subramanian et el, created and evaluated a PVA and PVP scaffold using the electrospinning technique and for tissue engineering and cell culture application and found good spreading and adhesion of NIG3T3 fibroblast cells cultured on the membrane. They suggest that the PVA/PVP membrane may spatially mediate cellular responses to promote cell attachment and proliferation (Subramanian et al. 2014). Synthetic polymers offer excellent mechanical properties, but they lack cell-recognition signals which is a major limitation of synthetic materials (Barbosa et al. 2016).

1.6.2 Natural Polymers in Dermal Tissue Engineering

Natural polymers and synthetic polymers have both been widely investigated for engineering skin tissue. Natural polymers can be obtained and isolated from a variety of sources including animal, seaweed or bacteria (Kang et al. 2018). Depending on their origin, these natural polymers can offer their own intrinsic signalling molecules for example, collagen and fibrin, while others such as alginate and agarose, do not (Lee and Mooney 2001). Both have their advantages. They display low toxicity and low chronic inflammatory response because of their abundance in skin and ability to be recognised by cell surface receptors (Barbosa et al. 2016).

Collagen and hyaluronic acid (HA; a GAG protein), are two components in the ECM of the skin and have been investigated and considered ideal biomaterials for wound repair (Wang et al. 2018). These naturally occurring biomaterials undergo enzymatic hydrolysis (Rosso 2005). Collagen promotes strong attachment and proliferation of keratinocytes and dermal fibroblasts and HA has low immunogenicity. Another essential component of human skin is elastin which provides structural and cell mediating functions (Wang et al. 2018). Natural collagen obtained from bovine or human sources poses a major risk of disease transmission. Eliminating or reducing the risk of disease transmission could be achieved either by using synthetic collagen-mimetic materials or recombinant-produced collagen (Rosso 2005).

Keratin is a protein-based polymer and represents the most important biopolymer in mammals after collagen (McKittrick et al. 2012). It has been widely utilised for various biomedical applications including skin tissue engineering due to its biocompatibility, biodegradability, bioactivity and natural abundance (Keskin, Urkmez, and Hames 2017). Keratin facilitates and supports fibroblast cell proliferation, promotes wound healing and reepithelization (Ku and Omary 2006, Wang et al. 2012). Its brittle nature and low molecular weight make it unsuitable for electrospinning, however, many polymers have been blended with keratin to facilitate the electrospinning process including PCL, PEO and PVA (Cruz-Maya et al. 2019, Ma et al. 2017, Park et al. 2015).

Other examples of natural materials are hydroxyapatites, polypeptides, hyaluronan, GAG, collagen, chitosan, and alginates (Barbosa et al. 2016). A widely investigated natural material is silk which is composed of two proteins, fibroin and sericin (Wang et al. 2018).

Chitosan is the second most abundant polymer after cellulose, the polysaccharide is widely employed for many biomedical applications such as in surgical thread, drug delivery carriers, bone healing and wound dressing materials (Lou 2008, Nho and Park 2002, Yang et al. 2008). It is commercially obtained by the alkaline deacetylation of chitin. Chitin is a natural polymer that is easily obtained from some insects, fungi and crustacea including shrimp, crab and lobster sources (Ranjha and Khan 2013). The ability to obtain chitosan from waste products after food processing means an unconstrained, sustainable supply is available and one which adds value to food waste (Mahoney et al. 2012). Chitosan is one of few natural polymers that is antibacterial. This offers the advantage of limiting infection in the wound and could reduce the need of adding antibacterial drugs. The positively charged chitosan attaches to the negatively charged residues on the bacterial surface, damaging the cell membrane (Helander et al. 2001). The polycationic nature of chitosan is also responsible for other therapeutic properties such as fast blood coagulation and electrostatic immobilization of wound microorganism (Moghaddam et al. 2014, Younes and Rinaudo 2015). Moreover, it possesses a structure that is similar to glycosaminoglycan (GAG), a major component of dermal ECM, making it an excellent candidate for tissue engineering (Mahoney et al. 2012). Gökmese and others said it could speed the synthesis of collagen in the early stages and accelerate tensile strength of wounds (Gökmeşe, Uslu, and Aytimur 2013).

Chitosan is only soluble in acidic media and some claim that this is not suitable for cell viability (Moghaddam et al. 2014). However, in this study, it was decided to prepare chitosan in a 2% acetic acid solution as used in other studies (Aytimur and Uslu 2014,

Gökmeşe, Uslu, and Aytimur 2013). The highly viscous nature of chitosan in an aqueous solution with increasing concentration makes the solution difficult to electrospin due to the presence of strong hydrogen bonding between -NH_2 and -OH groups of chitosan (Mahoney et al. 2012). Added to this, owing to its ionic nature, chitosan displays polyelectrolyte behaviour in solution form creating large repulsive forces between ionic groups while it is charged under an electric field resulting in a lack of continuous fibre formation during electrospinning (Mahoney et al. 2012). On the other hand, there is a risk of having insufficient material to produce solid fibres when using low polymer concentrations. The effect of parameters, such as conductivity and polymer concentration, on the formation and morphology of electrospun nanofiber are difficult to define for pure aqueous solution of chitosan (Mahoney et al. 2012).

The biological properties of natural polymers make them of interest in research and clinical applications, however, their low mechanical properties, the instability of material and deterioration which accompanies long-term implantation limits their clinical application (Rosso 2005). Blending chitosan with a synthetic polymers or organic acids is an effective strategy to overcome some of these challenges and successfully fabricate electrospun chitosan containing nanofibers (Mahoney et al. 2012).

1.6.3 Crosslinking

Acetic acid, a commonly used solvent to dissolve chitosan, cleaves the backbone structure of chitosan molecules to result in mechanically weak nanofibers that degrade very quickly in aqueous environments such as in body fluids (Mahoney et al. 2012). A way to reduce the solubility and increase the structural integrity of the chitosan scaffolds is by chemical crosslinking. However, even a trace amount of toxic chemicals in the scaffold can alter cytocompatibility. A variety of crosslinkers are used to crosslink chitosan through the amine groups. Some of these chemicals agents include diisocyanates, N,N-disuccinimidyl suberate, resimene, hexamethylene 1,6-di(aminocarboxysulfonate) and epichlorohydrin (Schiffman and Schauer 2007).

A popular crosslinking agent that has been highly utilised in more recent publications is glutaraldehyde (GA). Liu et al. used GA to crosslink porous collagen/chitosan scaffolds and found that the crosslinking degree is affected by the method of crosslinking used (2012). In general, a higher crosslinking degree resulted in scaffolds with a smoother surface and stronger internal structures leading to more controlled size (Liu 2012).

Chemical modification of chitosan by GA turns chitosan hydrophilic (Beppu et al. 2007). It is known that wet environments are much better for wound healing and therefore this is not

a desirable property to have for a skin substitute for burn wound treatment. In recent work, chitosan membranes have been crosslinked by immersing in sulfuric acid for 24 hours (Shang et al. 2020). GA crosslinks chitosan by two main mechanisms. The first is by Michael-type adducts with terminal aldehydes and the second is via Schiff base imine functionality (Schiffman and Schauer 2007). The potential toxicity of GA to cells have been reported by Alves and others (Alves et al. 2011).

Currently, there are two commercially available crosslinked engineered substitutes available in the market; GraftJacket and Integra™. GraftJacket is made from donated human tissue. The human tissue is treated to remove cellular components and epidermis. The remaining components; collagen, elastin, proteoglycans and the internal matrix of the dermis is chemically cross-linked to maintain the collagen architecture for cryopreservation (Nathoo 2014).

Integra™ Matrix Wound Dressing (Integra Life Sciences) is a composite of crosslinked bovine collagen and GAG with a semipermeable silicone covering. The semipermeable silicone membrane functions temporarily as the epidermal layer to control water vapour loss and provide structural integrity. The composite matrix recruits dermal fibroblasts to the damaged tissue, which then makes and secretes new ECM and facilitates healing. The matrix was crosslinked by high temperature vacuum dehydration at 105 ºC followed by immersion in 0.05 wt. % GA solution (Burke 1981). The two steps also sterilised the matrix during manufacturing resulting in a bacteria free membrane.

Residual GA is the main reason for cytotoxicity in scaffolds treated with GA for crosslinking. The use of GA means that additional treatments are needed for its removal for example, washing with Milli-Q water or oven drying. It is paramount that analysis, such as high-performance liquid chromatography, to detect residual GA must be performed following the removal step (Liu 2012).

Mi and others used genipin which is a naturally occurring crosslinking reagent to crosslink chitosan microspheres and compared its biocompatibility to glutaraldehyde crosslinked chitosan microsphere in a rat model (Mi et al. 2002). They found less inflammation and overall a better biocompatibility when using genipin.

A study compared three crosslinking methods to crosslink PVA/chitosan nanofibrous scaffolds; methanol immersion, glutaraldehyde crosslinking and heat treatment (180°C for 3h in a vacuum oven). They found that after immersing in water, methanol treated nanofibrous structures were totally destroyed, glutaraldehyde crosslinked scaffolds resulted

in some loss of nanofibrous structures while heat treated nanofibrous structure retained its structure after immersion in water (Çay, Miraftab, and Perrin Akçakoca Kumbasar 2014). Hence, the present study utilised heat treatment crosslinking method but at a lower temperature for a longer period of time in attempt to reduce structural damage in chitosan/PVA/PVP 3DENS.

2.0 The Current Project

The need for an artificial material capable of successfully substituting for skin, especially in the case of full thickness burns, have long been recognised. This need is also present in diseases or injuries where large areas of the skin are damaged. Despite products like Integra, GraftJacket, and other commercial products that have shown favourable clinical outcomes (Burke 1981), skin grafting remains to be the gold standard of treatment despite its many disadvantages.

It is generally well accepted that epidermal cells from the patient themselves would provide optimal epidermal covering. However, the use of artificially developed dermal matrixes offer several clinical advantages; it allows the material to be completely manufactured from nonviable materials in industrial batch processes and sterilized for immediate use. Secondly, because of it non-viable nature, they can be stored at room temperature over long periods of time. There is also the potential for mass production proving an opportunity for biological and economic use (Burke 1981). Chitosan is obtained from a renewable resource and add value to food waste material; while PVA and PVP are two of the most abundantly available synthetic polymers.

The novelty of this work is crosslinking 3DENS made with the combination of natural polymer chitosan, and synthetic polymers PVA and PVP. While scaffolds of this combination have been fabricated before, there had been no attempts to crosslink them. Moreover, a crosslinking method of heat treatment only was used successfully in the present study making it superior to those scaffolds that used chemical means to do so. The temperature of 120ºC used to crosslink chitosan/PVA/PVP used in the present study has not been reported before.

The combination of chitosan, PVA and PVP have previously been used to create electrospun constructs for wound dressing, tissue engineering and drug delivery applications (Aytimur and Uslu 2014, Gökmeşe, Uslu, and Aytimur 2013, Zhang et al. 2014). Researcher electrospun chitosan in the range of 20% to 67% dry weight concentration, by blending them with PVA and PVP (Aytimur and Uslu 2014, Gökmeşe, Uslu, and Aytimur 2013, Zhang et al. 2014). They successfully fabricated nanofibers used several techniques to characterise blend solutions and 3DENS physically and chemically. These scaffolds were not crosslinked and none of these studies tested the scaffolds biological activity. One study used heat crosslinking to crosslink chitosan/PVA scaffold by heating at 180°C in a vacuum oven for 3 hours and tested the scaffolds swelling ability

(Çay, Miraftab, and Perrin Akçakoca Kumbasar 2014), however our study is designed to expose the 3DENS to heat for a longer time at a lower temperature that would be less harmful to the surface structure.

The present work studied solution properties, physical and mechanical properties of the final crosslinked and crosslinked 3DENS as well as performed *in vitro* studies for cell viability and proliferation. A diagrammatic illustration of the study design is represented in Figure 2.

The aim of this work was to construct a three dimensional nanofibrous scaffold (3DENS) using a combination of chitosan, PVA and PVP using electrospinning as the method for fabrication and improve their mechanical properties using heat crosslinking method to thermally induce physical crosslinks in the 3DENS. It was hypothesised that the crosslinked scaffolds would exhibit superior physical properties compared to the uncrosslinked scaffold and that scaffolds containing higher percentage of chitosan would increase cell growth and viability. In order to achieve this aim, the objectives were set out as follows:

1. Optimise formulation blends of chitosan, PVA and PVP in order to electrospun scaffolds.
2. Characterise rheological properties of each formulation to evaluate the influence of changes in ratios of polymers in each formulation on electrospinning parameters.
3. Optimise electrospinning parameters for the fabrication of scaffolds for each formulation blend to obtain relatively uniform fibre morphology.
4. Physically crosslink the 3DENS using heating method.
5. Characterise the physical and mechanical properties of the scaffolds.
6. Evaluate the biocompatibility of the scaffold *in vitro* using human dermal fibroblasts (NHDF) and normal human cultured keratinocytes (HaCaT).

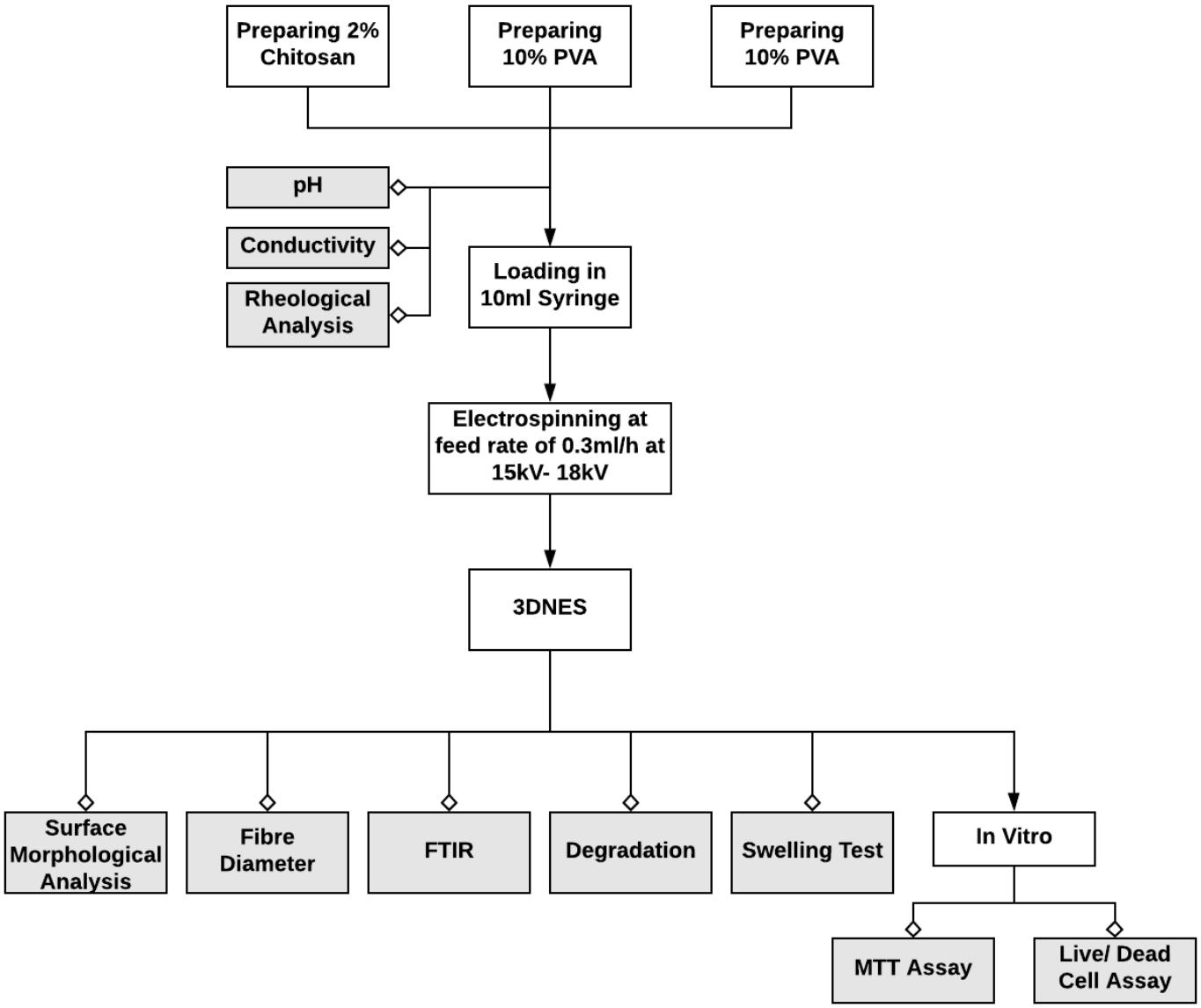

Figure 2. Overview of the study design

The figure illustrates the different characterisations performed (grey box) at each stage of the study design (white box).

3.0 Materials and Methods

3.1 Materials and Blend Formulations

Polyvinyl alcohol (PVA) and polyvinyl pyrrolidone (PVP) with an average molecular weight of 89 kDa and 360 kDa, respectively, were obtained from Sigma-Aldrich, USA. Chitosan with an average molecular weight of 890 kDa (75% deacetylation) was supplied by Shanghai Waseta Int'l Trading Company, China. All three polymers were used as received. PVA and PVP were dissolved by magnetic stirring in ultrapure water for 4 hours at 80°C and 90°C, respectively. Chitosan was dissolved in 2 % aqueous acetic acid solution at room temperature by magnetic stirring for one hour.

Formulations were made by mixing chitosan, PVA and PVP solutions in ratios outlined in Table 3 by stirring for 5 minutes until a homogenous mixture was formed. Homogeneity of the solution was confirmed visually, that is, no separate layers were seen.

3.2 Characterisation of Pure and Blend Polymer Solutions

3.2.1 Conductivity and pH of Formulations

The conductivity of the solution affects the net charge density carried by the jet in the electrospinning process where a higher net charge density increases the electrical force exerted on the jet leading to a decrease in fibre diameter (Gökmeşe, Uslu, and Aytimur 2013). The pH and conductivity of the polymer solutions was measured using Oakton pH/CON 700 Benchtop Meter (Thomas Scientific, USA).

3.3.2 Rheology

Rheology is a branch of physics that describes the deformation and flow behaviour of all kinds of materials under controlled testing conditions (Mezger 2006). Rheological measurements were performed on an advanced rheological expansion system (ARES) HAAKE™ Rheostress™ 1 (ThermoFisher Scientific, USA) equipped with a Peltier unit for temperature regulation (ThermoFisher Scientific, Waltham, USA) and a Thermo HAAKETM DC30-KIO self-contained refrigerated bath with immersion circulator (ThermoFisher Scientific, Waltham, USA). A cone – plate geometry was used in which a 60 mm titanium 1° cone plate (C60/T1°) and a 60 mm concentric parallel bottom plate was used. A gap of 52 μm and a temperature of 20°C was maintained throughout all tests (Cabral 2014).

Table 3. Formulations for electrospinning of nanofibrous mats (w./w.%)

Formulation	2% Chitosan sol	10% PVA sol	10% PVP sol	Total Solute Concentration
F10	10%	80%	10%	
Dry weight ratio	2	87	11	9.2%
F20	20%	70%	10%	
Dry weight ratio	5	83	12	8.4%
F30	30%	60%	10%	
Dry weight ratio	8	79	13	7.6%
F50	50%	40%	10%	
Dry weight ratio	17	66	17	6%
F70	70%	20%	10%	
Dry weight ratio	32	45	23	4.4%
Chitosan	100%	-	-	
Dry weight ratio	100			2%
PVA	-	100%	-	
Dry weight ratio		100		10%
PVP	-	-	100%	
Dry weight ratio			100	10%

All percentages are based on dry weight of materials as a percentage of total solution.

3.3.2.1 Flow Behaviour

Ideally viscous or Newtonian fluids such as water and mineral oil, have viscosities that are independent of shear rate and have a constant viscosity value (Mezger 2006). Shear-thinning and shear-thickening fluids have apparent viscosities corresponding to a specific shear rate. A decrease in viscosity with an increase in shear rate is characteristic of shear thinning behaviour of fluids (e.g. polymer solutions, polymer melts), while an increase in viscosity with increasing shear rate is characteristic of shear thickening behaviour (e.g. ceramic suspensions, dental composites). The graph in Figure 3 shows the viscosity curves for ideally viscous, shear thinning and shear thickening flow behaviour (Mezger 2006).

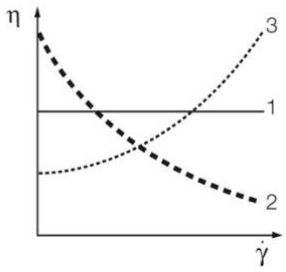

Figure 3. Typical viscosity curves

The graph represents viscosity curves for (1) ideally viscous, (2) shear-thinning, and (3) shear-thickening flow behaviour (Mezger 2006).

Newton's law states that shear stress, τ (Pa), is the result of the product of shear rate, (s^{-1}), and viscosity, η (Pas) (Mezger 2006). Therefore, viscosity can be defined by the following equation 1:

$$\eta = \frac{\tau}{\dot{\gamma}}$$

Equation 1. Viscosity as a function of shear stress and shear rate

The flow behaviour of formulations was studied in order to obtain viscosity functions. Shear rate ($\dot{\gamma}$) was set to 0 – 200 /s over 120 seconds. A shear rate of 20 /s was applied for 30 seconds to homogenise the sample and allowed to rest for 3 minutes before running sweeps.

3.3.2.2 Oscillatory Amplitude Sweep

Before performing a frequency sweep on an unknown sample, an amplitude sweep must be done to determine the range of frequency within which the sample behaves in a linear fashion. Beyond this range, the solution is permanently deformed (Tabilo-Munizaga and Barbosa-Cánovas 2005). This is called the linear viscoelastic range (LVR). In order to determine the LVR of the samples, an oscillation amplitude sweep was done for shear stress from 0.1 Pa to 20 Pa at frequency 0.1 Hz, 1 Hz, 10 Hz, 50 Hz, and 100 Hz at 20°C.

3.3.2.3 Oscillatory Frequency Sweep

The viscoelastic properties of the aqueous solutions of chitosan, PVA, PVP and blend formulations were followed through small-amplitude oscillatory shear experiments with oscillation frequency range from 0.1- 100 rad/s and strain amplitude $\dot{\gamma}$ = 1 % (within the LVR) defined by preliminary amplitude sweep (Section 3.3.2.2). The storage, G', and loss, G" moduli were recorded as a function of the oscillation frequency (ω).

3.4 Optimisation of Electrospinning Parameters for Fabrication of 3DENS

The 3DENS were fabricated using the electrospinning unit TL-BM (Tong Li Tech, Shenzhen, China) equipped with a metal rotating drum collector SS304, a positive high voltage supply device, a negative high voltage supply device, a V shaped spinneret holder (Tong Li Tech, Shenzhen, China), and a syringe pump. The polymer solution was supplied using a Luer Lock syringe, Luer Lock soft tubing and a 21 Birmingham Gauge needle (Figure 4).

The working parameters in the electrospinning process were optimized to obtain uniform, bead free and fine fibres. To obtain smooth fibres, polymer solutions were loaded into a 10ml syringe with a stainless-steel needle with inner diameter of 0.51 mm (21 gauge) which was attached to the positive electrode. A constant amount of polymer solution was supplied at a steady flow rate. Aluminium foil was placed over the rotating cylindrical collector which was attached to the negative electrode. The needle tip to collector distance was maintained at 15 cm. Nanofibers were obtained by electrospinning at a voltage range of 13 kV – 23 kV at room temperature under atmospheric pressure. The formulations were tested to see if better fibres could be obtained by altering the voltage. Table 4 outlines the parameters that were tried.

Table 4. Electrospinning Parameters

Sample ID	Voltage (kV)	Flow Rate (ml/h)	Distance (cm)
F10a	13	0.3	15
F10b	15	0.3	15
F20a	17	0.3	15
F20b	20	0.3	15
F30a	15	0.3	15
F30b	18	0.3	15
F50a	18	0.3	15
F50b	20	0.3	15
F70a	23	0.3	15

The different parameters applied to each formulation in the electrospinning process.

A)

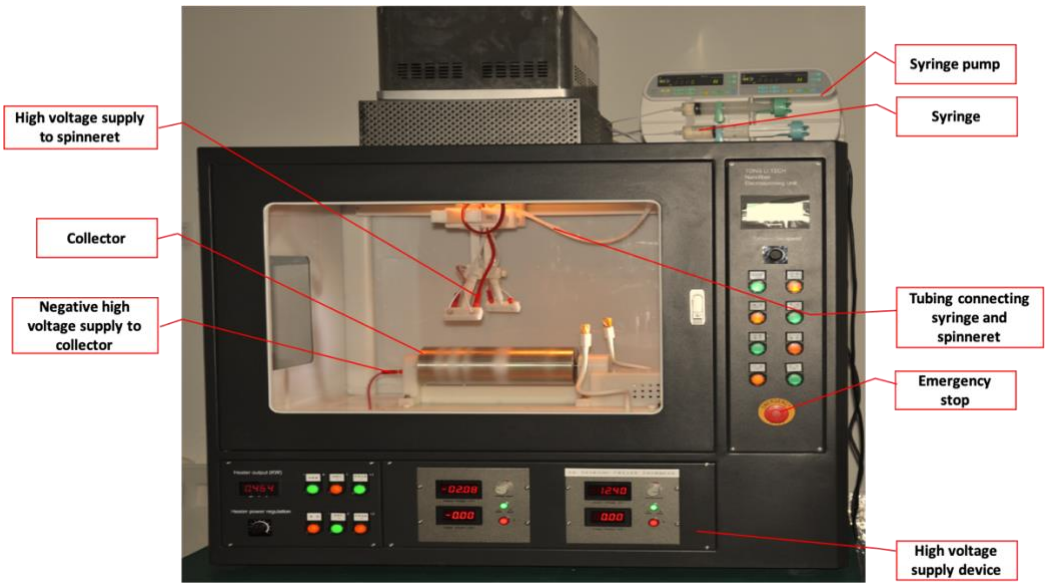

B)

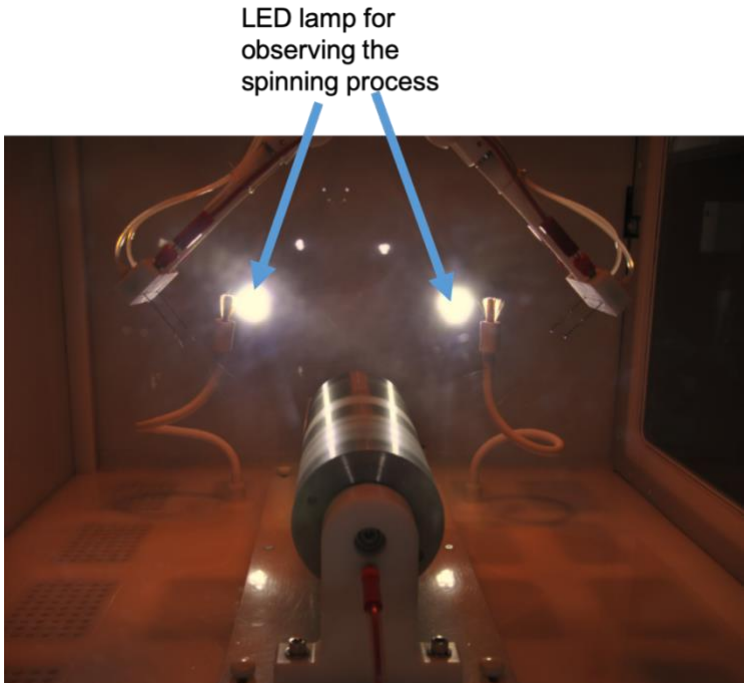

Figure 4.Electrospinning unit TL-BM (Tong Li Tech, Shenzhen, China)

The figure shows main components of the electrospinning unit (A), and side view of electrospinning unit showing LED lamps used for observing solution jets during the spinning process (B).

3.5 Crosslinking

A novel crosslinking method was utilised in the present study to thermally induce physical crosslinks in chitosan/PVA/PVP 3DENS by heating. The nanofibrous scaffolds were physically crosslinked by heating at 120°C in an oven for 24 hours.

3.6 Scanning Electron Microscopy (SEM)

In order to determine the optimal fibre morphology, SEM micrographs were used. 3DENS samples were mounted on aluminium stubs using double sided carbon tape and coated with 5 nm of gold palladium in an Emitech k575X Peltier-cooled high-resolution sputter coater (EM Technologies Ltd, Kent, England). They were viewed in a JEOL 6700F field emission scanning electron microscope (JEOL Ltd, Tokyo, Japan). Images were taken of two different field of views at 5000x and 15000x magnification.

ImageJ software (NIH, USA) was used to measure the fibre diameters from the SEM images (Schindelin 2012). A 7 x 5 grid was placed randomly on SEM micrographs and 35 diameter measurements were taken from each of the two field of views (n=70). The mean, standard deviation of the mean, minimum and maximum value are reported. A one-way ANOVA followed by a Tukeys Post Hoc test was performed using Graphpad Prism 8 software (version: 8.2.0, San Diego, CA, USA). Statistical significance was set at $p < 0.05$.

3.7 Fourier Transform Infrared Spectroscopy

Chemical characterisation of 3DENS were carried out on peeled fibrous membranes and for raw materials of chitosan, PVA and PVP powders using an Alpha II Fourier Transform Infrared Spectrometer (Broker Optik, Ettlingen, Germany) equipped with RockSolidTM interferometer, CenterGiowTM IR-Source, a single reflection Platinum-ATR monolithic diamond crystal measurement interface, and a temperature stabilised DTGS detector (MIRacle, Pike Technologies, Madison, WI, USA) (Figure 5).

The infrared spectra of the samples were calibrated to background spectra and measured over a wavelength range of 400 cm^{-1} to 4000 cm^{-1} with a resolution of 4 cm^{-1}. The final spectra were a mean of 24 scans to reduce spectral noise. Data was acquired using OPUS software (Bruker Optik, Ettlingen, Germany) and graphed using Origin software (Origin Lab Corporation).

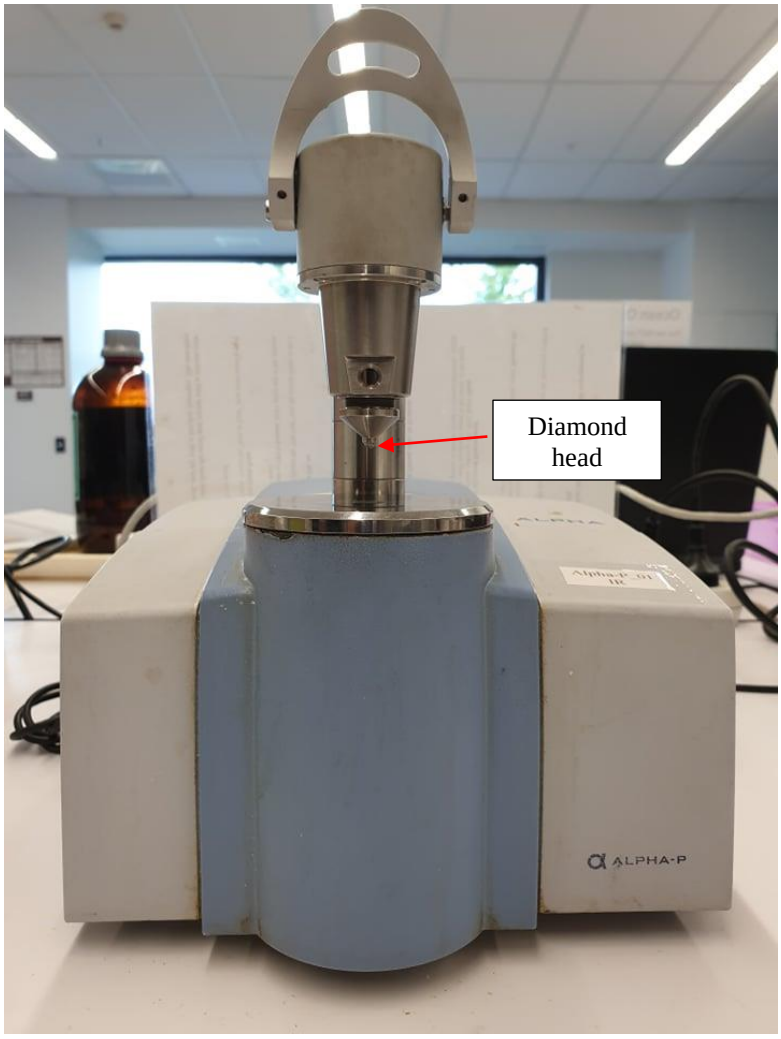

Figure 5. Alpha II Fourier Transform Infrared Spectrometer (Broker Optik, Ettlingen, Germany)

3.8 Swelling Test

Due to the hydrophilic nature of the polymers used to fabricate the scaffold, the water adsorption capacity of the nanofibrous scaffolds was determined by the swelling of the sample (Gu et al. 2009). The swelling ability of the scaffold was measured using the method described by Shavandi and others (Shavandi 2015). Firstly, a circular piece of the scaffold with a diameter of 11 mm was cut. Weight of the scaffold with foil was taken. The scaffold was removed from the foil by wetting the scaffold in phosphate buffered saline (PBS pH 7) and then carefully removed from the foil. The initial dry weight of the scaffold was calculated by subtracting the weight of the scaffold and foil by the weight of the foil only (W_d). The scaffold was then immersed in PBS in a 15 ml falcon tube and kept in a 37°C incubator for 24 hours. Then the excess PBS was removed from the sample by blotting using filter paper and weighed in wet condition (W_w). Swelling ratio was calculated according to the following equation (2):

$$Swelling\ (\%) = \frac{W_w - W_d}{W_d} \times 100$$

Equation 2. Calculation of the swelling ratio

Where W_d is the initial dry weight of the sample and W_w is the final wet weight of the sample. The experiment was replicated three times for each 3DENS sample (Gu et al. 2009).

3.9 Degradation

The degradation percentage of all samples were measured at 7 and 14 days. Weight of the scaffold with foil was taken. The scaffold was removed from the foil by wetting the scaffold in phosphate buffered saline (PBS pH 7) and then carefully removed from the foil. The initial dry weight of the scaffold was calculated by subtracting the weight of the scaffold and foil by the weight of the foil only (W_i). The scaffold was then immersed in PBS in a 15ml falcon tube and kept in a 37°C incubator for 7 and 14 days. Each 3DENS was removed and placed on a pre-weighed filter paper and dried in an oven at 50°C for 12 hours. The final weight (W_f) of the 3DENS was obtained by subtracting the weight of the filter paper from the weight of the filter paper and dried 3DENS. The degradation of the 3DENS was defined as the amount of weight lost as a percentage of initial weight. Degradation was calculated in accordance with the equation (3):

$$\text{Degradation (\%)} = \frac{Wi - Wf}{Wi} \times 100$$

Equation 3. Calculation of the rate of degradation

3.10 *In Vitro* Biological Characterisation

3.10.1 Cell Lines

This study utilised human adult low calcium, high temperature keratinocytes (HaCaT ATCC® CRL-2404), an immortalized human keratinocyte cell line, and neonatal human dermal fibroblasts from juvenile foreskin (NHDF ATCC® PCS-201-010). The Figure below shows NHDF observed using a 10X objective has a spindle shape compared to a cuboidal cell shape seen in HaCaT cells (Figure 6).

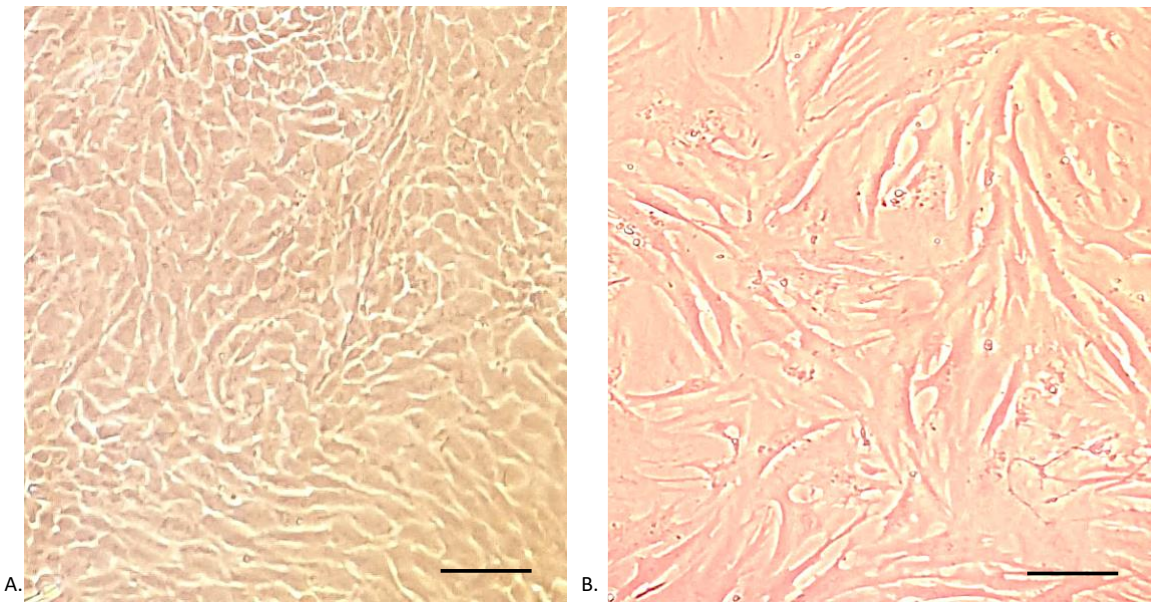

Figure 6. HaCaT and NHDF cells viewed under a microscope

The figure above shows A. HaCaT and B. NHDF cells under an inverted phase contrast microscope at 10x magnification. Scale bar represents 200µm.

3.10.2 Cell Revival

Frozen stocks of HaCaT (passage 19) and NHDF (passage 16) were removed from liquid nitrogen and warmed in a 37°C water bath for no longer then 60 seconds. All cell culture work was conducted in a HeraSafe 2030i 1.2, Class II Microbiological Safety Cabinet (ThermoFisher Scientific, Germany) which was disinfected using 70% ethanol in dH_2O followed by 15 minutes of UV sterilisation.

The thawed stock solution was transferred to a sterile $75cm_2$ culture flask and grown to 70%-90% confluence in sterile Dulbecco's Modified Eagle Medium (DMEM) supplemented with 1% Fetal Bovine Serum (FBS; Thermo Fisher, NZ) and 1% penicillin-streptomycin (Gibco, Canada). This will be referred to as complete DMEM (cDMEM). The flasks were kept in a humidified incubator with 5% CO_2 in atmosphere, maintained at 37°C. cDMEM was replaced every 3-4 days.

3.10.3 Passaging

In order to prolong the life of the cells in culture and maintain their proliferative state, passaging is done by transferring some cells from the previous culture to a fresh culture medium. The cells were passaged when they reached 70 % - 90 % confluence by trypsinization to maintain their proliferative state. The procedure was carried out by first removing existing media via suctioning. The adhered cells were rinsed with Dulbecco's PBS (DPBS; GIBCO) to remove any remaining media that can inhibit trypsin activity. Next, 4 ml of Trypsin (0.25 %) and ethylenediaminetetraacetic acid (EDTA) solution (Gibco) was added to the culture flask containing NHDF or HaCaT cells then returned to the incubator for 5 minutes or 15 minutes, respectively. At the end of the incubation period, the flasks were viewed under a binocular phase contrast microscope to confirm that the cells were suspended. Trypsin was inactivated by adding 8 ml of cDMEM. A further 20 ml of cDMEM was added to dilute the suspension. Cells were counted using Scepter™ 2.0 Handheld Automated Cell Counter (Merk Millipore) and seeded into plates as needed. The remaining cells were subcultured in cDMEM.

3.10.4 Scaffold Sterilisation

The scaffolds were cut into 9 mm diameter by hole punching. 3DENS were immersed in sterile PBS for easy removal and placed on the bottom of well plates. The plates were exposed to UV light with the lids open in HeraSafe 2030i 1.2, Class II Microbiological Safety Cabinet (ThermoFisher Scientific, Germany) at KW 254 nm LW 365 nm for 30 minutes to sterilise. Ethanol was investigated for sterilizing but was not used due to a visually observable change in morphology in the 3DNES when treated with ethanol.

3.10.5 Cell Viability Assay

To determine cell viability within the 3DENS, cell-scaffold constructs were stained using the live/dead cell viability/cytotoxicity assay. Calcein blue acetoxymethyl ester powder (calcein blue AM, CB; CAS no.: 54375-47-2, Sigma–Aldrich, USA) and propidium iodide (PI, 1.5 mM stock solution in PBS; Cat no.: 421301, BioLegend, San Diego, CA, USA) were used for fluorescence microscopy. Sterilized 3DENS were placed at the bottom of the well on a cover slip. A glass cover slip without any 3DENS was used as the control.

Cells (5 x 10_3 /ml) were seeded into each well containing scaffold and a control well and supplemented with 1 ml of cDMEM. Experiment was performed in triplicate (n=3). All work was done in HeraSafe 2030i 1.2, Class II Microbiological Safety Cabinet.

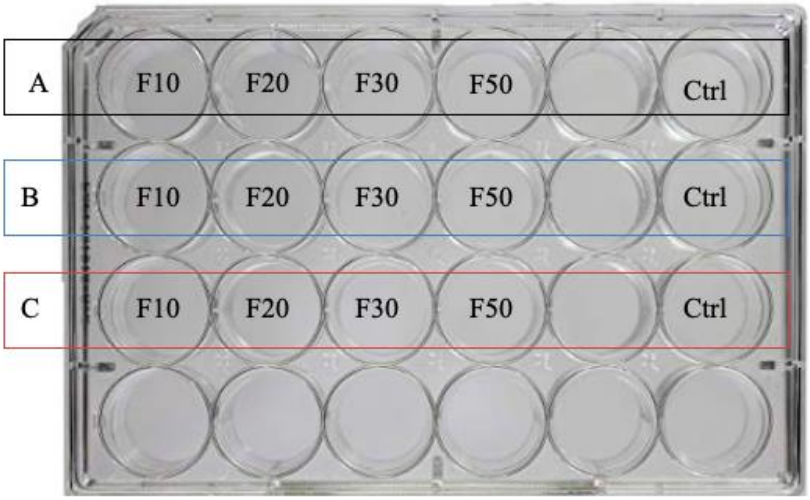

Figure 7. 24-well plate layout for Live/Dead cell assay

The figure showed the plate layout used to seed cells for Live/dead cell assay.

Cell viability of HaCaT (passage 20) and NHDF (passage 17) cells were measured separately at 24, 48 and 72 hours for all 3DENS. All plates were organised in the same manner as shown in Figure 7.

Assay solution was prepared for each plate by pipetting 1.5µL calcein AM (Molecular Probes/Invitrogen #C3099) and 6 µL PI (Molecular Probes #P-3566) into 1 ml of DPBS. First the culture media was removed from each well and discarded. Approximately 30 µL of assay solution was added to the wells, ensuring the scaffold was completely covered. The glass cover slip with the scaffold was then removed carefully from the bottom of the well and placed scaffold side down onto a glass slide for viewing under BX51 microscope with a

fluorescent attachment (Olympus Corp., NY, USA) and images were captured using Olympus cellSens imaging Software (Life Science Solutions). Live cells were indicated by green fluorescence (excitation 528 nm, emission 617 nm) as calcein stains the intact cell membrane, and, dead cells were indicated by red fluorescence (excitation 528 nm, emission 617 nm) as PI stains the cell nuclei. For quantitative analysis, cell counts were performed using three random field of views per 3DENS and control using 4x objective for each time point. The cell viability for each image was calculated according to the following equation:

$$\text{Cell Viability (\%)} = \frac{\text{Number of Live Cells}}{\text{Total Cell Number}} \times 100$$

Equation 4. Calculation of cell viability

3.10.6 Proliferation MTT Assay

Methylthiazolyldiphenyl-tetrazolium bromide (MTT) was obtained from Sigma Aldrich. This assay can quantify the number of viable cells in a sample by relying on the conversion of tetrazolium salt into a formazan product by dehydrogenases present in metabolically active cells. The insoluble formazan has a purple colour (Figure 8) which can be solubilised to form a coloured solution that can then be quantified by reading the absorbance of the media on a spectrometer. Cell number can be calculated by reference to a standard curve.

Cell proliferation was assessed for crosslinked and uncrosslinked samples using HaCaT (passage 21) and NHDF (passage 18) cell lines at 24, 48 and 72 hours. Sterile scaffolds were placed in the bottom of 48-well plates and organised as shown in Figure 5. The experiment was done in triplicate and repeated twice (n=6). All work was done in HeraSafe 2030i 1.2, Class II Microbiological Safety Cabinet.

Cells (5 x 10^3 /ml) were plated on to each well containing scaffold and a control well (without a scaffold and cells, i.e. media only) and supplemented with 0.5 ml of complete DMEM. Wells containing 80 x 10^3, 40 x 10^3, 20 x 10^3, 10 x 10^3, 5 x 10^3, 2.5 x 10^3 cells/ml were plated to create a standard curve. These were also supplemented with cDMEM and were plated in duplicate. Control wells (blanks) contained cDMEM without any cells, and were also plated in duplicate. The plates were organised as shown in Figure 9 for all time points.

MTT (12 mM) stock solution was prepared by adding 1ml of sterile PBS to 5mg of MTT and vortexed until dissolved. MTT solution was wrapped with aluminium foil to protect it from light and kept in 4°C. Stock solution of 10% sodium dodecyl sulphate (SDS) and 1M hydrochloric acid (HCl) in ultrapure MilliQ water was also prepared. To count the cells after the incubation period, assay solutions was prepared by mixing MTT solution in colour free media at a ratio of 1:5 (MTT solution: media). The cDMEM media was removed from each well and 200µL of the assay solution was added to each well and the plate was incubated for 4 hours. During incubation, acidified SDS was prepared by mixing 10 µL of HCl per 1ml of SDS and kept at room temperature. At the end of the 4-hour incubation of the cells in MTT containing assay solution, 100 µL of acidified SDS was added to each well and left in the incubator overnight. The next day, each well was mixed thoroughly and 100 µL of solution from each well was transferred to a 96-well plate for reading in a spectrometer at 570 nm absorbance. Graphpad Prism 8 software (version: 8.2.0, San Diego, CA, USA) was used to plot the unknown cell numbers against the known standard curve.

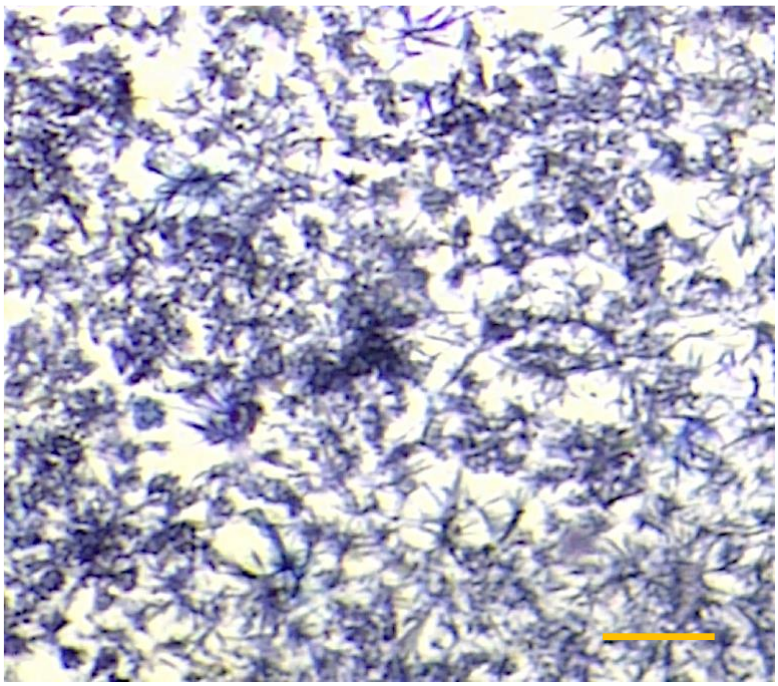

Figure 8. MTT stained live cells forming crystals

The image shows purple staining produced by presence of formazan formed by conversion of tetrazolium salt into formazan by dehydrogenases present in metabolically active cells. The scale bar represents 200 µm.

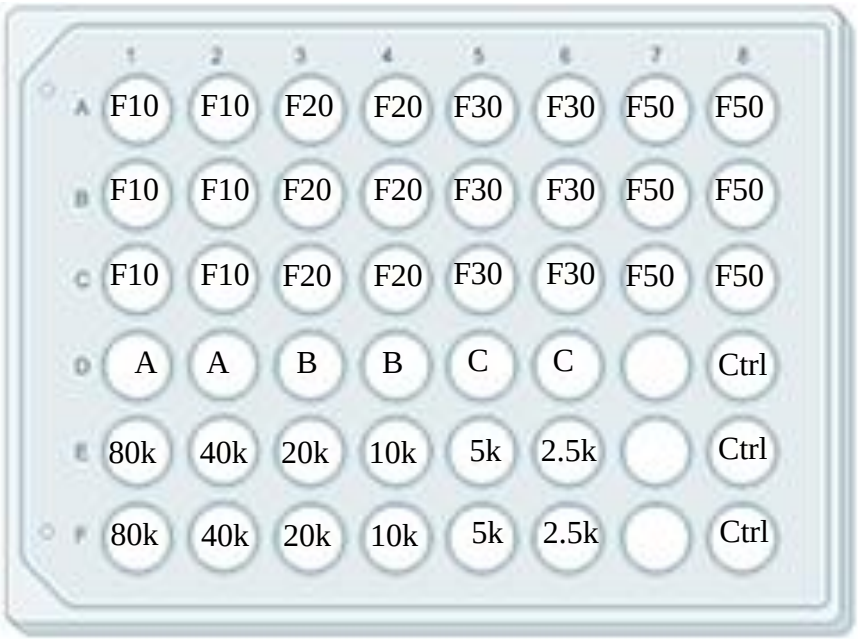

Figure 9. MTT assay plate set

The figure showed the plate layout used to seed cells for MTT cell assay.

3.11 Statistical Analysis

For experiments comparing more than three groups or more, the one-way ANOVA was used with a Tukey post hoc analysis. For experiments comparing the two groups of crosslinked versus uncrosslinked, the paired or unpaired t-test was employed. A p-value of < 0.05 was considered as statistically significant. All conditions were done in at least triplicates. All results were expressed as mean ± SEM. Graphpad Prism 8 software (version: 8.2.0, San Diego, CA, USA) was used for statistical analysis and graph generation.

4.0 Results

4.1 pH and Conductivity

The pH and conductivity values of each of the formulation solutions are listed in Table 5. All three polymer solutions were in the acidic pH range (pH < 7). Chitosan had the lowest pH at 3.88, followed by PVP at 4.58 and PVA having the highest pH at 5.86. The pH of blend formulations decreased from F10 to F70 (4.35, 4.25, 4.16, 4.03, and 3.96, respectively)

Chitosan had the highest conductivity (3962 μS/cm), followed by PVA (566 μS/cm) and PVP had the lowest (116 μS/cm). As the percentage of chitosan increased in the blend formulations (F10 to F70), the conductivity of the polymer solution also increased (752 μS/cm, 938 μS/cm, 1165 μS/cm, 1733 μS/cm, and 3926 μS/cm, respectively).

4.2 Viscosity

The graphs in Figure 10 represent viscosity as a function of shear rate ($\dot{\gamma}$ for solutions of chitosan (A), PVA (B), PVP (C), F10 (D), F20 (E), F30 (F), F50 (G) and F70 (H) at 20° C. For all the polymer solutions, viscosity decreased as shear rate increase. This is characteristic of shear-thinning behaviour (figure 3).

Viscosity of a shear- thinning fluid is shear dependence hence, the apparent viscosity (η_a) of each sample at a shear rate ($\dot{\gamma}$) of 200/s is reported in Table 5 in centipoise (1 mPas = 1 cP). PVA and PVP solutions had similar viscosities (η ($\dot{\gamma}$ = 200/s) = 190 cP and 200 cP, respectively). Chitosan had the lowest viscosity, η ($\dot{\gamma}$ = 200/s) = 140 cP.

Table 5. Composition and physical properties of polymer

Formulation	**2% Chitosan sol**	**10% PVA sol**	**10% PVP sol**	**Total Solute Concentration**	**pH**	**Conductivity (µS/cm)**	**Viscosity[1] (η_a) (cP)**
F10	10%	80%	10%		4.35 ± 0.08	725 ± 38	230
Dry weight ratio	2	87	11	9.2%			
F20	20%	70%	10%		4.25 ± 0.07	938 ± 70	230
Dry weight ratio	5	83	12	8.4%			
F30	30%	60%	10%		4.16 ± 0.07	1165 ± 94	220
Dry weight ratio	8	79	13	7.6%			
F50	50%	40%	10%		4.03 ± 0.13	1733 ± 144	210
Dry weight ratio	17	66	17	6%			
F70	70%	20%	10%		3.96 ± 0.12	3962 ± 190	200
Dry weight ratio	32	45	23	4.4%			

Chitosan	100%	-	-		3.88 ± 0.14	3962 ± 416	140
Dry weight ratio	100			2%			
PVA	-	100%	-		5.86 ± 0.01	566 ± 24	190
Dry weight ratio		100		10%			
PVP	-	-	100%		4.58 ± 0.11	116 ±15	200
Dry weight ratio			100	10%			

The table above outlines the components of blend formulations F10 to F70 and reports values of pH, conductivity and viscosity of all polymer solutions including pure chitosan, PVA and PVP (n=3).[1]The viscosity reported here is apparent viscosity (η_a) at shear rate of $\dot{\gamma}$ =200/s.

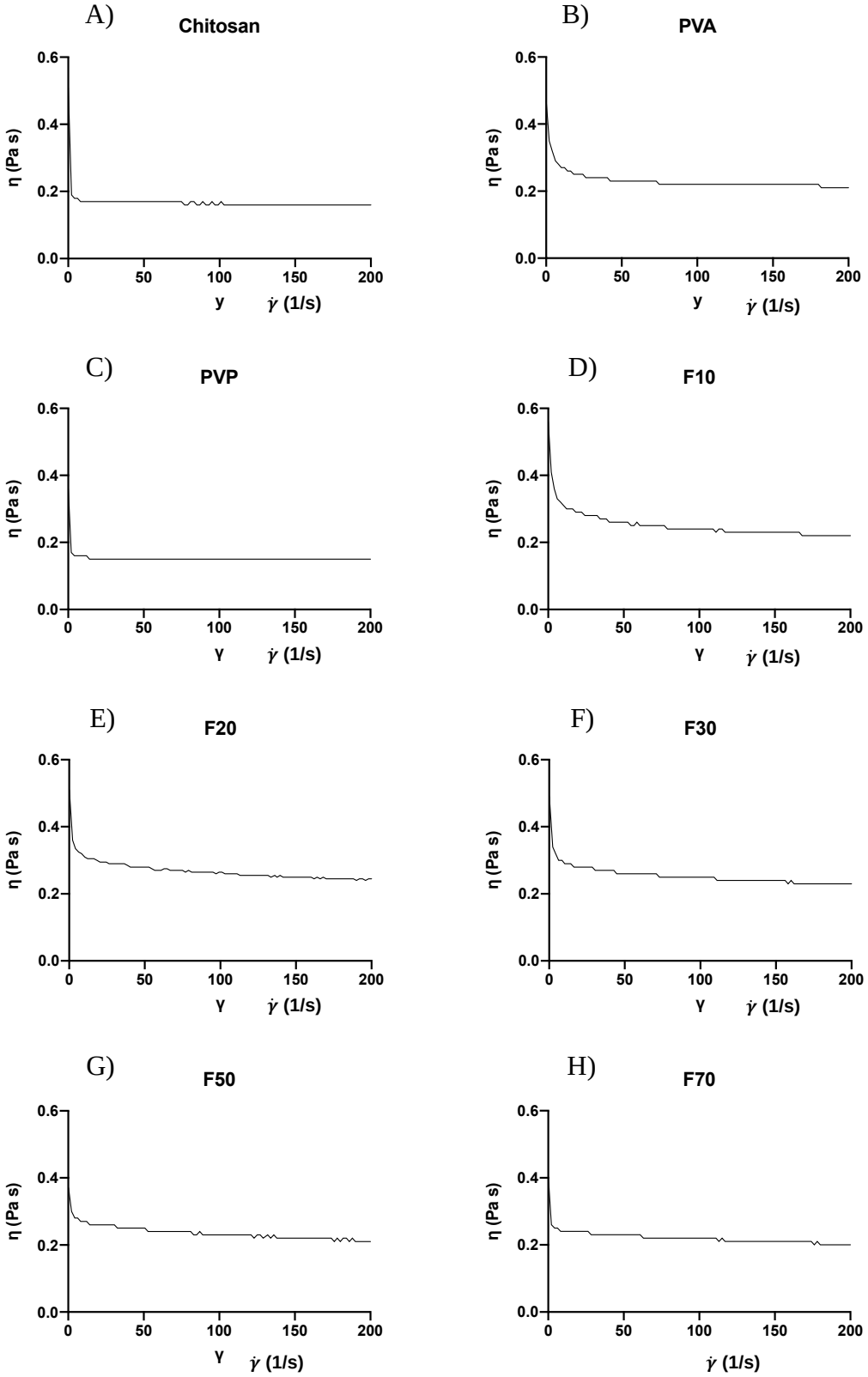

Figure 10. Viscosity curves of polymer solutions

The graphs above represent viscosity as a function of shear rate ($\dot{\gamma}$) for solutions of chitosan (A), PVA (B), PVP (C), F10 (D), F20 (E), F30 (F), F50 (G) and F70 (H) at 20 °C (n=3).

4.3 Viscoelastic Properties

4.3.1 Oscillatory Amplitude Sweep

The results of the amplitude sweep are shown in Figure 11**.** The samples are not within the LVR at frequencies above 10 Hz.

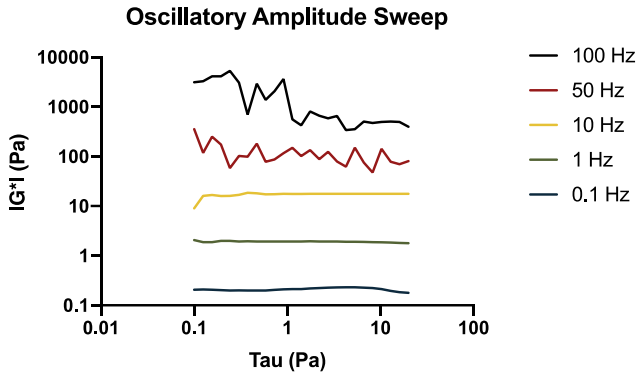

Figure 11. Amplitude sweep

X and y values are in log 10 scale.

4.3.2 Oscillatory Frequency Sweep

A frequency sweep study was performed to determine G', and G" as a function of frequency (ω) at a fixed temperature of 20°C. The storage modulus (G') represents the elastic/solid behaviour of a sample and measures the amount of deformation energy stored in the sample during shearing. On the other hand, the loss modulus (G"), represents the viscous/fluid behaviour of a sample and measures the amount of deformation energy used up in the sample during shearing (Mezger 2006). $G' > G''$ demonstrates behaviour that is more elastic or solid while $G'' > G'$ demonstrates viscous or more liquid behaviour (Tabilo-Munizaga and Barbosa-Cánovas 2005).

The dependence of storage G' and loss G" modulus on the angular frequency are shown in Figure 12 for solutions of chitosan (A), PVA (B), PVP (C), F10 (D), F20 (E), F30 (F), F50 (G) and F70 (H) at 20° C. For chitosan, PVP, F10, F20, F30, and F50 solutions, the stronger dependence of G' on frequency and higher loss modulus (G") indicates that the polymer solution is a viscous fluid with weak networks (Figure 11, A and C-H). On the other hand, PVA, behaved as a structured fluid characterised by having a higher storage modulus than loss modulus (G'> G") as can be observed in Figure 11, B (Bercea et al. 2020).

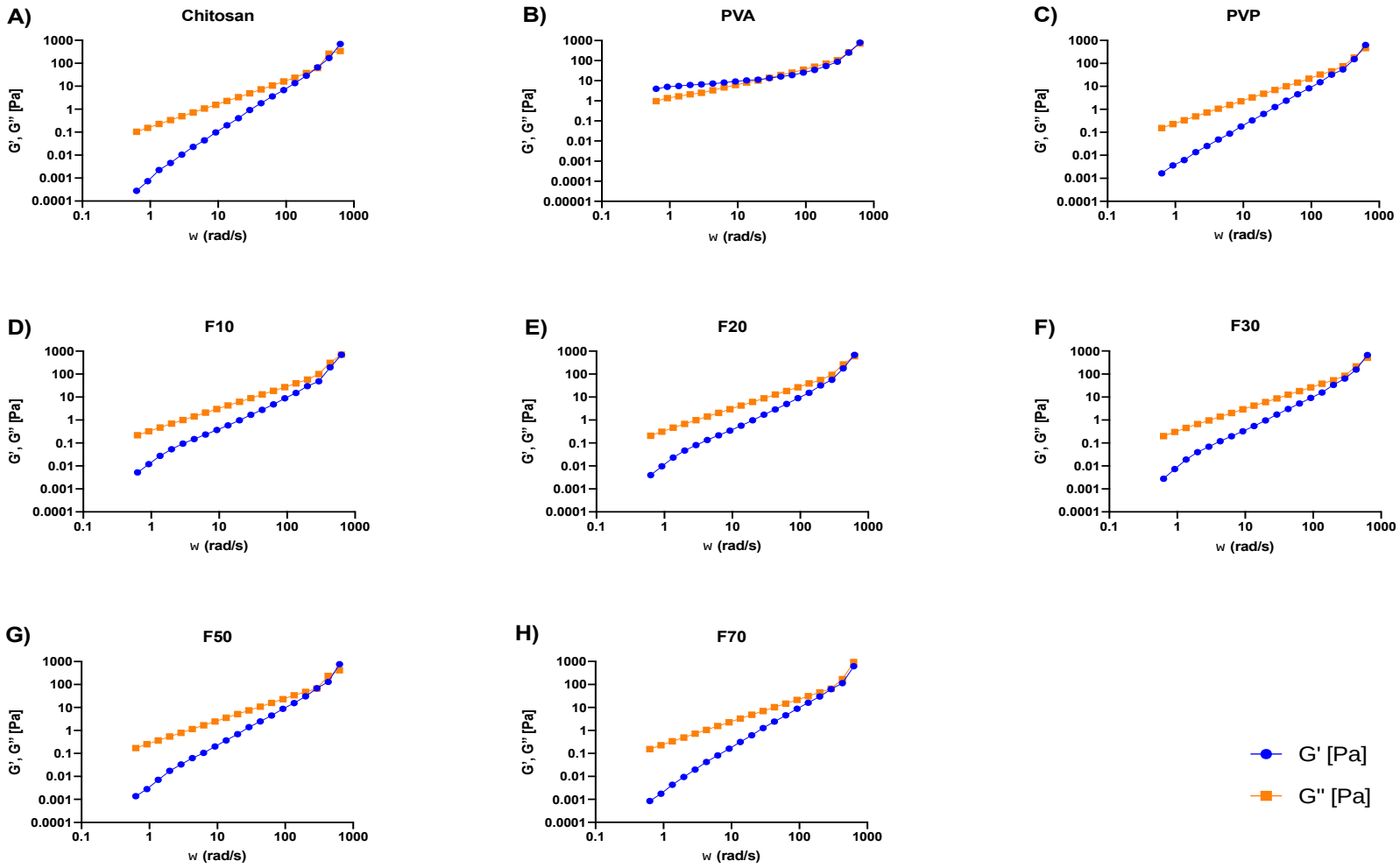

Figure 12. Graph of G', G" plotted against omega

The storage (G') and loss (G") modulus as a function of frequency (ω) is plotted for chitosan (A), PVA (B), PVP (C), F10 (D), F20 (E), F30 (F), F50 (G), and F70 (H). The x and y axis are represented in log (10) scale. (n=3)

4.4 Surface Morphology (SEM)

SEM micrographs were used to evaluate the fibres produced by electrospinning at a flow rate of 0.3ml/hour with needle tip to collector distance maintained at 15 cm for each formulation at voltages ranging from 13 kV to 23 kV and are presented in Figure 13. The specific electrospinning parameters applied to each formulation have been outlined previously (Table 4). The best processing parameters are outlined in Table 6 below.

Table 6. Best processing parameters

Formulation	Voltage (kV)	Flow rate (ml/h)	Distance (cm)
F10	15	0.3	15
F20	17	0.3	15
F30	18	0.3	15
F50	18	0.3	15

kV= Kilovolts

As seen from the micrograph of synthesised nanofibers, formulation F10 produced at a voltage of 15 kV using flow rate of 0.3 ml/h, 15 cm away from the collector (Figure 12. F10b) formed linear and bead free fibres.

For F20, fibres produced using 15 kV and 17 kV look similar under SEM therefore the lower voltage was used to produce the final scaffold (Figure 12 F20a and F20b). F20 fibres are not linear and have a small amount of spindle shaped beading but thinner fibres were produced. F30 and F50 scaffold were also not linear and had an increasing number of beads with the beads getting rounder in shape, however, the fibres became thinner (Figure 12, F30a to F50b). A voltage of 18 kV was selected for spinning the final scaffold for formulation F30 and F50 as the fibres in SEM images look similar compared to the higher voltage tried.

SEM image of F70a (Figure 12) showed that spraying had occurred rather than the production of a continuous jet, which resulted in polymer deposition as a powder rather than a fibre on the collector. F70 was excluded from further studies due to its inability to form a fibre.

F10a)

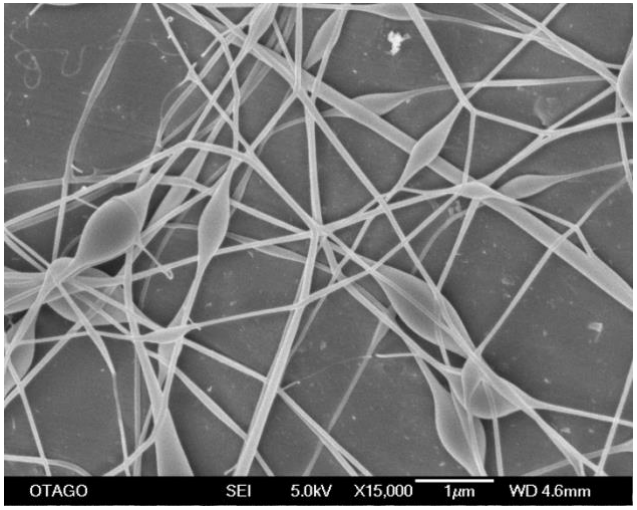

F10b)

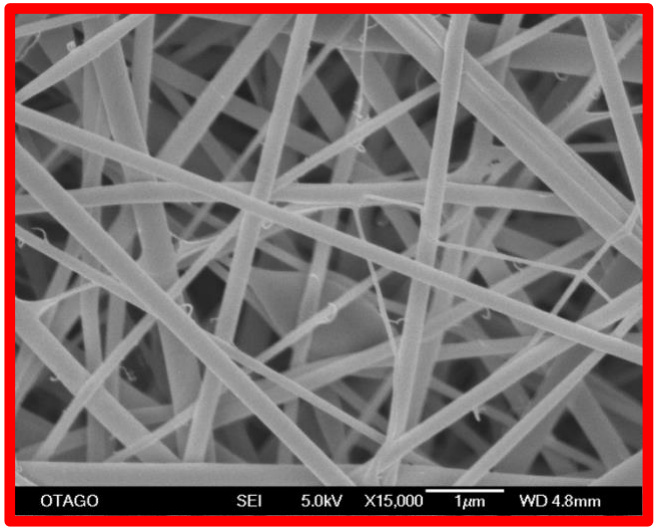

F20a)

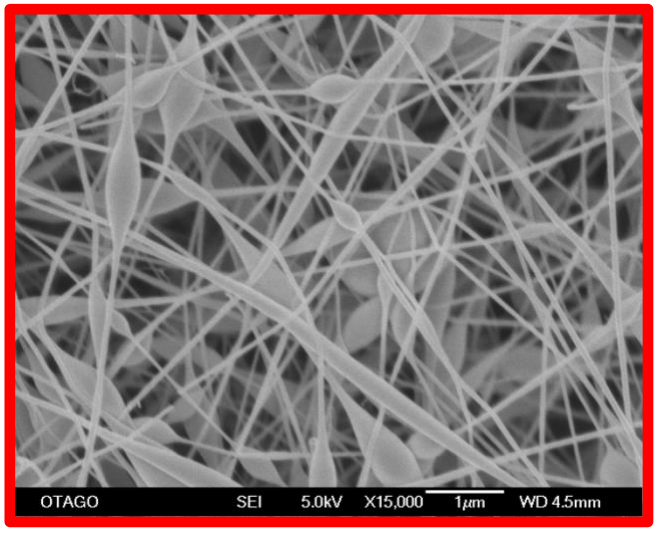

F20b)

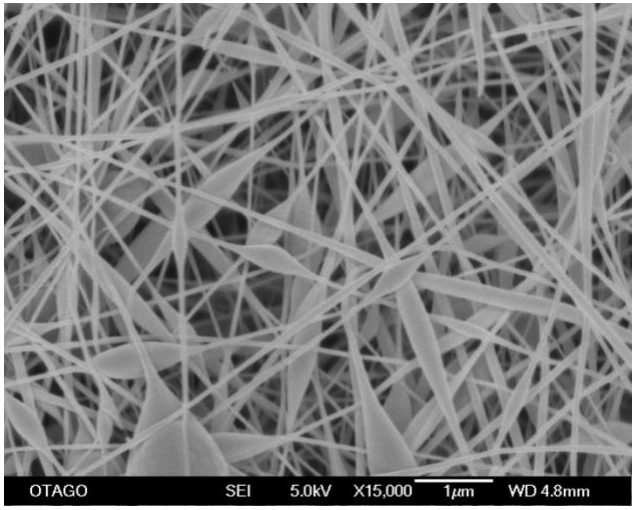

F30a)

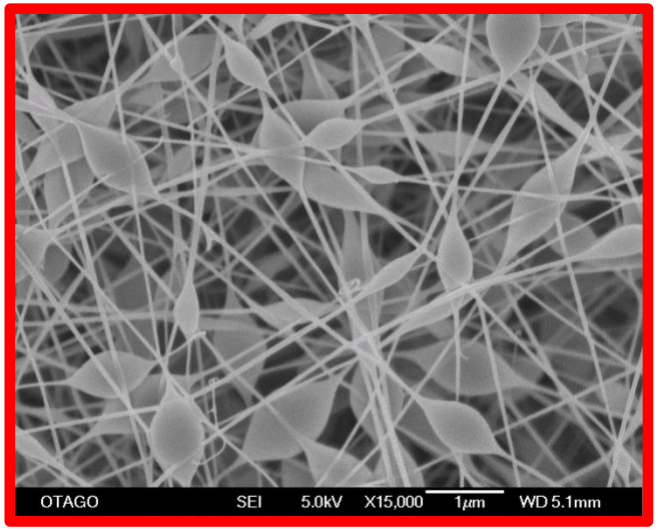

F30b)

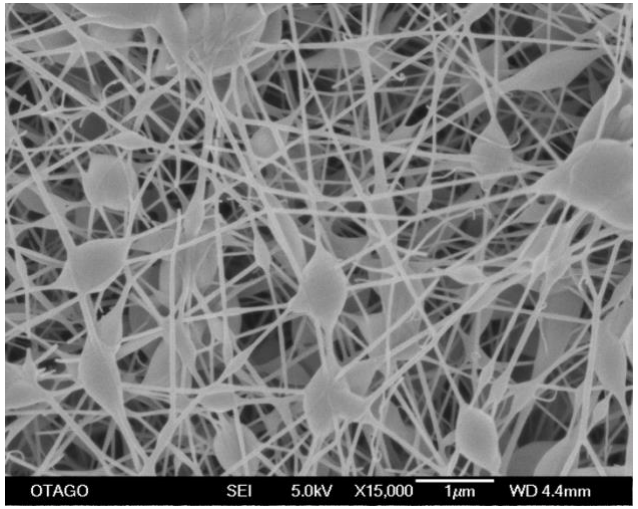

F50a)

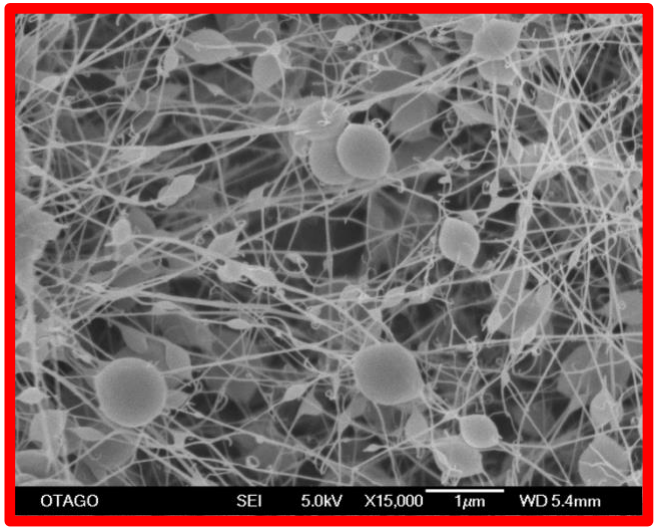

F50b)

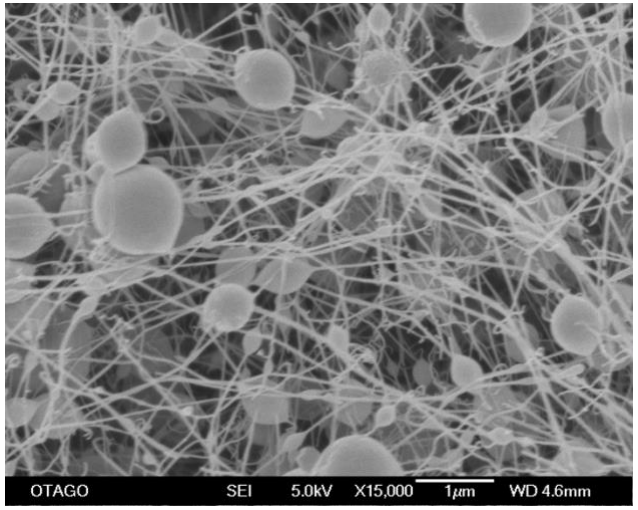

F70a)

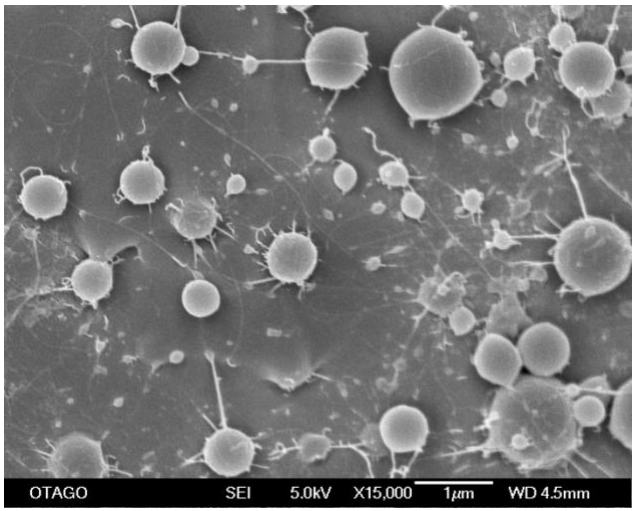

Figure 13. SEM images x15000 magnification

SEM Images of Formulations 1- 4 electrospun at a flow rate of 0.3 ml/h from a distance of 15 cm from the tip to the collector at varying voltages. Minimum voltage required to produce a polymer jet was used. Images outlined in red represented the best observed fibre morphology and their corresponding processing parameters were used for fabrication of final 3DENS.

4.5 Fibre Diameter

In order to calculate fibre diameter for each of the different 3DENS formulations, 35 fibre diameters were measured randomly from SEM images of two different field of views for each 3DENS at 15000x magnification using ImageJ software. The mean, standard deviation of the mean, and the range of the 70 measurements are reported in Table 7.

A one-way ANOVA followed by a Tukey's multiple comparisons test was carried out using prism software for all 3DENS formulation diameters ($p<0.0001$). Overall, the fibre diameter decreased from F10 to F50. A t-test was used to compare the mean of each 3DENS fibre diameter to the others. The fibre diameter of F10 was significantly smaller than all other 3DENS (221 ηm, $p < 0.0001$). Fibre diameter of F20 was significantly larger than F50 (86 ηm and 53 ηm, respectively, $p = 0.0024$) but not from F30 (72 ηm, $p=0.43$). The difference between the diameters of F30 and F50 fibres were not found to be statistically significant (72 ηm and 53 ηm, respectively, $p = 0.17$). Out of all the formulations, fibre diameter distribution is comparatively very narrow for F30 (41 ηm- 131 ηm). A wide fibre diameter distribution was observed for F10 (81 ηm-415 ηm) and for F50 (17 ηm -410 ηm).

Table 7. Fibre diameter of 3DENS

	F10	**F20**	**F30**	**F50**
Mean	221	86	72	53
SD	78	80	18	63
MIN	81	48	41	17
MAX	415	228	131	410
	334	180	90	393

All measurements are in ηm, n=70.

4.5 FTIR

The FTIR spectra of 3DENS of chitosan, PVA, PVP, and the blend of chitosan/PVA/PVP for the different formulations were obtained and the results are shown in Figure 14. In the PVA spectrum, a weak broad transmittance at 3282cm^{-1} on the spectra can be assigned to the O-H stretching vibration of hydroxyl group of PVA (Subramanian et al. 2014). The peak occurring at 2938cm^{-1} corresponds to the C-H vibration (alkyl groups) and the band corresponding to CH_2 asymmetric stretching (methylene group) vibration occurs at 2907cm^{-1} (Subramanian et al. 2014). The bending, wagging of CH_2 vibrations are at 1235cm^{-1} and 1416 cm^{-1} (Subramanian et al. 2014). C-O stretching of acetyl groups present on the PVA backbone corresponds to the sharp band at 1089cm^{-1} (Subramanian et al. 2014).

The infrared spectrum of PVP is characterised by strong C=O transmission peak from amide group of PVP at 1645 cm^{-1}. C-N group appeared at 1227 cm^{-1}. Peaks observed at 1423 cm^{-1} and 2950 cm^{-1} correspond to .C-H stretching and bending vibrations (Subramanian et al. 2014).

Characteristic transmittance bands for chitosan can be assigned to 1645 cm^{-1} corresponding to C=O (amide-I) stretching vibration and 1590 cm^{-1} corresponding to a combination of C-N stretching and N-H bending (amide II) vibrations (Costa-Júnior, Pereira, and Mansur 2009).

The characteristics peaks of pure materials as listed above are present in the 3DENS of different formulations. The shifts in the IR peaks are characterised for each 3DENS in Table 8. The observed broad band around 3278 cm^{-1} – 3292 cm^{-1} in the 3DENS is attributed to OH stretching vibrations of PVA+PVP in the formulations. The stretching vibration of C=O of PVP is responsible for the strong band at 1655 cm^{-1} – 1658 cm^{-1} in the 3DENS. The strong band at 1082 cm^{-1} – 1091 cm^{-1} is assigned to the characteristic C-O stretching of PVA influenced by hydrogen bonding along with C-H and O-H bending (Subramanian et al. 2014).

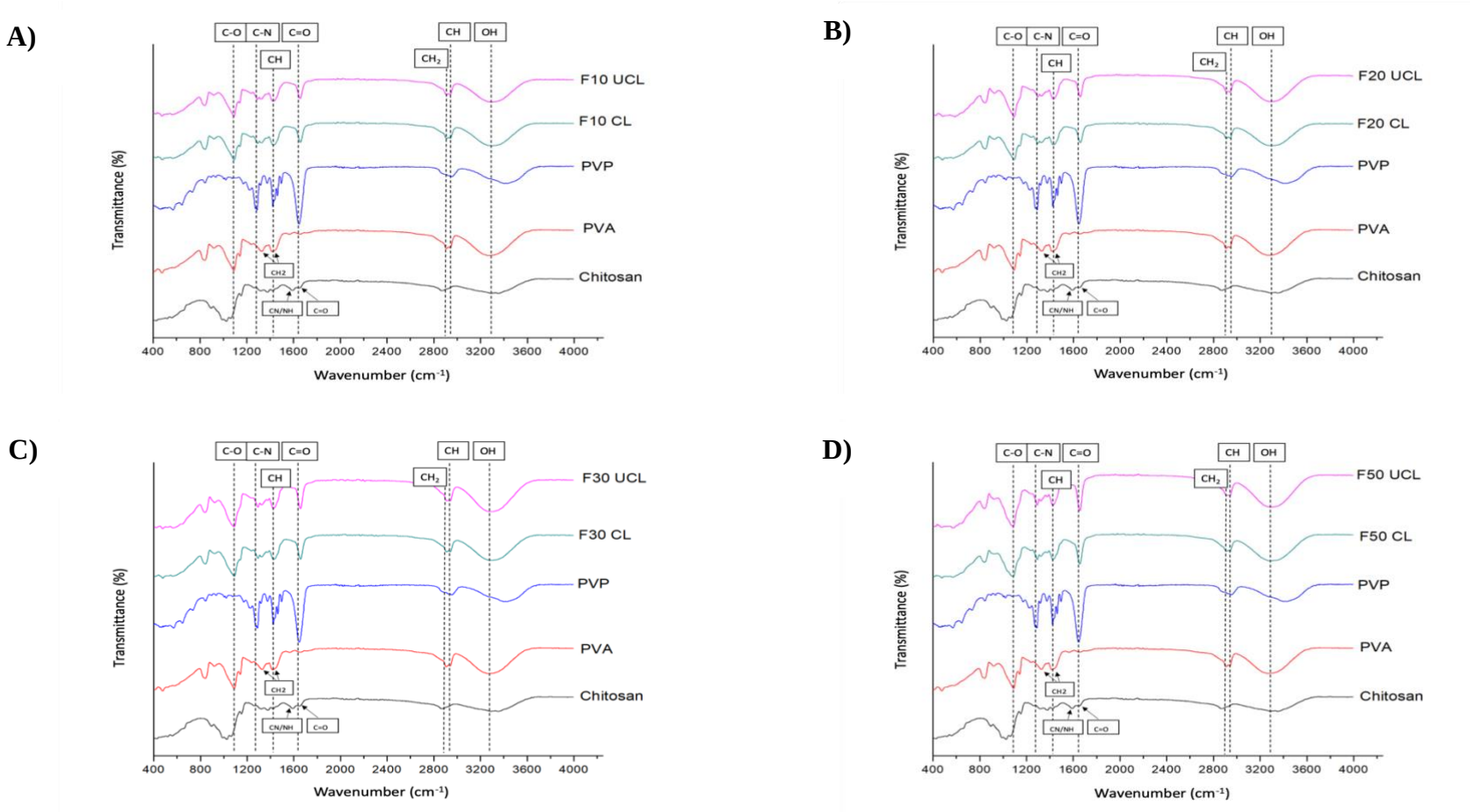

Figure 14. FTIR spectra graphs of F10, F20, F30 and F50

The graphs show FTIR spectra for F10 (A), F20 (B), F30 (C) AND F50 (D) along with FTIR spectra of chitosan, PVA, and PVP.

Table 8. The characteristic IR peaks and their assignments to varying formulations of 3DENS

3DENS	Peak wavenumber (cm^{-1})	Assignments
F10 UCL	3292	O-H stretching
F20 CL, F30 CL, F50 UCL	3288	
F10 UCL, F30 UCL	3286	
F20 UCL	3282	
F50 UCL	3278	
F10 CL, F20 UCL, F20 CL, F30 CL, F50 CL	2940	C-H vibration
F10 UCL, F30 UCL, F50 UCL	2938	
F10 UCL, F20 UCL, F30 UCL, F50 UCL, F50 CL	2911	CH_2 stretching
F10 CL, F20 CL, F30 CL	2909	
F10 UCL, F10 CL, F20 UCL, F20 CL	1658	C=O stretching and N-H bending
F30 UCL, F30 CL, F50 UCL, F50 CL	1655	
F10 CL, F20 UCL, F20 CL, F50 CL	1425	C-H bending
F10 UCL, F30 UCL, F30 CL, F50 UCL	1423	
F10 UCL, F10 CL, F20 UCL, F30 UCL, F50 UCL	1237	C-N stretching
F20 CL, F30 CL	1235	
F50 CL	1231	
F10 CL, F20 CL	1091	C-O stretching
F10 UCL, F20 UCL, F30 UCL, F30 CL, F50 UCL	1089	
F50 CL	1082	

4.7 Degradation at Day 7 and Day 14

The degradation rate of crosslinked and uncrosslinked 3DENS were measured at day 7 and day 14. Figure 15 shows photographs of all samples immersed in PBS on day 7. The increasing delicacy of the scaffolds from F10 to F50 in both the crosslinked and uncrosslinked samples can be observed from the images in Figure 15; F50 CL, F30 UCL and F50 UCL samples appear as feathers floating in the PBS. Another important observation that can be made from these images are the yellow colour of the crosslinked scaffolds compared to the white colour of the uncrosslinked 3DENS.

The rate of degradation of the various 3DENS as a percentage of initial weight at day 7 and 14 of the experiment is represented by the graphs in Figure 16.

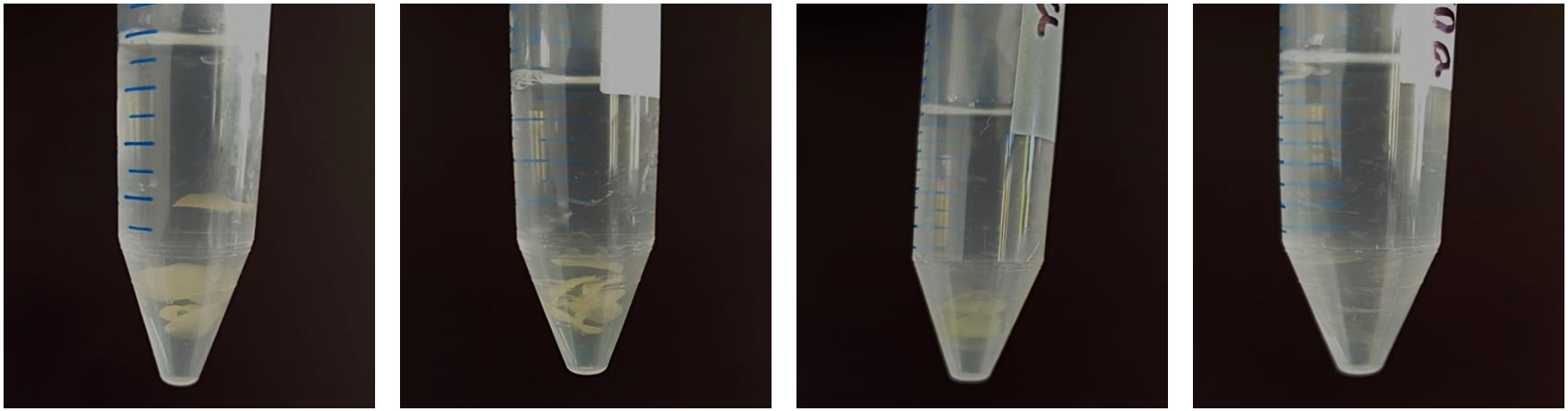

A) F10-CL B) F20-CL C) F30-CL D) F50-CL

E) F10-UCL F) F20-UCL G) F30-UCL H) F50-UCL

Figure 15. Degradation of 3DNES at day 7 in PBS at 37 °C

The figure shows images taken of uncrosslinked and crosslinked 3DENS immersed in PBS (pH 7.4) after 7 days of incubation at 37 °C.

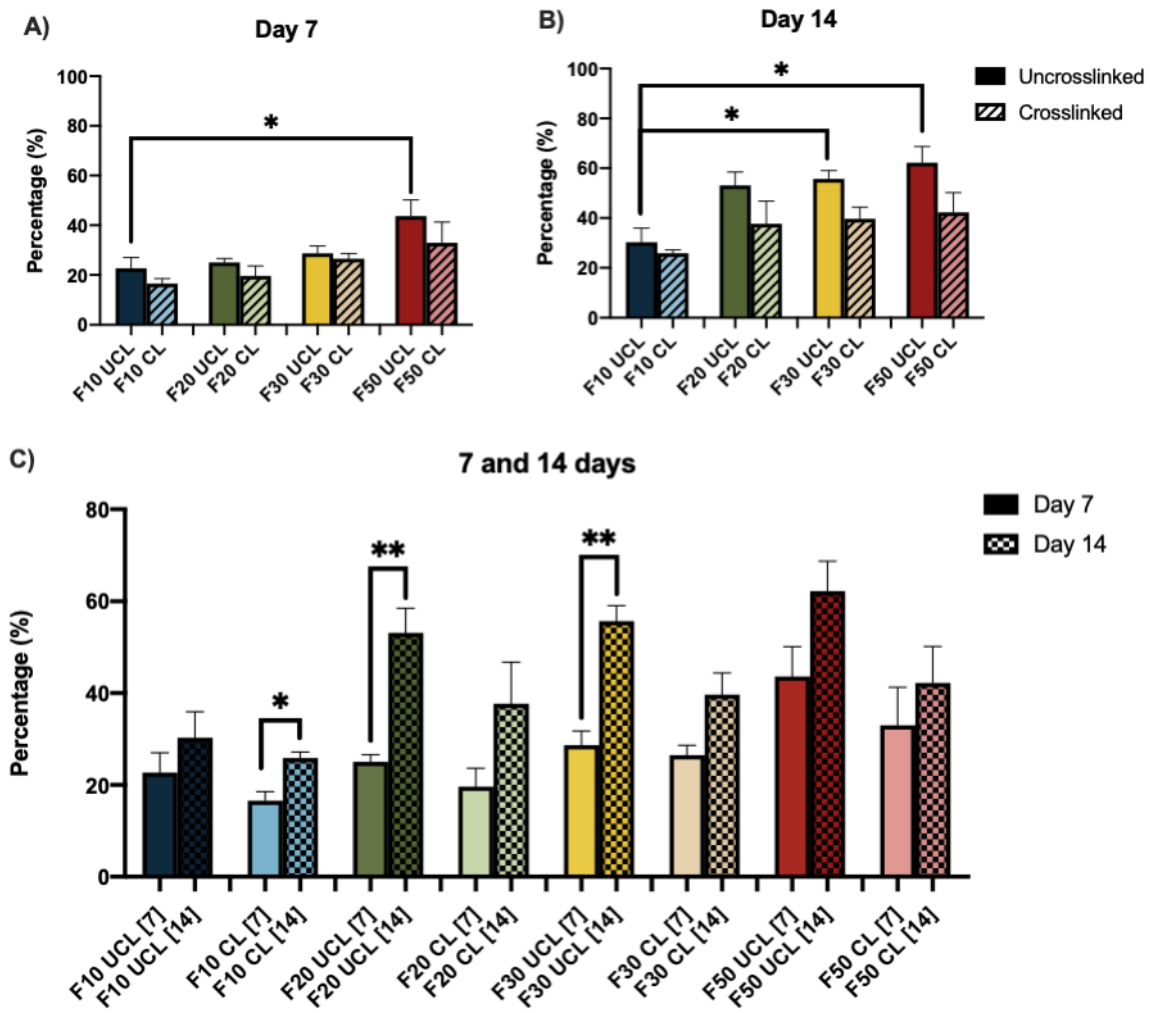

Figure 16. Degradation profiles of 3DENS in PBS (pH=7.4) at 37º C

The Figure shows the percentage of weight lost after 7 days for each UCL and CL 3DENS samples (A), percentage of weight lost after 14 days for all UCL and CL 3DENS samples (B) and compares the percentage of weight lost at day 7 and day 14 for each of the 3DENS. (<0.05, **<0.005, n=3)*

The one-way ANOVA showed that F50 UCL degraded significantly faster than F10 UCL (p = 0.03) at day 7 however, no significant differences were seen between CL 3DENS (p = 0.15) (Figure 16 A). By day 14, F30 UCL and F50 UCL showed a higher degradation rate than F10 UCL (p = 0.01) (Figure 16 B). CL 3DENS showed no significant differences between formulations at day 14 (p = 0.36) (Figure 16 B).

Figure 15 C compares degradation at day 7 and 14 for each 3DENS. A one-way ANOVA is not suitable for comparing two samples so T tests were done to compare degradation at day 7 to day 14 for all UCL and CL 3DENS. The results showed that the increase in

degradation rate on day 14 was not significantly higher than day 7 for F10 UCL (p = 0.35), F20 CL (p = 0.14), F30 CL (p = 0.06), F50 UCL (p = 0.11) and F50 CL (p = 0.47). 3DENS degraded significantly more at day 14 compared to day 7 for formulation F10 CL (p = 0.02), F20 UCL (p = 0.007), and F30 UCL (p = 0.004).

4.8 Swelling

Figure 17 shows the swelling rate of F10 UCL, F10 CL, F20 UCL, F20 CL AND F30 CL in PBS at 37°C. It was not possible to obtain swelling data for samples F10 UCL, F10 CL, F20 UCL, F20 CL and F30 CL due to the samples being too delicate to handle when wet in order to get an accurate reading as seen in (Figure 15).

The one-way ANOVA showed no significant differences between F10 CL, F20 CL, and F30 CL (p = 0.11). A one-way ANOVA is not suitable for comparing two samples therefore a T-test was used to compare F10 UCL and F20 UCL; no differences were found (p = 0.79). T-tests confirmed that crosslinked 3DENS held significantly higher adsorption compared to uncrosslinked 3DENS in F10 and F20 formulations (p = 0.26 and p = 0.026, respectively).

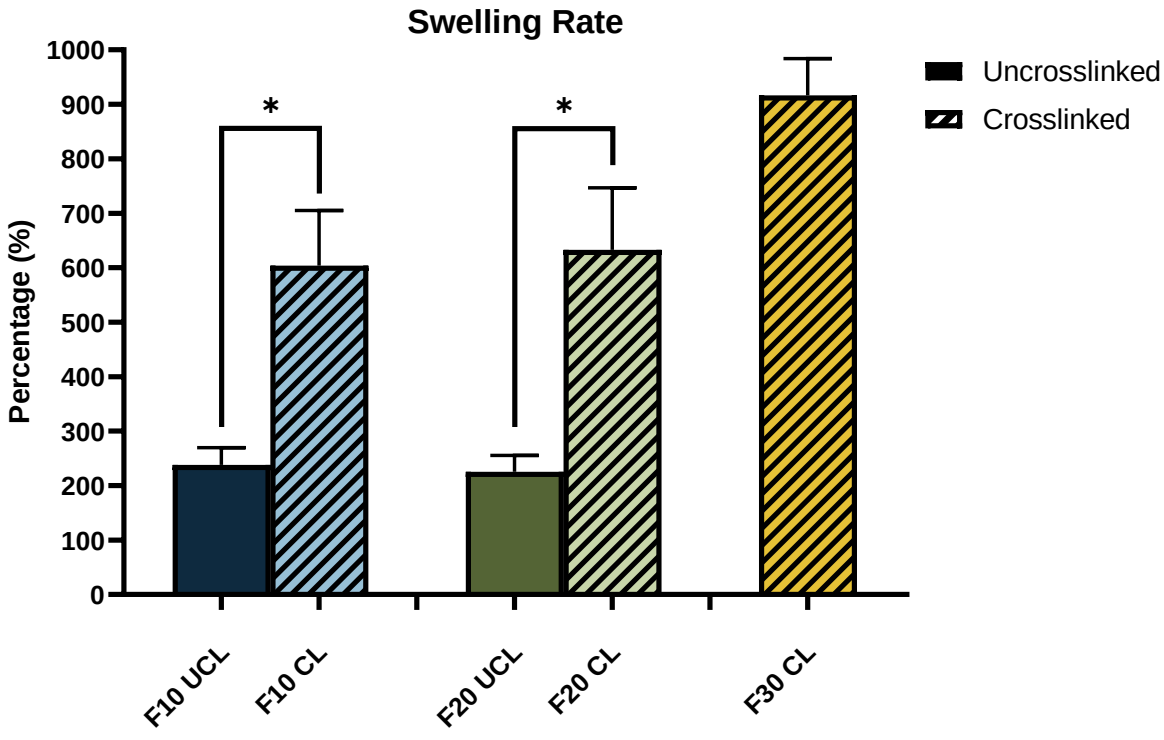

Figure 17. The swelling ratios of various 3DENS

*The figure above shows the swelling ratio for F10 UCL, F10 CL, F20 UCL, F20 CL and F30 CL 3DENS in PBS (pH 7.4) at 37℃ (n=3, *p < 0.05, error bars represent ± SEM).*

4.9 Biological Analysis

4.9.1 Live/Dead assay using HaCaT

Figures 19-21 show images of 3DENS seeded with HaCaT cells at 24, 48 and 72 hours. The green fluorescence indicates live cells stained by calcein dye and the red fluorescence indicates dead cells stained by propidium iodide. The images clearly show more live cells then dead cells which is confirmed by the positive viability percentage shown in the graphs in Figures 22-24. for all 3DENS. The fluorescence images also indicated a tendency of HaCaT cells to infiltrate into deeper layers of the 3DENS.

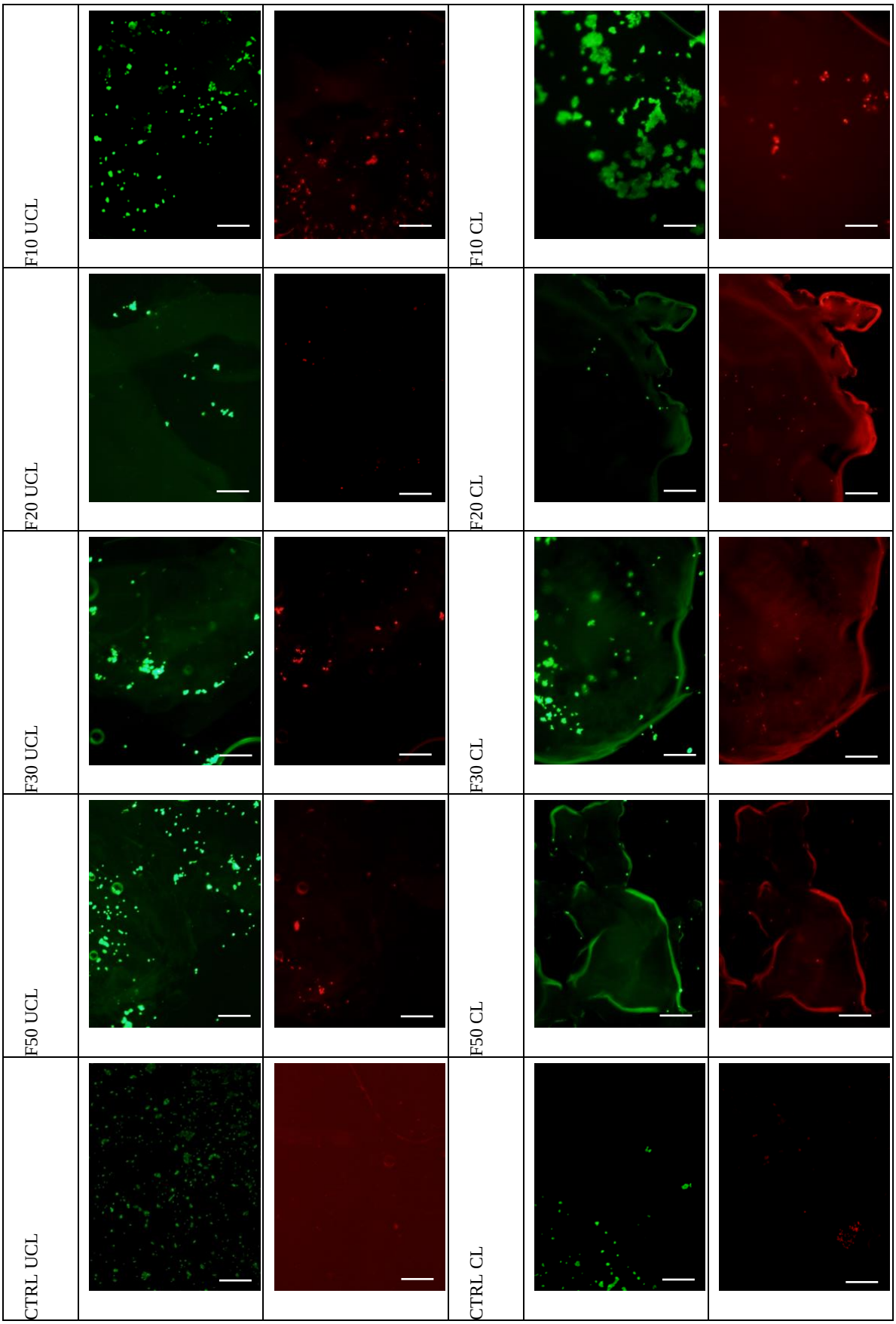

Figure 18. Fluorescence images of the 3DENS seeded with HaCaT cells after undergoing the Live/Dead viability assay at 24 hours

Control groups were cells seeded into wells without any 3DENS. Green indicates live cells stained by calcein and red indicates dead cells stained by propidium iodide. Scale bar represents 200μm.

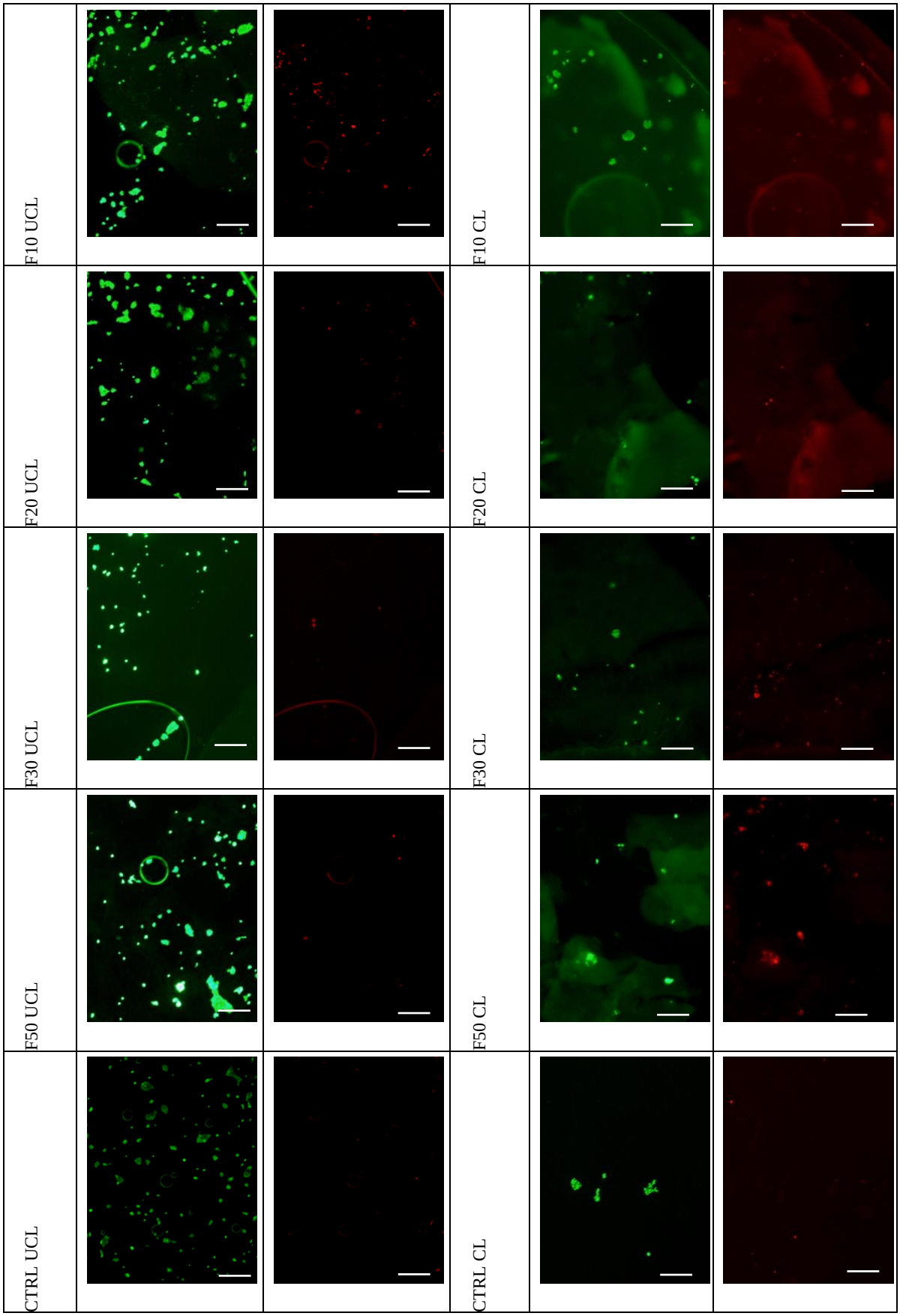

Figure 19. Fluorescence images of the 3DENS seeded with HaCaT cells after undergoing the Live/Dead viability assay at 48

Control groups were cells seeded into wells without any 3DENS. Green indicates live cells stained by calcein and red indicates dead cells stained by propidium iodide. Scale bar represents 200 μm.

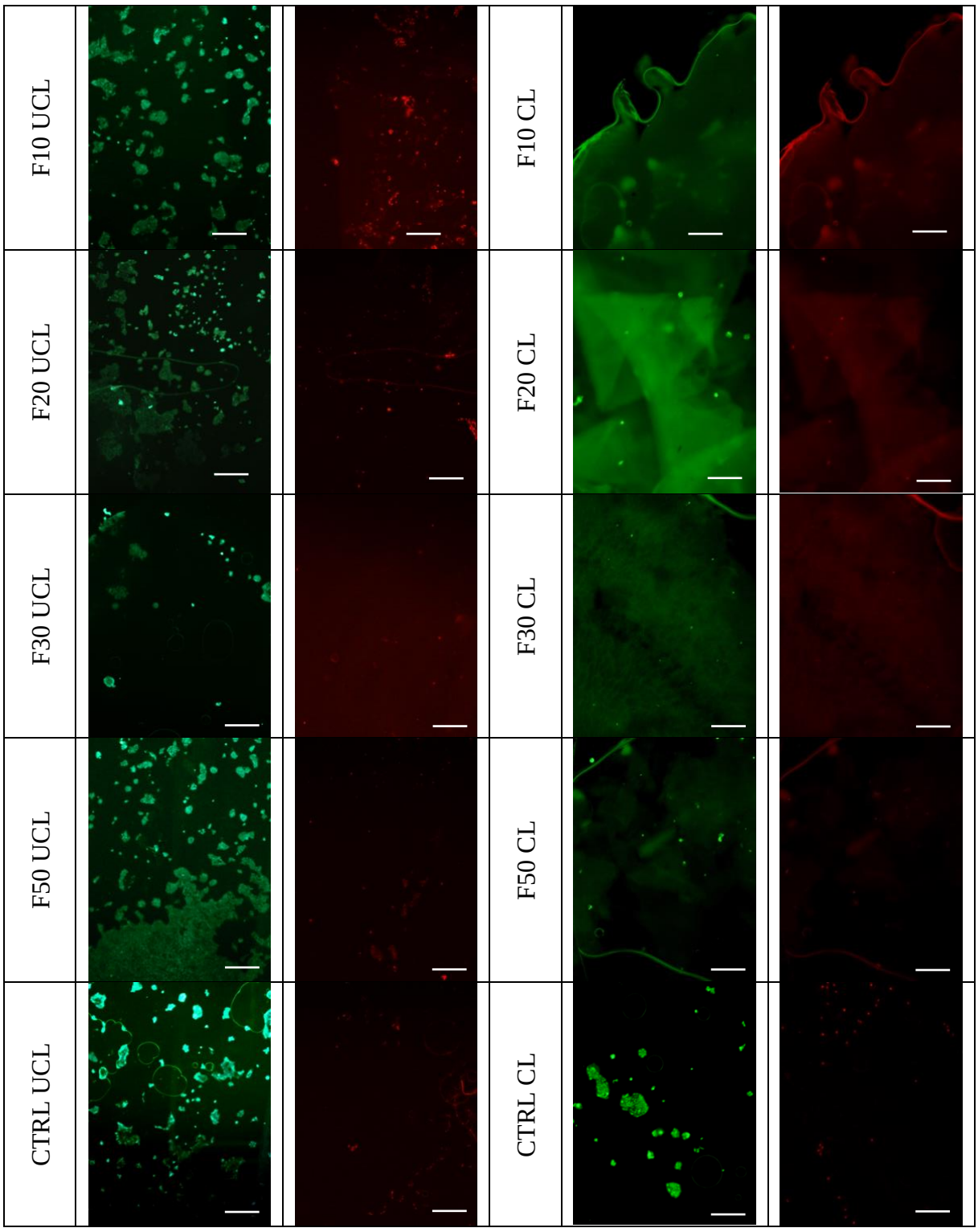

Figure 20. Fluorescence images of the 3DENS seeded with HaCaT cells after undergoing the Live/Dead viability assay at 72 hours

Control groups were cells seeded into wells without any 3DENS. Green indicates live cells stained by calcein and red indicates dead cells stained by propidium iodide. Scale bar represents 200 μm.

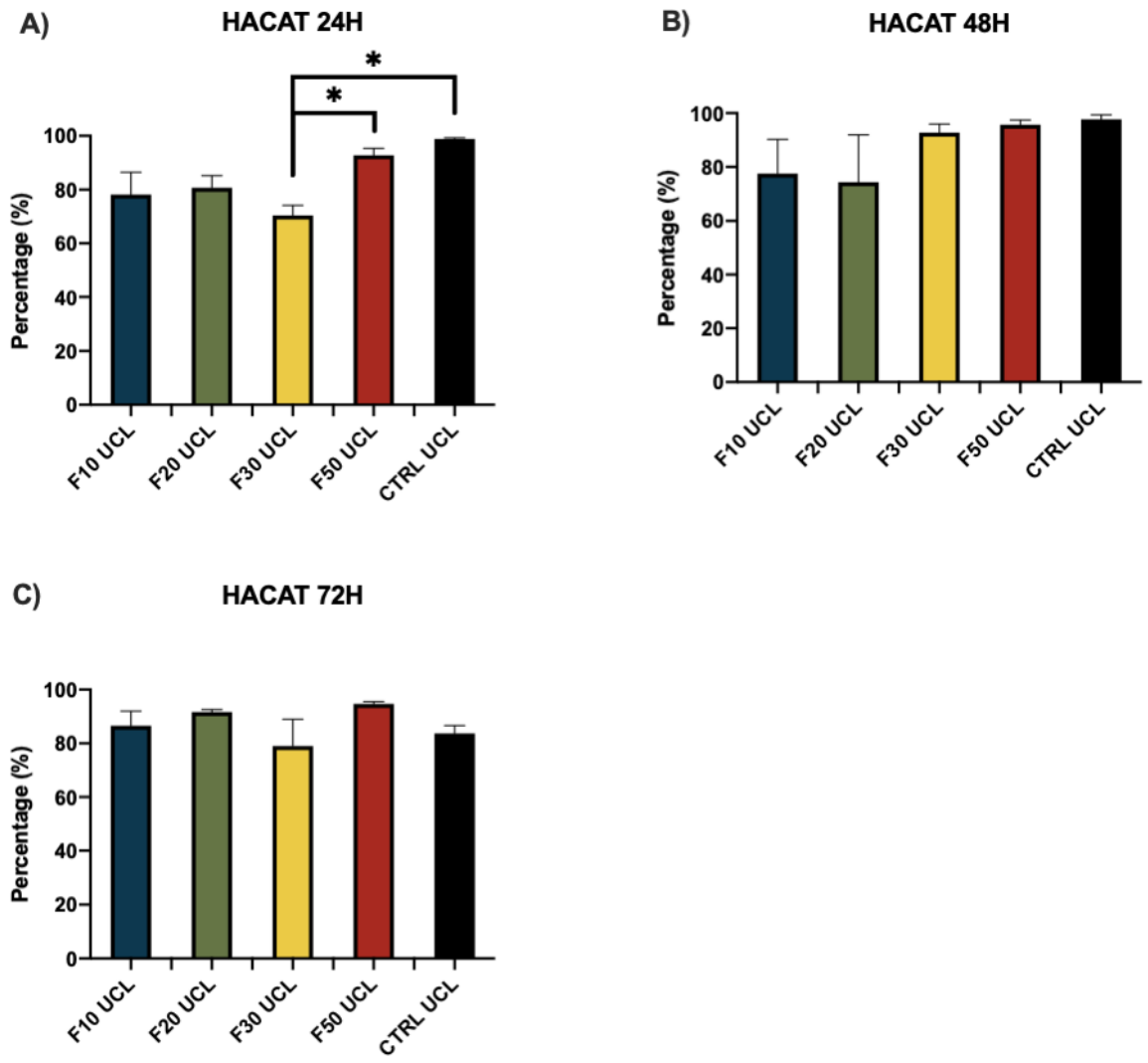

Figure 21. Viability of HaCaT cells on uncrosslinked 3DENS

*The graphs represent HaCaT cell viability on uncrosslinked 3DENS as a percentage at 24h (A), 48h (B) and 72h (C) (n=3, *p<0.05, error bars represent ± SEM).*

HaCaT cells showed good viability (> 70 %) in all uncrosslinked 3DENS at 24, 48 and 72 hours (Figure 22. Results of the one-way ANOVA test confirmed that F30 showed significantly lower cell viability at 24 hours compared to F50 and control (p = 0.01). At 48 and 72 hours, cell viability remained above 70% however none of the 3DENS performed significantly different compared to the others (p = 0.37 and p = 0.30, respectively).

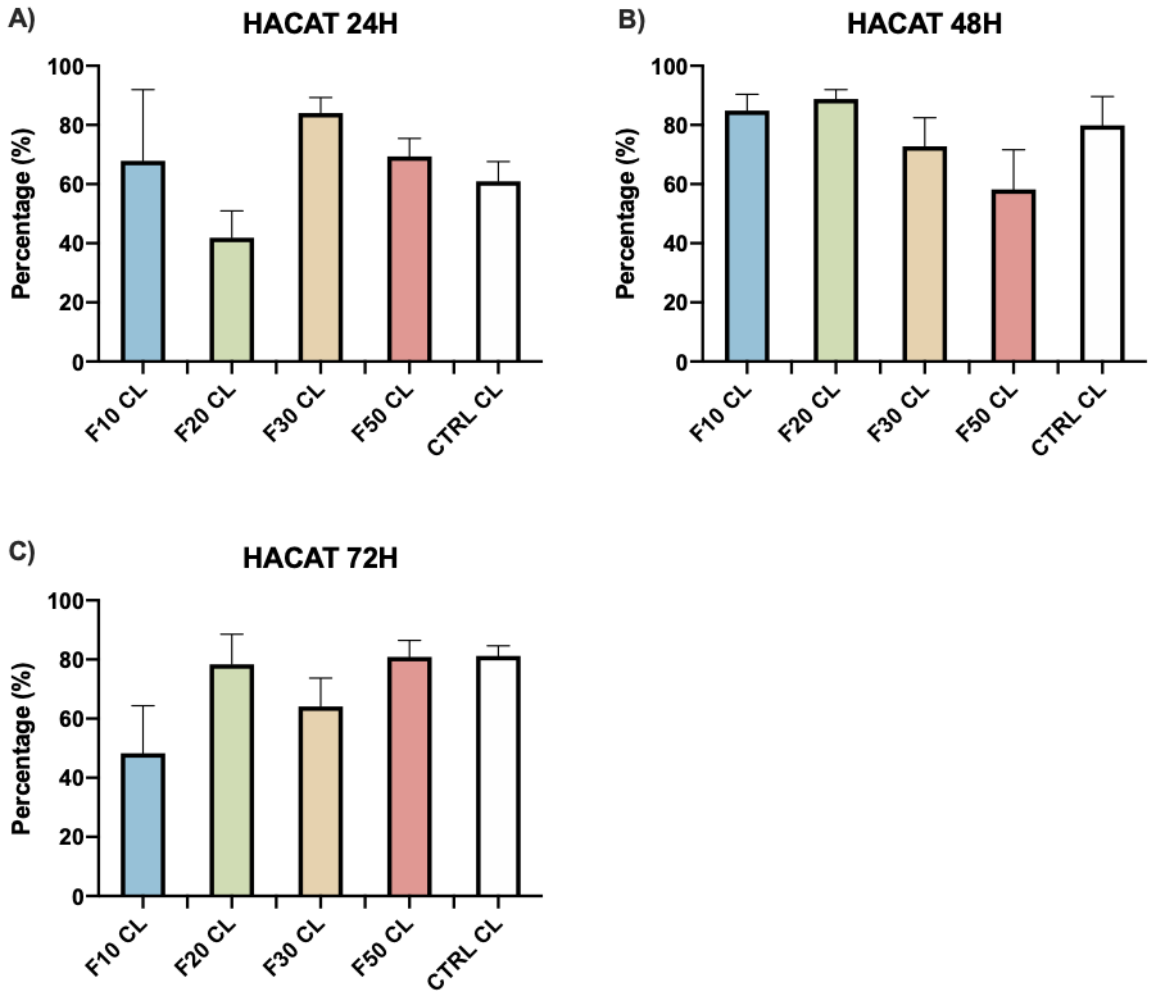

Figure 22. Viability of HaCaT cells on crosslinked 3DENS

The graphs represent HaCaT cell viability on crosslinked 3DENS as a percentage at 24h (A), 48h (B) and 72h (C) (n=3, error bars represent ± SEM).

In the crosslinked 3DENS, F20 CL showed the lowest cell viability (42 %), followed by F10 CL (68 %) however F30 CL and F50CL showed good viability (> 70 %) (Figure 23). At 48 hours, F10 CL, F20 CL and F30 CL showed good viability (> 70 %) while F50 CL showed the lowest HaCaT viability (58 %). By 72 hours F10 CL and F30 CL had viability below 70% and F20 CL and F50 CL had viability of approximately to 80 %. However, results of the one-way ANOVA test showed no significant differences in HaCaT cell viability between different CL 3DENS at 24, 48 and 72 hours (p = 0.27, p = 0.21 and p = 0.45, respectively).

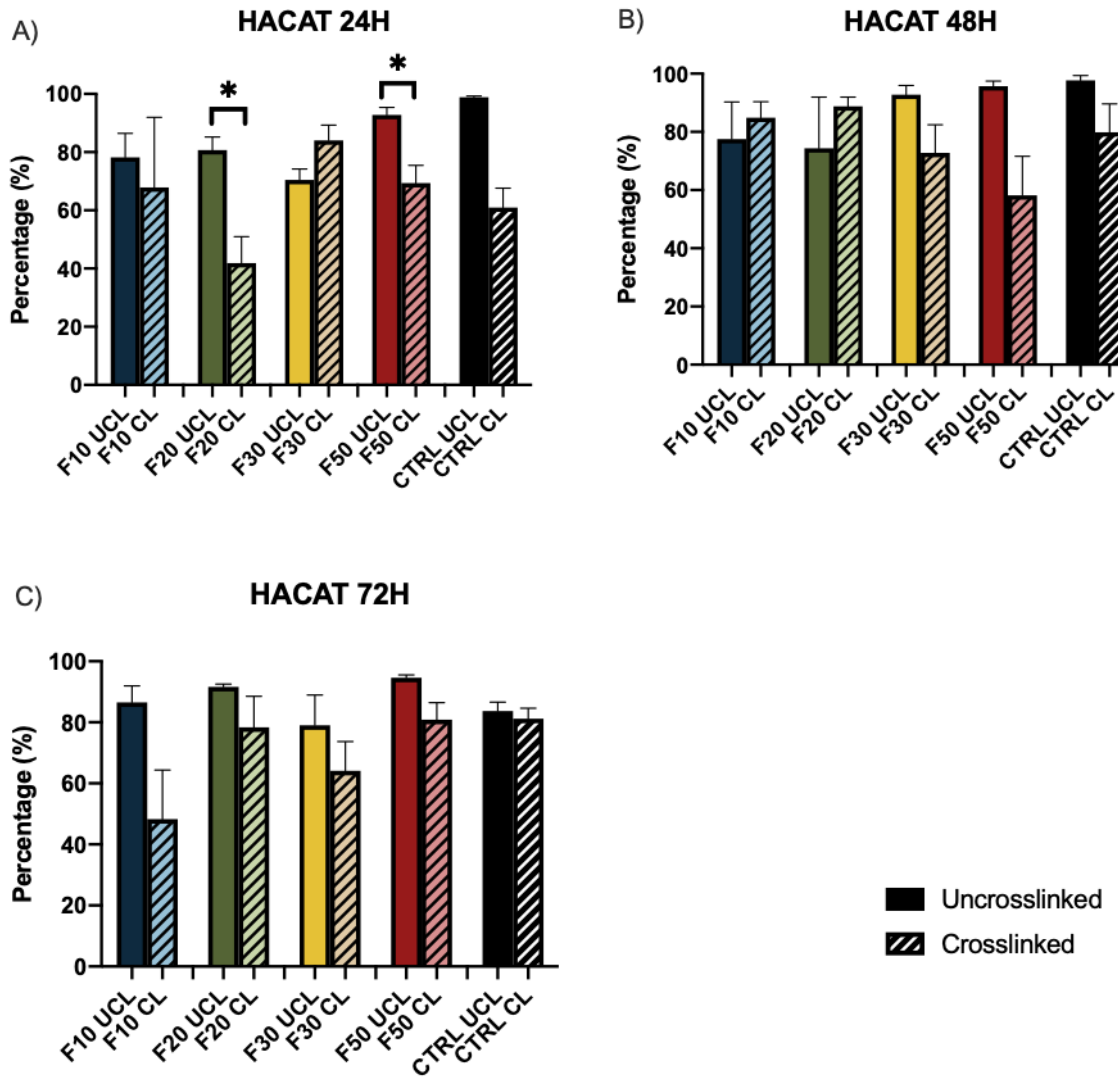

Figure 23. Viability of HaCaT cells on uncrosslinked and crosslinked 3DENS

*The graphs compare HaCaT cell viability on uncrosslinked and crosslinked 3DENS at 24h (A), 48h (B) and 72h (C) (n=3, *p < 0.05, error bars represent ± SEM).*

A one-way ANOVA is not suitable for comparing two samples. Results of a t-test were used to comparing uncrosslinked to crosslinked 3DENS, uncrosslinked 3DENS F20 and F50 showed significantly higher cell viability than crosslinked 3DENS F20 and F50 at 24 hours ($p = 0.02$ and $p = 0.02$, respectively) (Figure 24). The difference between uncrosslinked and crosslinked 3DENS for all formulations at 48 hours were not significant ($p > 0.05$). At 72 hours, uncrosslinked 3DENS showed a higher cell viability for all formulations, however, this difference was not significant ($p > 0.05$).

4.9.2 Live/Dead Assay using NHDF

Figures 25-27 show fluorescence images of 3DENS seeded with and NHDF cells at 24, 48 and 72 hours.

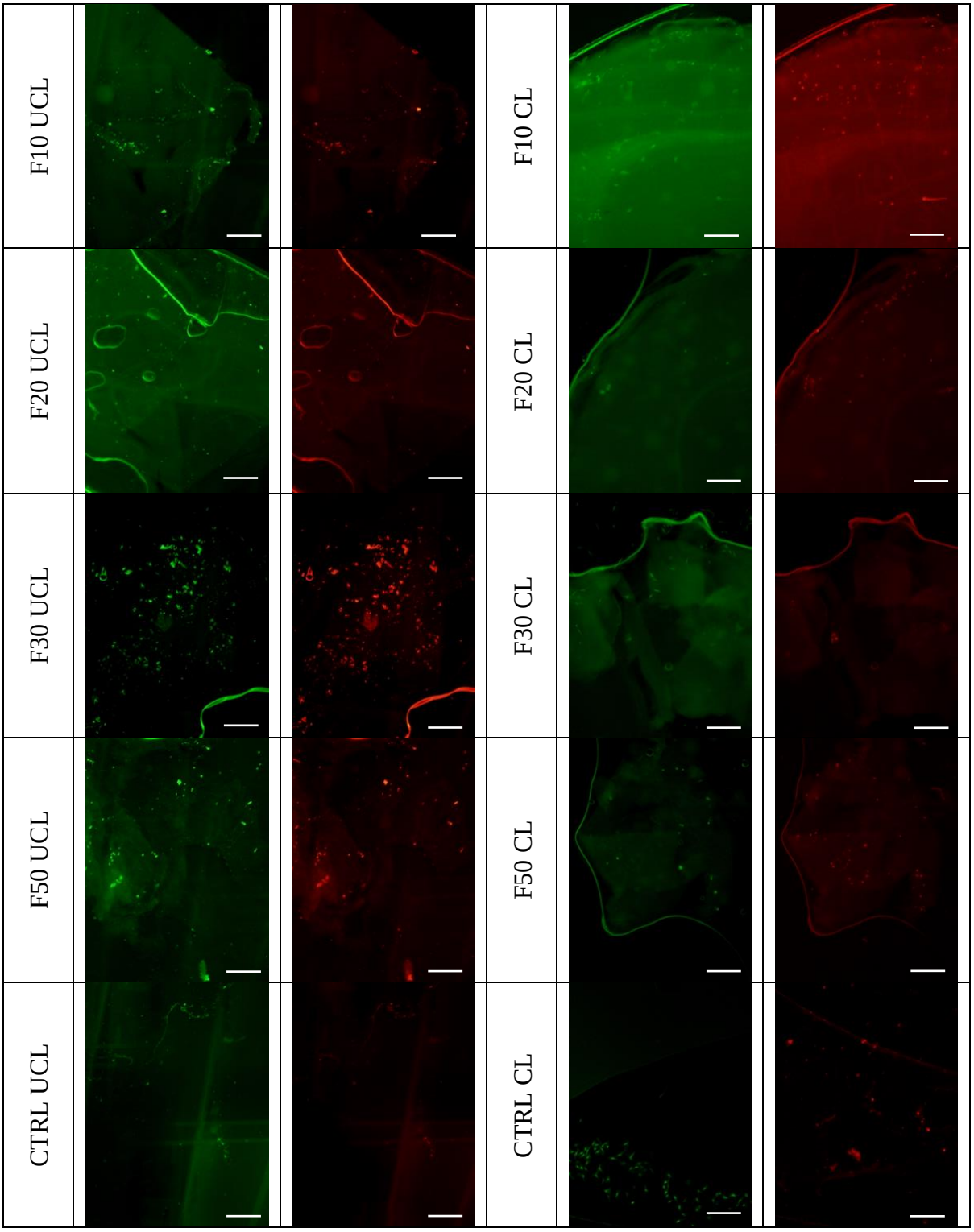

Figure 24. Fluorescence images of the 3DENS seeded with NHDF cells after undergoing the Live/Dead viability assay at 24 hours

Control groups were cells seeded into wells without any 3DENS. Green indicates live cells stained by calcein and red indicates dead cells stained by propidium iodide. Scale bar represents 200 μm.

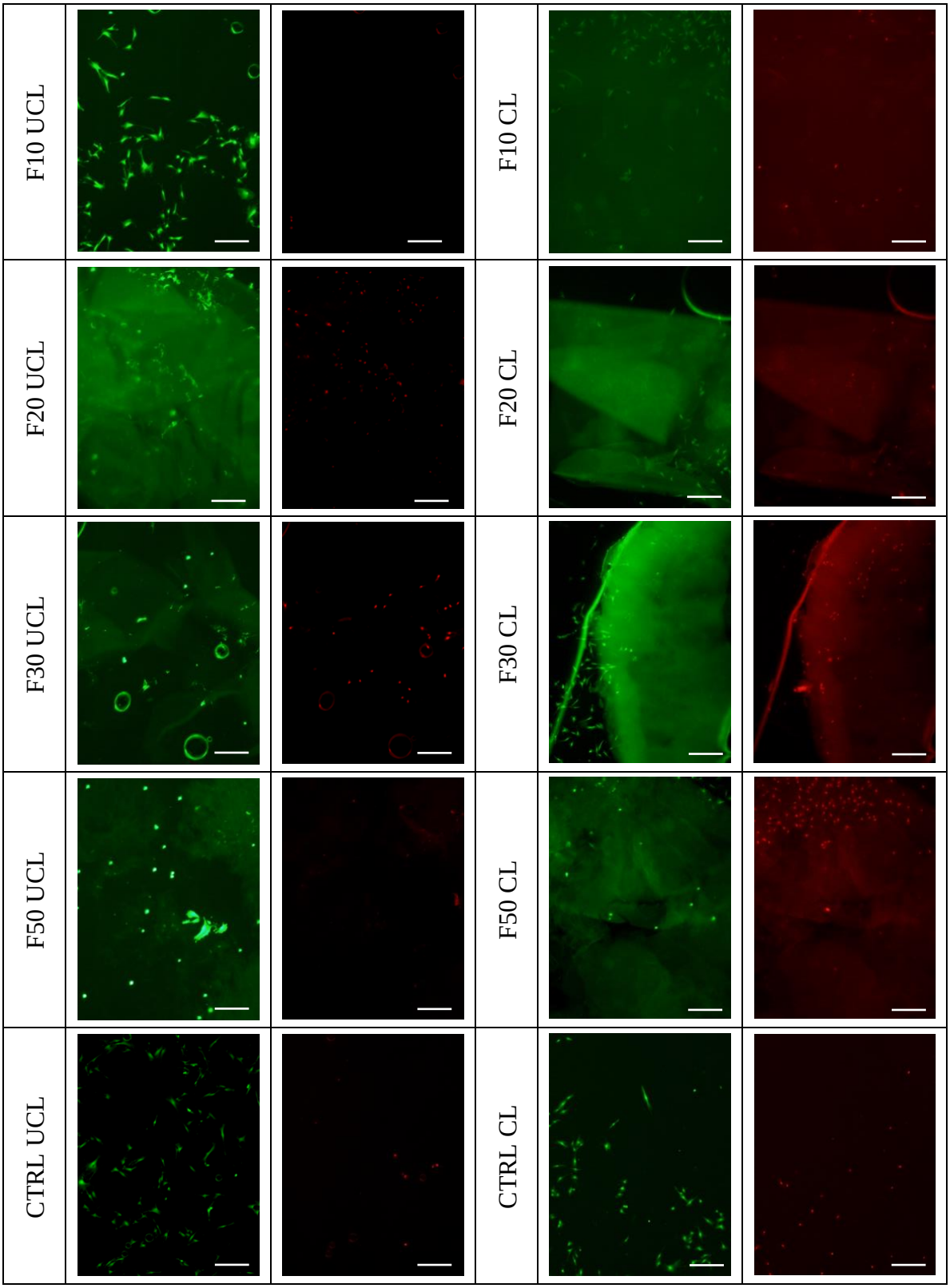

Figure 25. Fluorescence images of the 3DENS seeded with NHDF cells after undergoing the Live/Dead viability assay at 48 hours

Control groups were cells seeded into wells without any 3DENS. Green indicates live cells stained by calcein and red indicates dead cells stained by propidium iodide. Scale bar represents 200 μm.

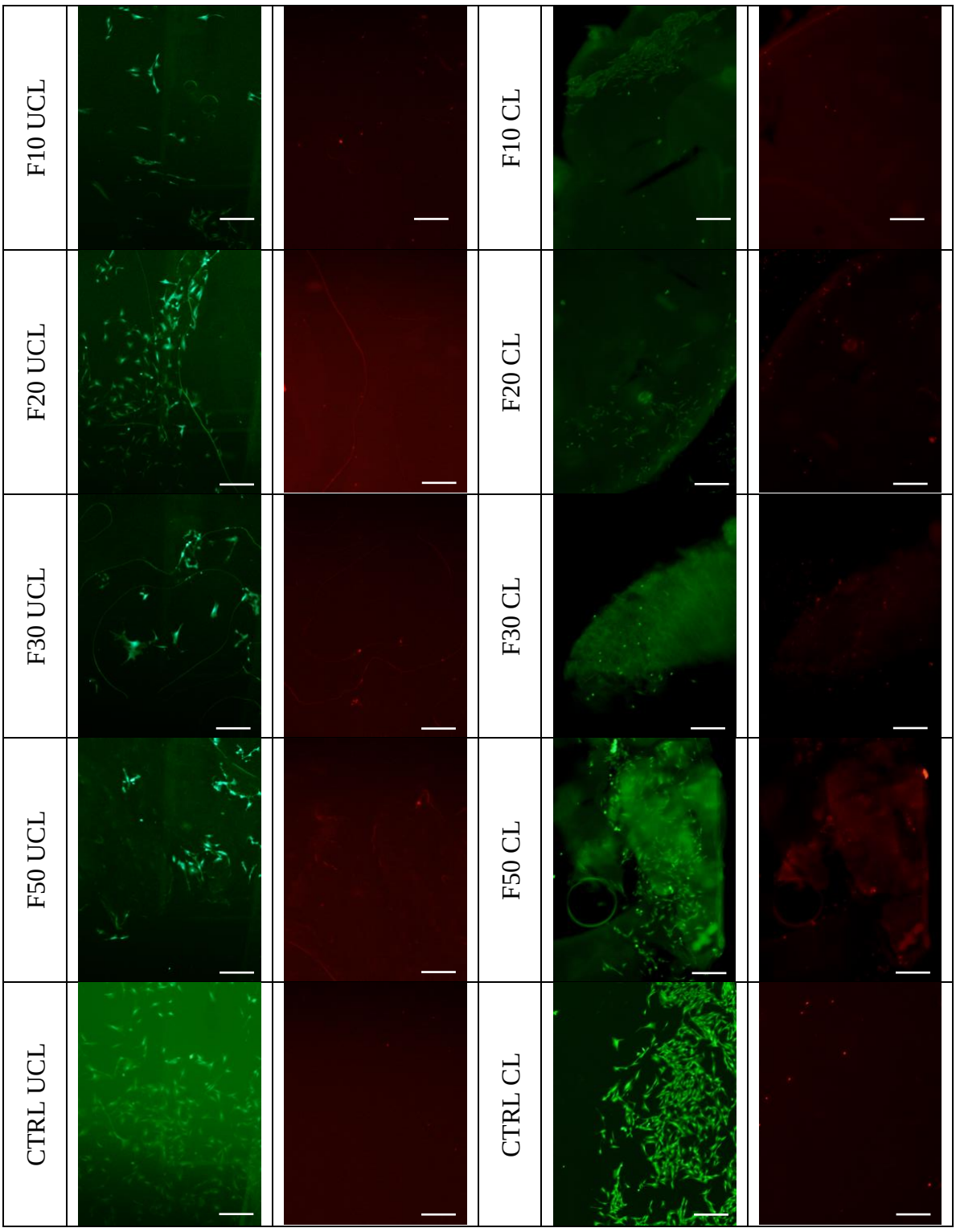

Figure 26. Fluorescence images of the 3DENS seeded with NHDF cells after undergoing the Live/Dead viability assay at 72 hours

Control groups were cells seeded into wells without any 3DENS. Green indicates live cells stained by calcein and red indicates dead cells stained by propidium iodide. Scale bar represents 200 μm.

As stated previously for fluorescence images, the green fluorescence indicates live cells stained by calcein dye and the red fluorescence indicates dead cells stained by propidium iodide. The positive viability percentage shown in the graphs in Figure 27, attest to the presence of more live cells then dead in the 3DENS fluorescence images. The images clearly show more live cells then dead cells which is confirmed by the positive viability percentage shown in the graphs in Figures 28-30 for all 3DENS. The fluorescence images also indicated a tendency of NHDF cells to infiltrate into deeper layers of the 3DENS.

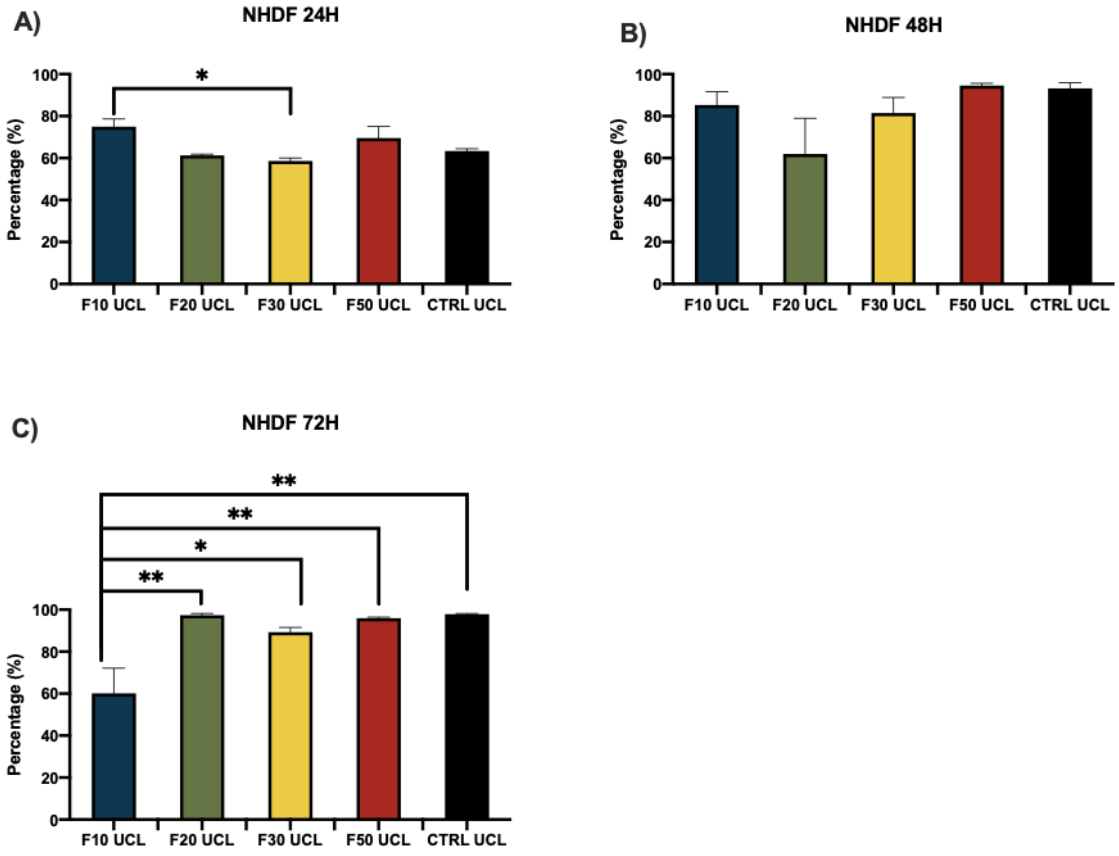

Figure 27. Viability of NHDF cells on uncrosslinked 3DENS

*The graphs represent NHDF cell viability on uncrosslinked 3DENS as a percentage at 24h (A), 48h (B) and 72h (C) (n=3, *p<0.05, **p<0.01, error bars represent ± SEM).*

The one-way ANOVA showed that in crosslinked 3DENS, NHDF cell viability was significantly higher in F10 UCL than F30 UCL (p = 0.02) (Figure 28). Uncrosslinked 3DENS F20, F30, and F50 had cell viability between 58 %- 70 %. At 48 hours, cell viability increased for all 3DENS with F50 showing the highest viability (94 %), followed by F10 (85 %), F30 (82 %) and F20 having the lowest at 62 %. Cell viability at 48 hours were not significantly different for any 3DENS formulation (p=0.14). By 72 hours, F10 UCL showed significantly lower cell viability compared to all other 3DENS and the control (p = 0.003). Cell viability for uncrosslinked 3DENS F20 to F50 was at 90 % or above.

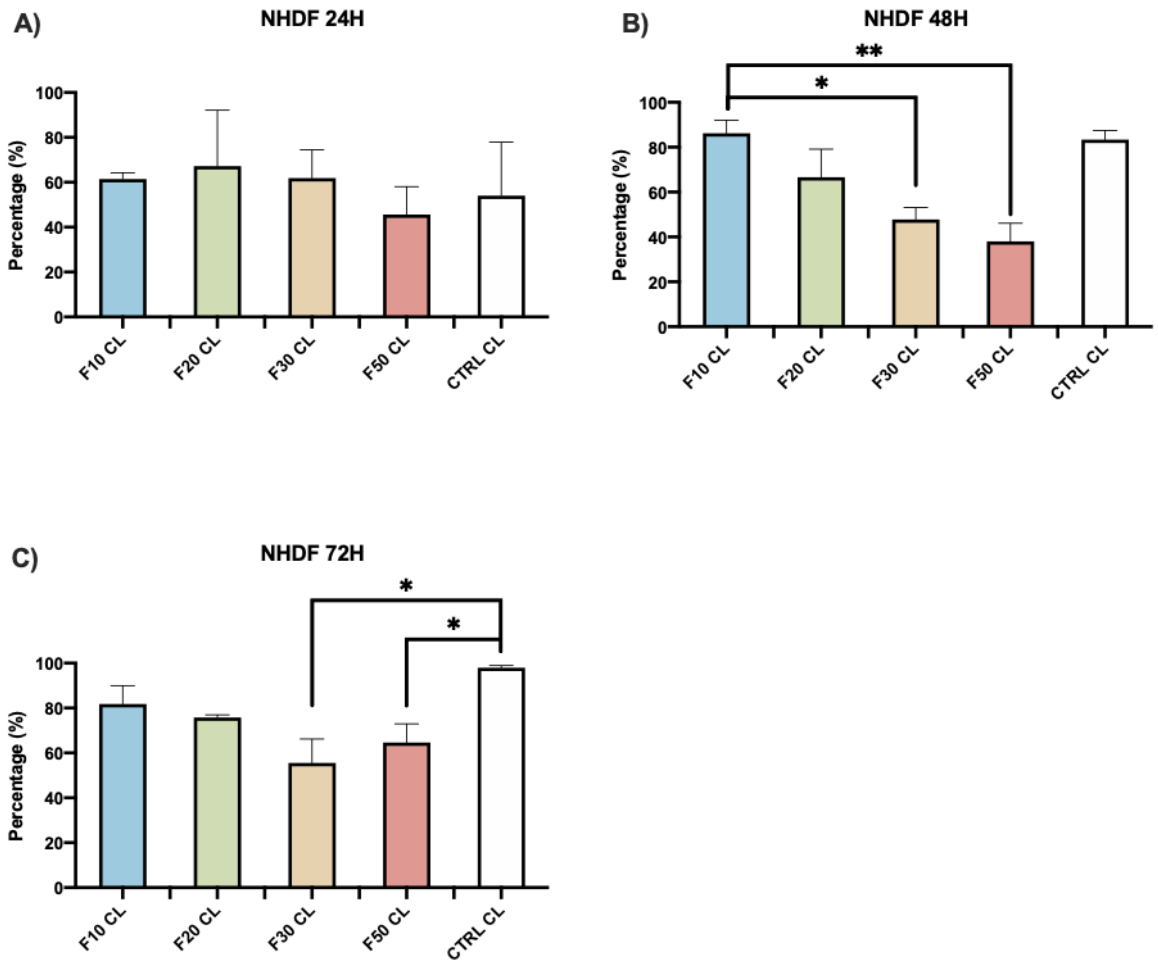

Figure 28. Viability of NHDF cells on crosslinked 3DENS

*The graphs represent NHDF cell viability on crosslinked 3DENS as a percentage at 24h (A), 48h (B) and 72h (C) (n=3, *p < 0.05,**p < 0.01, error bars represent ± SEM).*

Cell viability of NHDF on the various crosslinked 3DENS scaffolds were less than 70 % which are generally not considered viable however, the one-way ANOVA showed no significant differences between the different formulations at 24 hours (p = 0.23) (Figure 29). At 48 hours, cell viability gradually decreased from F10 CL to F50 CL. F10 CL showed significantly higher cell viability than F30 CL and F50 CL (p = 0.005). By 72 hours, F30 CL and F50 CL showed significantly lower cell viability than the control (p = 0.02).

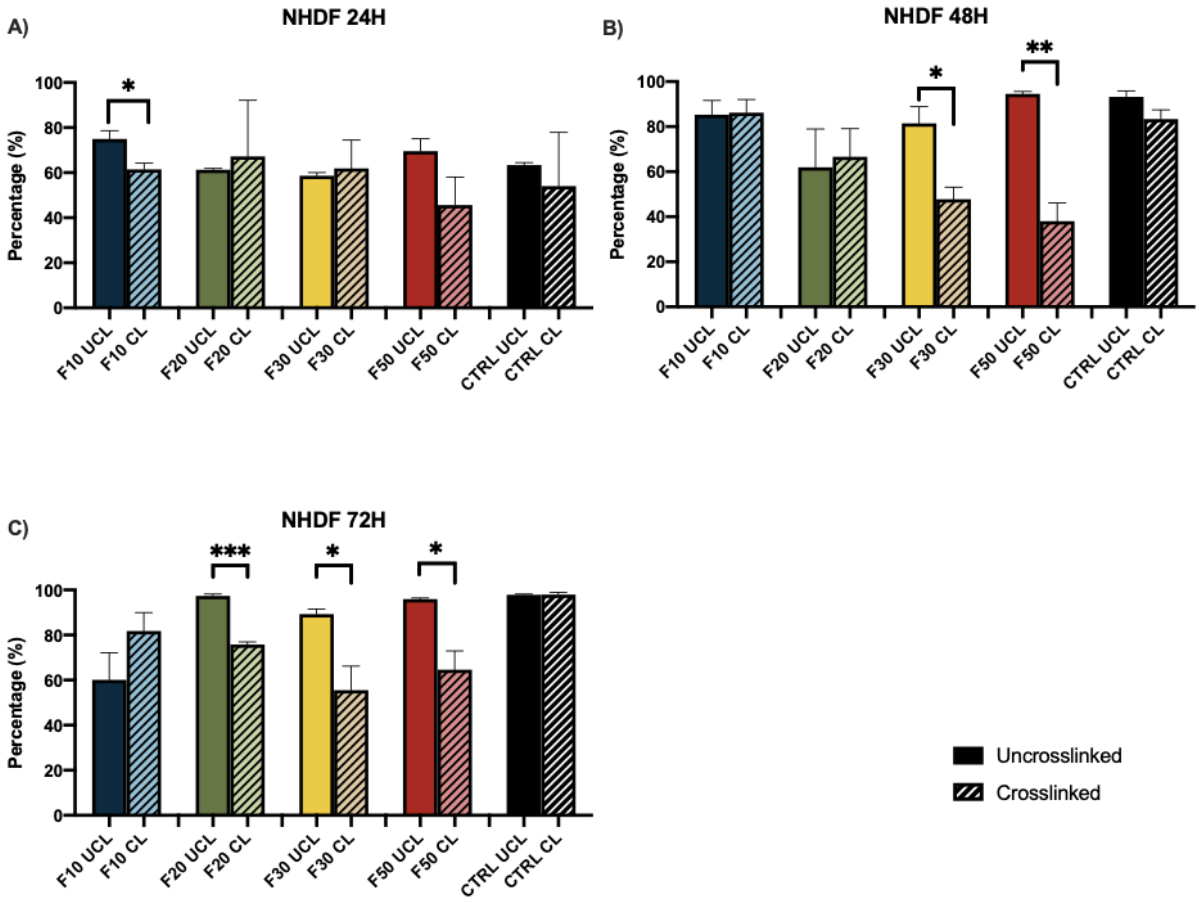

Figure 29. Viability of NHDF cells on uncrosslinked and crosslinked 3DENS

*The graphs compare NHDF cell viability on uncrosslinked and crosslinked 3DENS as a percentage at 24h (A), 48h (B) and 72h (C) (n=3, *p < 0.05, **p < 0.01,***p < 0.001, error bars represent ± SEM).*

The cell viability of NHDF of uncrosslinked 3DENS and crosslinked 3DENS was compared using a T-test (Figure 30). At 24 hours, F10 UCL performed significantly better than F10 CL ($p = 0.04$), and there were no significant differences between the uncrosslinked and crosslinked 3DENS for F20, F30 and F50 ($p > 0.05$). At 48 hours, uncrosslinked 3DENS F30 and F50 performed significantly better than the crosslinked formulation ($p = 0.02$ and $p = 0.002$, respectively). At 72 hours, uncrosslinked 3DENS F20, F30 and F50 performed better than crosslinked 3DENS ($p = 0.001$, $p = 0.04$ and $p = 0.02$, respectively).

4.9.3 Cell Proliferation using HaCaT Cell Line

The proliferation of HaCaT cells were measured on uncrosslinked and crosslinked 3DENS at 24h, 48, and 72h. The number of cells present in each 3DENS at various time points are presented in the graphs shown in Figures 29-30.

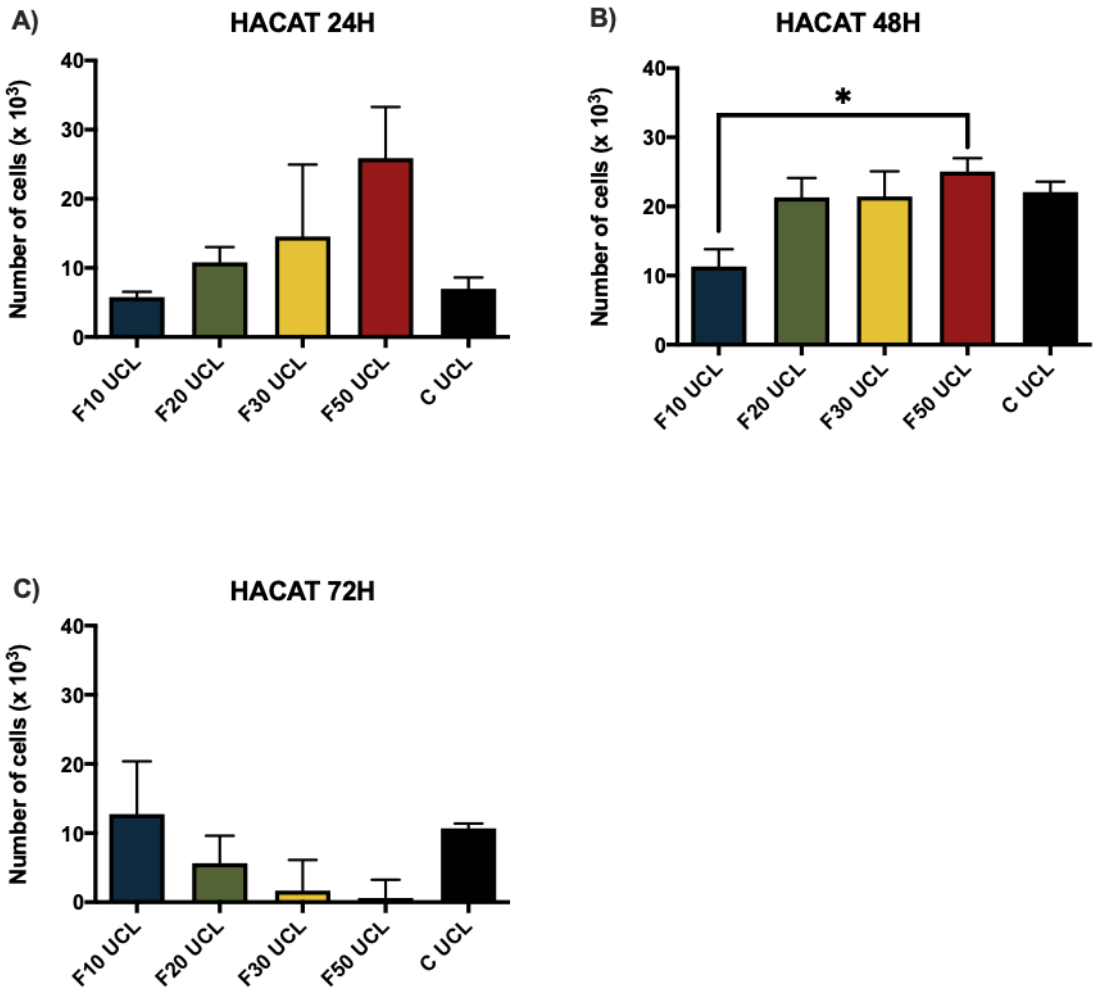

Figure 30. Proliferation of HaCaT cells on uncrosslinked 3DENS

*The graphs represent the number of HaCaT cells on uncrosslinked 3DENS at 24h (A), 48h (B) and 72h (C) (n=6, *p < 0.05, error bars represent ± SEM).*

At 24 hours, the proliferation rate of HaCaT cells increased as the percentage of chitosan in the uncrosslinked 3DENS formulations increased from F10 to F50 (Figure 31). These differences were not significant ($p = 0.19$). At 48 hours, UCL F50 performed significantly better than UCL F10 ($p = 0.03$). By 72 hours, the proliferation rate dropped for 3DENS F20 to F50 while F10 maintained its proliferation and had the highest cell count. However, no

significant differences were found between the uncrosslinked 3DENS at 72 hours (p = 0.30).

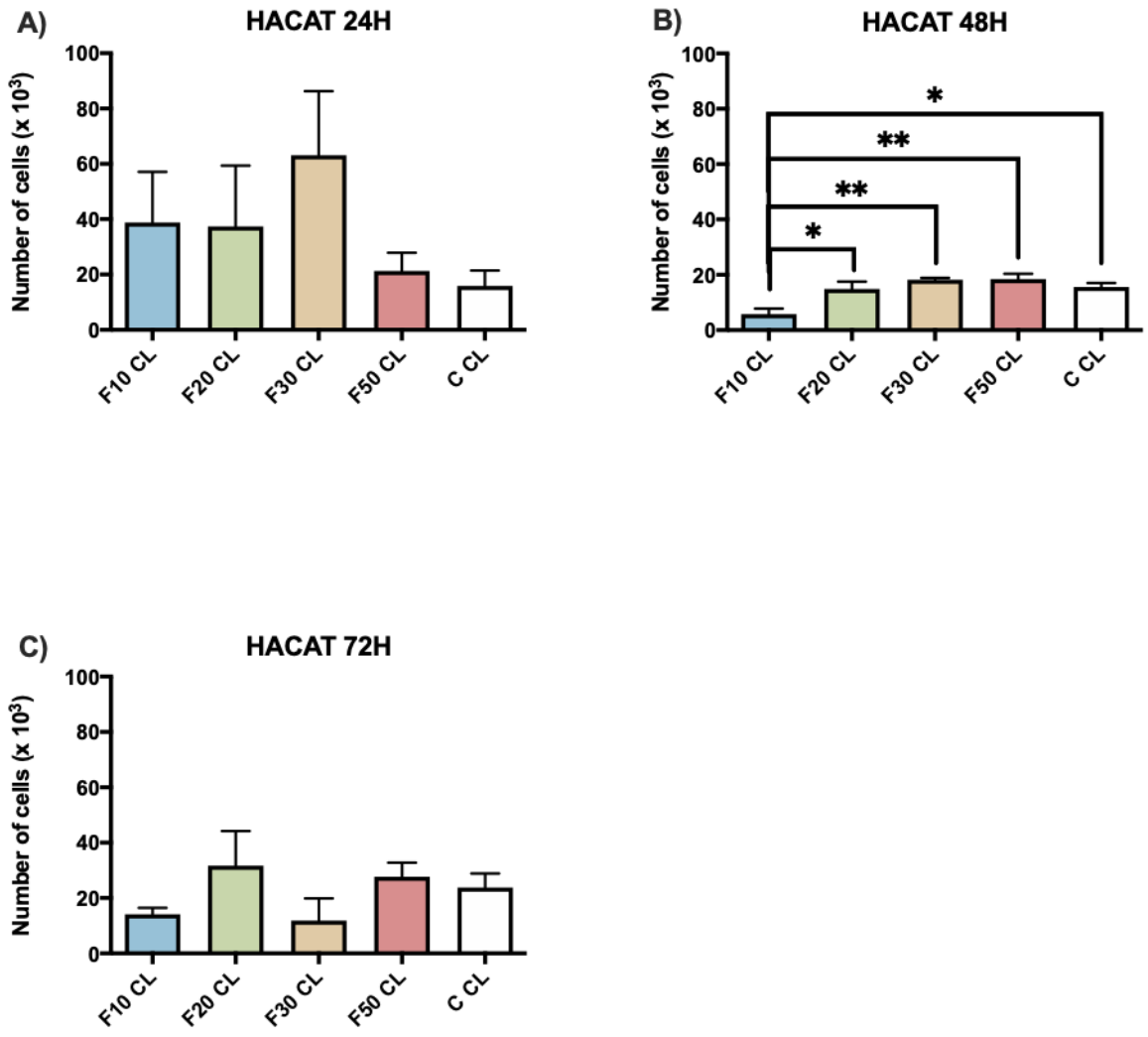

Figure 31. Proliferation of HaCaT cells on crosslinked 3DENS

*The graphs represent the number of HaCaT cells on crosslinked 3DENS at 24h (A), 48h (B) and 72h (C) (n=6, *p < 0.05, error bars represent ± SEM).*

In the crosslinked 3DENS, no significant difference was found in the proliferation rate of HaCaT cells at 24 hours (p = 0.37) (Figure 32). At 48 hours, F10 CL had significantly lower proliferation rate than all other formulations and the control (p = 0.004). By 72 hours, the were no significant differences between any of the 3DENS and the control (p = 0.33).

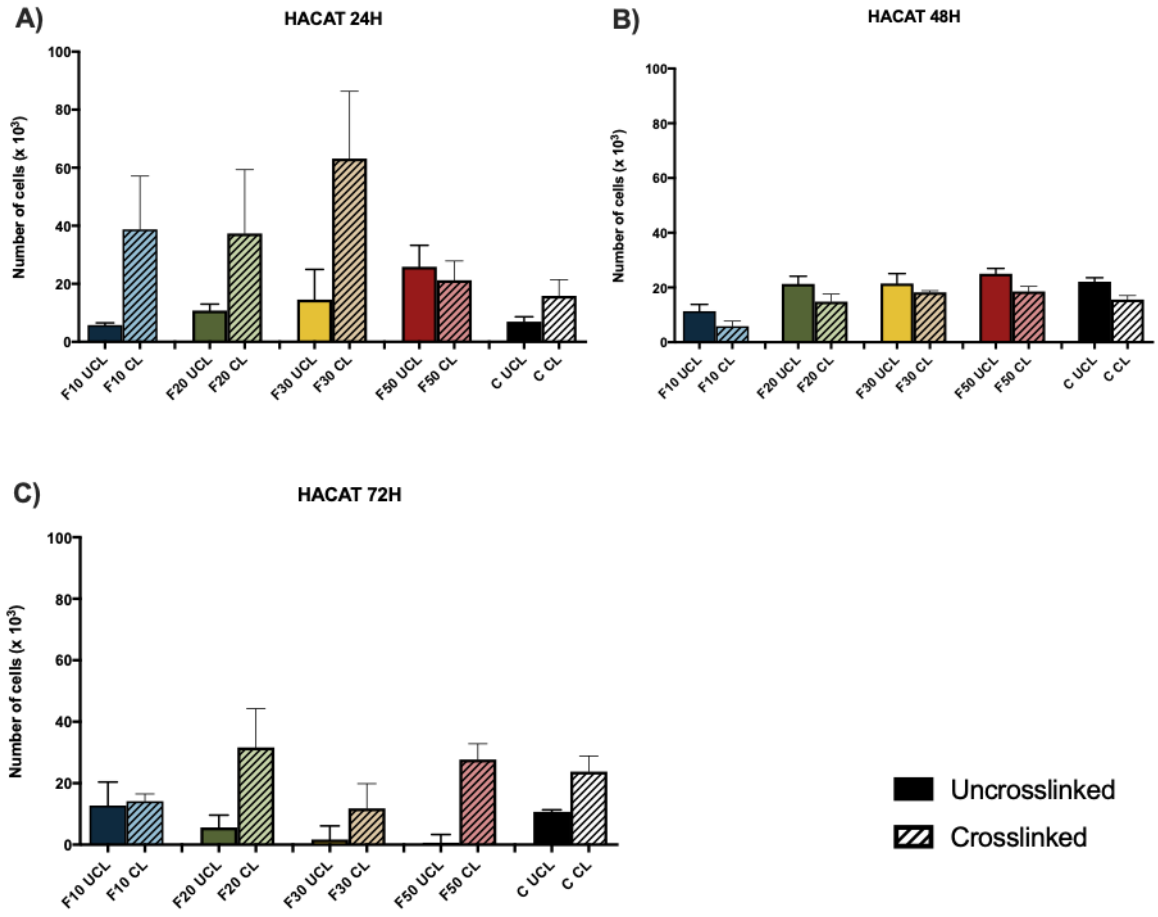

Figure 32. Proliferation of HaCaT cells on uncrosslinked and crosslinked 3DENS

The graphs compare the number of HaCaT cells on uncrosslinked and crosslinked 3DENS at 24h (A), 48h (B) and 72h (C) (n=3, error bars represent ± SEM).

A t-test was used to compare the proliferation of HaCaT cells in uncrosslinked and crosslinked scaffold for each formulation at 24, 48 and 72 hours. At 24 hours (Figure 33). the crosslinked 3DENS appeared to perform better than uncrosslinked 3DENS, however this difference was not significant ($p > 0.05$). There were no significant differences between the proliferation rate of HaCaT cells in the uncrosslinked and crosslinked 3DENS at 48 and at 72 hours ($p > 0.05$).

4.9.4 Cell proliferation using the NHDF cell line

The proliferation of NHDF cells were measured on uncrosslinked and crosslinked 3DENS at 24h, 48, and 72h. The number of cells present in each 3DENS at various time points are presented in the graphs shown in Figures 34-36.

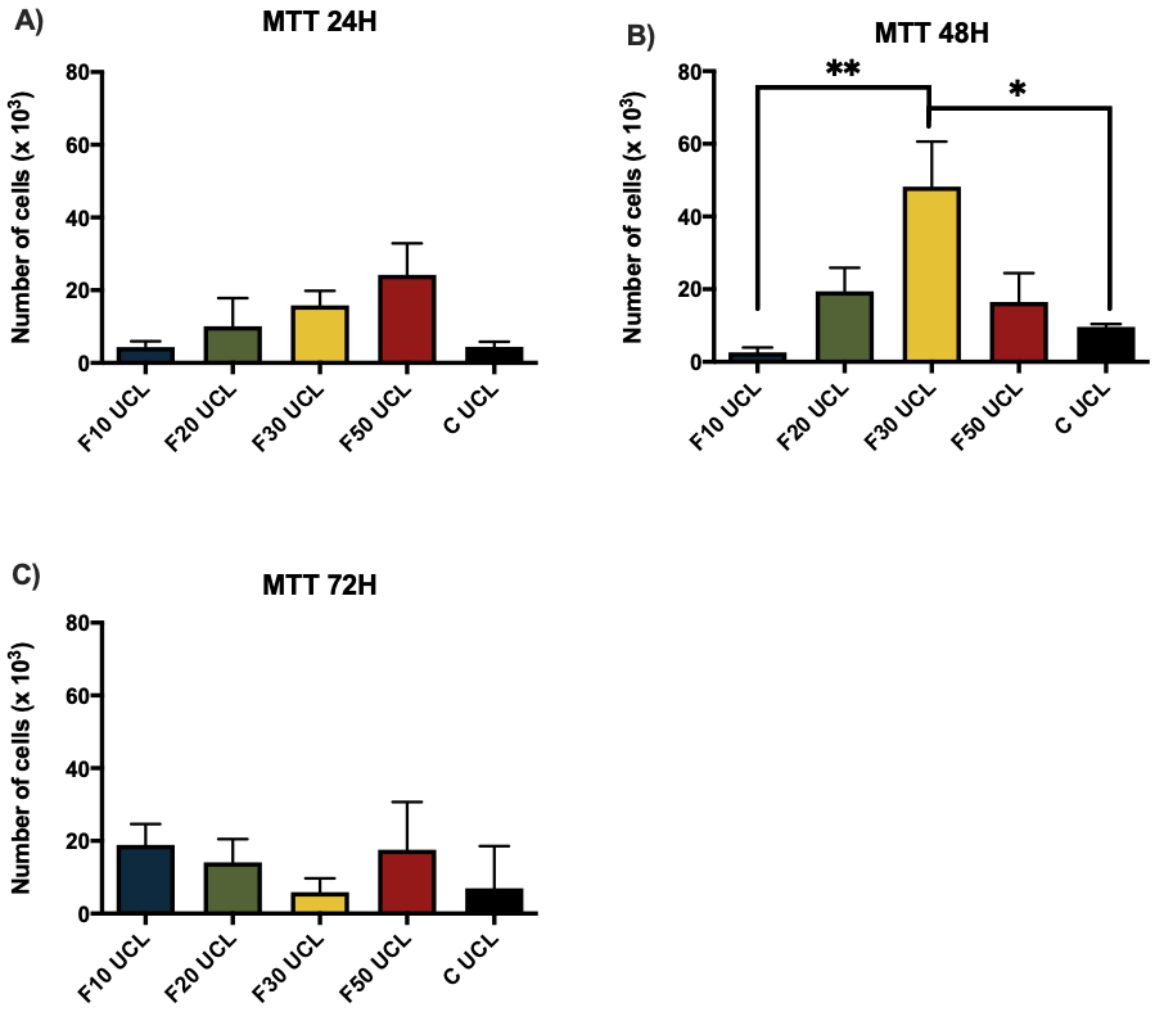

Figure 33. Proliferation of NHDF cells on uncrosslinked 3DENS

*The graphs represent the number of NHDF cells on uncrosslinked 3DENS at 24h (A), 48h (B) and 72h (C) (n=6, *p < 0.05, p < 0.01, error bars represent ± SEM).*

The number of proliferative cells on the 3DENS at 24 hours increased from F10 UCL to F50 UCL but no significant differences were seen ($p = 0.13$) (Figure 34). At 48 hours, F30 UCL had the highest rate of proliferation and it was significantly higher than F10 UCL and the control ($p = 0.01$). By 72 hours, there were no significant difference in the proliferation rate of NHDF cells between any uncrosslinked 3DENS ($p = 0.77$).

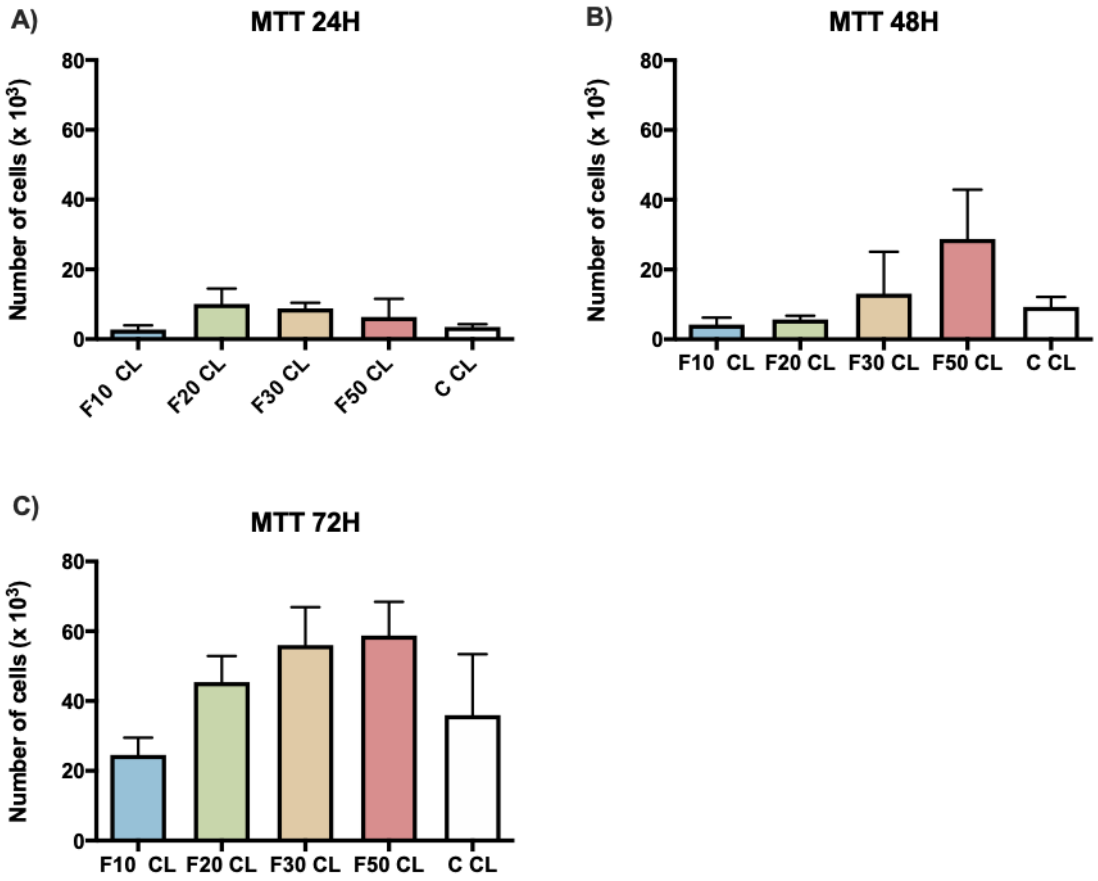

Figure 34. Proliferation of NHDF cells on crosslinked 3DENS

The graphs represent the number of NHDF cells on crosslinked 3DENS at 24h (A), 48h (B) and 72h (C) (n=6, error bars represent ± SEM).

The proliferation assay of NHDF cells on crosslinked 3DENS showed no differences between the different formulations at 24 and 48 hours ($p = 0.44$ and $p = 0.32$, respectively) (Figure 35). At 72 hours, the number of proliferative cells seemed to increase from F10 CL to F50 CL however, this increase was not significant ($p = 0.23$). At 72 hours, the number of NHDF cells on F20 CL, F30 CL and F50 CL 3DENS were higher than the control group but no significant differences were seen ($p > 0.05$).

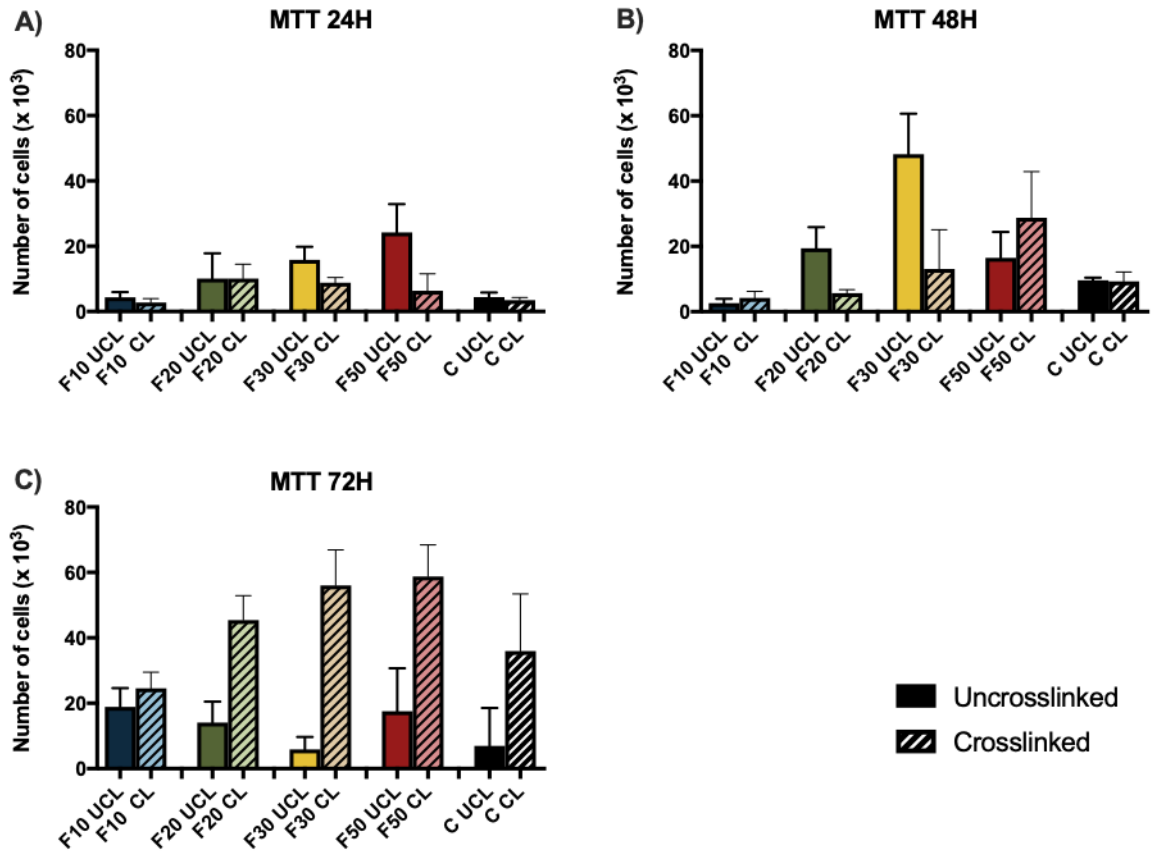

Figure 35. Proliferation of NHDF cells on uncrosslinked and crosslinked 3DENS

The graphs compare the number of NHDF cells on uncrosslinked and crosslinked 3DENS at 24h (A), 48h (B) and 72h (C) (n=3, error bars represent ± SEM).

T-tests were used to compare the proliferation of NHDF cells on uncrosslinked 3DENS compared to crosslinked 3DENS. There were no significant differences between them for any formulation at 24 hours ($p > 0.05$) (Figure 36). At 48 hours, uncrosslinked F20 and F30 had higher cell numbers than crosslinked F20 and F30, however, these differences were not significant ($p > 0.05$). By 72 hours, the number of proliferative NHDF cells were higher in crosslinked 3DENS than uncrosslinked 3DENS, however the differences were not significant for any formulation ($p > 0.05$).

4.9.5 Summary of Biological Analysis

The findings of the biological assays are summarised as follows:

- HaCaT and NHDF cells were viable in all uncrosslinked and crosslinked 3DENS. UCL 3DENS performed significantly better than CL 3DENS.
- At 48 hours, HaCaT cell proliferation was significantly higher in CL and UCL 3DENS with a higher amount of chitosan, however, by 72 hours, there were no differences between the formulations.
- F30 UCL had the highest number of proliferative NHDF cells at 48 hours, however, at 72 hours, the UCL 3DENS were not different from each other. CL 3DENS showed no differences either.

5.0 Discussion

At present, there are no studies using thermal crosslinking without any added chemical crosslinking agents to crosslink chitosan-based scaffolds. While chitosan, PVA and PVP blend 3DENS have been fabricated and characterised physically, no biological characterisations have been done for this combination for the application of dermal tissue regeneration. In the present study, the overarching aim was to use electrospinning technology to fabricate a 3DENS using combination of chitosan, PVA and PVP, and to assess its suitability as a dermal tissue regenerative scaffold *in vitro*. To achieve this aim, the spinning solutions where physically characterised, electrospinning parameters were optimised, the 3DENS were characterised physically and chemically, and the *in vitro* biological compatibility of the scaffolds were assessed. The main results of the study are as follows:

1. The pH of the blend solutions gradually decreased with the increase in the amount of chitosan.
2. The addition of 2 % chitosan decreased the electrical conductivity of the blend solutions.
3. The decrease in viscosity of the blend solutions was attributed to the decrease in the amount of PVA in the solution as the proportion chitosan increased.
4. Blend formulations of chitosan, PVA and PVP displayed shear thinning behaviour. PVA behaved as a structured fluid.
5. The voltage required to produce a Taylor cone with a continuous jet increased as the amount of chitosan in the formulation increased.
6. The average fibre diameter decreased from 0.22 ηm to 0.05 ηm from F10 to F50.
7. 3DENS degraded faster as the amount of chitosan increased.
8. Crosslinked 3DENS displayed higher water adsorption capacity than uncrosslinked 3DENS.
9. Both HaCaT and NHDF cells showed good viability in all uncrosslinked and crosslinked 3DENS. UCL 3DENS performed significantly better than CL 3DENS in terms of NHDF viability.

10. Cell proliferation of both HaCaT and NHDF cell lines on uncrosslinked and crosslinked scaffolds were similar regardless of formulation and were comparable to the control groups at various time points.

5.1 3DENS Fabrication Parameters and Fibre Morphology

Electrospinning technique was used as it creates a scaffold that mimics ECM architecture. Fresh 3DENS scaffolds were prepared in the lab for experiments throughout the duration of the study. The same electrospinning parameters were used successfully to spin new 3DENS each time. However, if the 3DENS was to be made in a different lab in a different region or country, environmental factors such as temperature and humidity should be taken into account as these have a direct influence on the electrospinning parameters.

Chitosan was chosen due to its structural similarity to GAG which is a key component of the ECM as previously discussed (section 1.1). 3DENS were successfully produced using chitosan, PVA and PVP; confirmed by the presence of IR peaks characterises of the raw materials in the 3DENS in FTIR graphs. A polymer concentration should be high enough, but not above the critical value that could induce blockage, to generate molecular chain entanglements needed to prevent the breaking up of the polymer jets and allow electrostatic stresses to elongate them (Taylor 1969). Therefore, PVP was kept a constant concentration of 10% to ensure the solution had the necessary viscosity to be electrospun independent of chitosan and PVA concentrations. Despite these efforts, not all formulations produced fibres. Successful concentration of chitosan solution in the blend formulations that could be electrospun were <70 % (<32 % dry weight of chitosan). The successful fabrication of fibres for formulations F10, F20, F30 and F50 suggests that they had chain entanglements greater than 2.5 entanglements per chain (Shenoy et al. 2005). Unlike in the present work, previous studies successfully electrospun polymer solutions containing dry weight ratio of chitosan greater than 32%. This disparity could be due to the higher concentration of chitosan solution used in these studies. In the present study, the total solute concentration decreased as the proportion of chitosan increased. This means that the number of chain entanglements also decreased as the chitosan component of each electrospinning solution increased where F70 had chain entanglements less than 2.5 entanglements per chain and was unable to produce a fibre. The parameters used for the generation of the 3DENS were a 10 ml syringe supplying polymer solution at a flow rate of 0.3 ml/h to a needle (0.51 mm inner diameter) connected to a positive electrode placed 15 cm away from a cylindrical collector; which was wrapped in aluminium foil connected to a negative electrode for the collection of nanofibers under varying amounts of voltage (between 15 kV and 20 kV). A

distance of 15 cm was used by all of the three studies that spun solutions containing chitosan, PVA and PVP (Aytimur and Uslu 2014, Gökmeşe, Uslu, and Aytimur 2013, Zhang et al. 2014). Table 9 provides a summary of the polymers, parameters, characterisation methods tested in this works. The studies focused on physical and chemical characterisations.

Table 9. Summary of previous work fabricating 3DENS using Chitosan, PVA and PVP

Polymer	Dry Weight Composition Ratio	Parameters	Tests	Application	Reference
10 % Chitosan (Mw: 400 kDa) 10 % PVA (Mw: 85k Da-146 kDa) 10 % PVP K-30 (Mw: 40 kDa)	CS/PVA/PVP 50/30/20 67/20/13	Needle size: n.s. Flow Rate: 0.5 ml/h Voltage: 20 kV Distance: 15 cm	SEM FTIR DSC Viscosity Conductivity Contact angle	Wound dressing	(Gökmeşe, Uslu, and Aytimur 2013)
10 % Chitosan (400 kDa) 10% PVA (Mw: 85 kDa-124 kDa) 10 % PVP K30 (Mw: 40 kDa)-	CS/PVA/PAA/PVP K30 20/31/40/9	Needle size: n.s. Flow Rate: 0.5 ml/h Voltage: 15-20 kV Distance: 15 cm	DSC FTIR SEM	Wound dressing	(Aytimur and Uslu 2014)

10 % Chitosan 10 % PVA 10 % PVP *No information on Mw*	CS/PVA/PVP 40/60/0 50/50/0 50/20/30	Needle size: 0.47 mm Flow Rate: n.s. Voltage: 9.5 kV Distance: 15 cm	SEM XRD FTIR	Tissue engineering Drug delivery	(Zhang et al.)

Mw= molecular weight, n.s. = not specified, kDa= kilodalton.

The minimum voltage needed to produce a continuous jet was used to spin each formulation followed by a higher voltage to compare the nanofiber structures produced using SEM micrographs. Gökmese et al., and Aytimur et al. showed SEM micrographs with similar fibre morphology of chitosan, PVA and PVP fibres that were similar to those demonstrated here (Aytimur and Uslu 2014, Gökmeşe, Uslu, and Aytimur 2013). The voltage required to produce a Taylor cone and continuous polymer jet increased as the proportion of chitosan in the solution increased. The polymer jet became more unstable as formulations with higher chitosan were spun. The voltage range used to produce the final 3DENS in this study was 15 kV for F10 which had the lowest amount of chitosan and increasing up to 20 kV for F50 which had the highest amount of chitosan. This range is consistent with voltage used in two of the previous work, however, the flow rate used in these studies were higher than the current study (0.5 ml/h and 0.3 ml/h) (Aytimur and Uslu 2014, Gökmeşe, Uslu, and Aytimur 2013). The molecular weight (Mw) of chitosan used in previously done studies was half the Mw of chitosan used in the present study (400 kDa and 800 kDa, respectively), so it would be expected that they would require a lower voltage to spin the solution. However, Gökmeşe and others used more than twice the concentration of chitosan than the current study (2013). On the other hand, Aytimur and others used 20 % dry weight concentration of chitosan which was comparable to F50 which had 17 % chitosan in dry weight but still used 15 kV-20 kV to produce a fibre despite having a lower molecular weight of chitosan (2014). Zhang and others used a voltage of 9.5 kV to produce fibres but did not provide information on the molecular weight of the polymers or the flow rate that was used (2014).

Chitosan had the lowest pH and highest conductivity from the three polymer solutions. Its proportional increase in the blend formulations caused an overall decrease in pH and increase in conductivity. In terms of conductivity, chitosan was 7 times more conductive than PVA and 34 times more conductive than PVP. Therefore, it is no surprise that the addition of chitosan had the greatest influence on increasing the conductivity of the blend formulations as a result of the protonation of –NH2 groups of chitosan in acetic acid aqueous solution (Çay, Miraftab, and Perrin Akçakoca Kumbasar 2014). F70 which was made up of 70 % chitosan solution had a similar pH to pure chitosan solution (3.96 and 3.88, respectively) and the same conductivity (3962 μS/cm). Its similarity to pure chitosan may be the reason for the lack of success in spinning this formulation which resulted in spraying in a powder form instead of collection of well-formed fibres.

The influence of conductivity on the morphology of the nanofibers are consistent with the literature which states that an increase in conductivity decreases fibre diameter (Ramakrishna et al. 2006). Thinner fibres are a result of an increased electrical force enhancing electrostatic repulsive force on the polymer jet (Aytimur and Uslu 2014). Similar to pure chitosan, the very high conductivity of F70 likely caused a negative effect on the Taylor cone and resulting in electro-spraying instead of polymer solution instead of fibres formation as seen in the SEM images in Figure 13 (Haider, Haider, and Kang 2018). A voltage of 23 kV was required to form a Taylor cone at a flow rate of 0.3 ml/h. Flow rate higher than 0.3 ml/h will demand a voltage higher than 23 kV in order to produce Taylor cone and polymer jet.

Polymer solutions contain molecules and particles; when put into motion, they are forced to slide along each other. The flow resistance caused by this internal friction is viscosity (Mezger 2006). In general, chitosan is very viscous and at 5 %- 10 % solution concentrations of chitosan, its addition to PVA/PVP blend would have increased the solution viscosity (Aytimur and Uslu 2014). However, because only a 2 % chitosan solution was use, when the proportion of chitosan solution increased in the formulation, the total solute concentration decreased as seen in Table 3 leading to a decrease in the viscosity of the blend formulations from F10 to F70. All the samples in this study displayed shear thinning behaviour, therefore its viscosity was reported at specific shear rate (200/s).

In higher viscosity spinning solutions, a higher number of chain-entanglements are present making it easier to produce a stable jet and obtain better fibres as seen for F10, which had the highest viscosity (Zhang et al. 2014). Haider et.al also stated that a decrease in viscosity leads to bead formation; this was observed in the SEM micrographs from the present study (Figure 13) (Haider, Haider, and Kang 2018). Smooth fibres were obtained for F10 which had the highest viscosity, and a higher number of beads were found in F20, F30 and F50.

The beads initially seen in F10 electrospun at 13 kV were removed when F10 was electrospun at 15 kV. Since all other parameters were maintained, the removal of beads can be attribute to the increase in voltage. Using voltages higher than 15 kV may produce fibres with smaller diameter (Sill and von Recum 2008). When voltage was increased from 15 kV to 18 kV at the same flowrate for F30, the beads became more circular indicating that the higher voltage caused more stretching resulting in thinner fibres. The formation of beaded fibres seen formulations F20 to F50 could also be attributed to the increase of repulsive forces between ionic groups (Çay, Miraftab, and Perrin Akçakoca Kumbasar 2014).

Overall, fibre diameter decreased from F10 to F50 which is consistent with the literature which states that fibre diameter decreases as the viscosity of the polymer solution decreases and as conductivity increases (Haider, Haider, and Kang 2018, Ramakrishna et al. 2006).

Analysis of fibre diameter showed that F10 produced thicker and linear fibres than all the other formulations. This finding is in line with the expected theoretical correlation between strong mechanical properties and structural integrity and is further supported by the frequency sweep data. The graphs showed that PVA displayed more elastic properties (Figure 12, B). This explains why F10, which had the highest PVA component, was able to form uniform fibres. The formulations with higher PVA component resisted deformation during the ES process and resulted in smoother fibres owing to PVA's structural integrity.

It should be noted that these measurements are true for a temperature around 20°C. It has been shown that G' dependence on ω changes with temperature while G" remains unaffected. PVA displays more viscous properties than elastic (G" > G') at higher temperatures (Bercea et al. 2020). This would be an important consideration of the fabrication of the 3DENS were to take place in hotter climates as electrospinning parameters would be affected if the viscoelastic properties of the polymer solutions change.

Formulation F10 which had the highest component of PVA, showed G' very close to G", hence it was able to store energy under deformation and create solid fibres as seen in the SEM analysis. As the component of PVA decreased from F10 to F70, G' and G" shifted further apart indicating that the viscous properties becoming more dominant.

5.2 Crosslinking of 3DENS

A thorough literature search yielded no results on crosslinking of chitosan, PVA or PVP using only heat without any added chemical crosslinkers. Our study thermally induced physical crosslinking in the 3DENS by applying heat at 120°C for 24 hours to increase the mechanical strength of our scaffolds, thus removing the need for toxic chemicals.

There were no clear differences observed in the FTIR peaks between the crosslinked and uncrosslinked 3DENS. One possible reason for this is that PVA and PVP peaks could be masking other peaks because the amount of chitosan used was minimal. However, the successful crosslinking of the 3DENS is evident from the degradation and swelling results seen in the study.

Our experiment exhibited the same colour change as Schiffman observed, which is, the mats changed colour from white (when spun) to yellow after crosslinking (Schiffman and Schauer 2007). Moreover, as the amount of chitosan in the 3DENS increased, the yellow

colour also became more saturated. The successful crosslinking of 3DENS are clearly supported by the swelling and degradation data. Crosslinked 3DENS degraded slower than uncrosslinked 3DENS due to having higher mechanical strength. As expected, a faster degradation rate was observed in 3DENS as the amount of chitosan in the formulation increased. Chitosan degrades much faster in physiological environment compared to PVA and PVP (Mahoney et al. 2012). The higher synthetic polymer concentration in lower chitosan containing 3DENS, contributes to their stronger mechanical properties and resistance to degradation. Schiffman et al, studied the degradation of uncrosslinked compared to crosslinked chitosan electrospun mats in acidic, neutral and basic environment and found that crosslinked scaffolds were able to resist degradation. The crosslinked chitosan scaffold survived all three environments where as the uncrosslinked scaffold only survived in basic environment (Schiffman and Schauer 2007).

Liu and others measured the degradation rate of crosslinked chitosan/gelatin and chitosan/gelatin/HA scaffolds and found a degradation rate of 46 % and 55 % at 14 days, respectively (Liu 2007). The scaffold in the previous study contained 20 % chitosan in dry weight ratio. The crosslinked 3DENS F50 in the current study is comparable to that (17 %) chitosan and showed a similar degradation rate of 42 % at day 14.

The commercially available Integra™ Matrix Wound Dressing (Integra Life Sciences) graft matrix degrades in 2-3 weeks leaving behind the silicone covering which can then be removed (Turner 2015). Crosslinking the membrane preserved the matrix's resistance to biodegradation and increased tensile strength. A similar outcome was observed in the present study. The crosslinked 3DENS fabricated in the present study displayed slower biodegradation compared to the uncrosslinked 3DENS and it was also easier to handle and did not break as easily. The rate of degradation for the 3DENS fabricated in the present study was 40%-60% at two weeks. However, the degradation rate of the 3DENS rate could be increased by manipulating polymers concentrations and testing different electrospinning parameters.

In this study, crosslinking was successfully used to preserve the matrix's resistance to biodegradation and increase tensile strength. The higher tensile strength means that the handling of the 3DENS would be easier for use in clinical settings. Moreover, in-vitro biological analysis using dermal tissue cell lines showed promising results for its use in dermal tissue engineering.

Swelling data was unobtainable for 3DENS with chitosan percentages greater than 30%, due to their delicate nature. F30 crosslinked was measurable but not F30 uncrosslinked given its weaker structural integrity compared to the crosslinked scaffold. Findings of the swelling study attests to the success of the crosslinking method used. Swelling data showed significantly higher water adsorption capability in crosslinked F30 compared to lower chitosan containing formulations. This finding is consistent with the literature that states that an increase in water adsorption capacity can be expected with increasing amounts of chitosan due to the presence of hydroxyl groups and amino groups of the chitosan which have strong affinity towards water (Smitha, Sridhar, and Khan 2004). Crosslinked 3DENS's were able to hold a significantly larger amount of water within its structure. The higher water adsorption capacity seen in crosslinked 3DENS compared to uncrosslinked 3DENS could be attributed to a higher number of functional hydrophilic groups created by crosslinking. This provides further evidence that the crosslinking method used was successful in crosslinking the 3DENS thereby creating a mechanically stronger scaffold. Moreover, the scaffolds in the present study showed higher swelling ratios than Çay et al. (2014). The increase in swelling ratio could be attributed to the lower heating temperature used being less damaging to the structure (Çay, Miraftab, and Perrin Akçakoca Kumbasar 2014). It is well known that wet environments are more suitable for wound healing. Crosslinked 3DENS fabricated in this study could provide the architecture and wet conditions required for optimal wound healing.

5.3 Analysis of Biological Compatibility of the 3DENS

The nano-dimensional porous structure created by the electrospinning technique resembles the native ECM of skin tissue. The porous nature of the scaffold should also encourage cell migration and provide cells with an increased number of sites for attachment and proliferation. The 3DENS fabricated in the current study displayed good structural integrity and mechanical properties. Therefore, they may be considered suitable as a substitute for skin tissue regeneration. In order to adequately represent human skin, fibroblasts and keratinocyte cell types were chosen to assess the biological activity of the 3DENS as they are the predominant cell types found in the dermis and epidermis, respectively. The HaCaT cell line was used in the study as it can be used for extended periods of time compared to primary cell lines. Dermal fibroblasts are available as the primary cell line NHDF (normal human dermal fibroblasts). HaCaT and NHDF were used as they were quick to culture and readily available. To our knowledge, chitosan/PVA/PVP 3DENS have not been studied *in vitro* for dermal tissue regeneration.

HaCaT and NHDF cell lines were both used perform the in vitro assays. The same experimental and environmental conditions were used with both cell lines. Three separate flasks for each of the cell lines were used to maintain n=3. Each test, MTT and Live/Dead cell assay, was reproduced three times using three different samples (n=3). Within each of those groups, the experiment was replicated and the results averaged to maintain triplicate.

The most important fact to note that based upon observations, both HaCaT and NHDF cells penetrated deeper layers of the 3DENS's. The gold standard of all scaffolds is that they have the ability to attract the cells and the cells are able to penetrate the structure and remain viable and proliferative. Both cell types were seen at different focal planes under the microscope indicating that they penetrated the scaffold.

Overall, HaCaT cells showed viability around 80% on all uncrosslinked 3DENS, above the 70% which is considered to be an acceptable criterion for viable proliferation. The viability levels remained at or higher than the controls of cells alone. The crosslinked scaffolds showed low HaCaT cell viability on F10 and F20 (<70 %) and good viability for F30 and F50 (>70 %) at 24 hours. The difference in viability between the crosslinked formulations were not significant at any time point. However, F10 CL was markedly lower than the control group at 72 hours. When comparing crosslinked to uncrosslinked 3DENS for the same formulations. There were no significant differences in performance between uncrosslinked and crosslinked 3DENS in terms of HaCaT cell viability. The results were very similar to the uncrosslinked and crosslinked control groups.

In terms of proliferation, HaCaT cells showed higher proliferation with increasing amounts of chitosan in uncrosslinked 3DENS (F10 to F50) at 24 and 48 hours. F20 UCL to F50 UCL were higher than the control group. However, at 72 hours, the opposite was observed. F10 had the lowest proliferation rate at 48 hours, maintained its number of cells and was the highest rate at 72 hours. The number of HaCaT cells decreased as the amount of chitosan in uncrosslinked 3DENS increased at 72 hours. In the crosslinked samples, there were no significant differences between any of the crosslinked 3DENS at any time point. At 72 hours, F20, F30 and F50 appeared to perform better than F10 but all values remained around the cell numbers in the control group.

For NHDF cell viability on uncrosslinked scaffolds, at 72 hours, F20 UCL, F30 UCL, and F50 UCL all showed good cell viability (>70 %). In the crosslinked 3DENS, F10 CL initially showed low cell viability however, it was significantly higher than other 3DENS at 72 hours. In terms of overall cell viability when comparing uncrosslinked 3DENS to crosslinked 3DENS, the uncrosslinked scaffolds showed significantly higher NHDF cell viability; where formulations F20, F30 and F50 showed the best NHDF cell viability at 72 hours. Due to its positive charges, chitosan is a bio-adhesive (He, Davis, and Illum 1998). This could attribute to the higher number of viable cells counted in the uncrosslinked scaffolds which had more chitosan available to interact with NHDF cells.

The proliferation of NHDF on uncrosslinked 3DENS initially showed no significant differences between the 3DENS at 24 and 72 hours. At 48 hours, F30 UCL had a significantly higher cell count, however, by 72 hours, it appeared to have the lowest. In crosslinked scaffolds, NHDF proliferation was low for all 3DENS but gradually increased by 72 hours. There were no significant differences between the 3DENS although the number of cells increased on crosslinked 3DENS as the amount of chitosan increased. When comparing the proliferation of NHDF on uncrosslinked 3DENS compared to crosslinked 3DENS, the crosslinked 3DENS reported much higher cell counts than uncrosslinked. However, this finding was not significant.

Abdull Rasad and others performed cell viability assay using NHDF cells on chitosan/PVP sheets and found that chitosan containing sheets (3-5% chitosan) showed significantly higher cell viability compared to the control at 24 hours. They also saw a higher cell viability at 48 and 72 hours, however this was not significantly different to the control (Abdull Rasad 2010).Although it was not significant, a similar trend was seen in the current study; uncrosslinked 3DENS with chitosan in the range of 2-5% showed higher cell viability at 24, 48 and 72 hours compared to control.

The author was unable to find in-vitro studies for the commercially available Integra™ Matrix Wound Dressing (Integra Life Sciences). It could be possible that since the product was studied in the 1980's, that such a study does not exist. Results of in-vitro analysis performed on the 3DENS fabricated in the current study using two dermal cell lines strongly suggests that the environment is suitable for supporting dermal tissue regeneration.

The overall finding of this cytotoxicity study seemed to be that all formulations proliferated at a similar rate and had a similar viability to the cells only control. The cells whether in the presence of the crosslinked or uncrosslinked scaffold remained at similar levels. The cells penetrated through the scaffold indicating that the 3DENS environment was favourable for cell viability and growth. Crosslinked chitosan/PVA/PVP 3DENS could potentially serve as a template for the construction of a synthesised "neodermis" by slowly biodegrading and being reabsorbed by the body over several months.

5.4 Conclusion

A three dimensional nanofibrous scaffold (3DENS) using a combination of chitosan, PVA and PVP using electrospinning was fabricated. The method used to thermally induce physical crosslinking in the 3DENS was successful and improved the hydrophilicity and mechanical properties of the 3DENS. The crosslinked scaffolds exhibit similar biological properties compared to the uncrosslinked scaffolds and the control group. The cells successfully penetrated into deeper layers in the 3D scaffold.

The electrospinning technique was used in this project due to its ability to produce porous scaffolds in the nano-dimension. Moreover, electrospinning is relatively cheap compared to other nano-fabrication technology and is able to mass produce scaffolds. Cost-effectiveness is an important consideration for the clinical translation of the product to low- and middle-income countries where resources are limited. Chitosan was selected for its biological advantages. Chitosan comes from the crustacean shell which a renewable resource and adds value to waste material. However, it is difficult to electrospin chitosan on its own and carrier polymers, PVA and PVP, were used in order to make spinning easier.

The proportion of chitosan in the electrospinning solution had the greatest effect on the pH and conductivity of the solutions. Rheological studies of the polymer solutions revealed that PVA behaved as a structured solid therefore, had the greatest influence on the viscosity of the solution. All blend formulations behaved like shear-thinning fluids. The voltage required to produce a Taylor cone with a continuous jet increased as the amount of chitosan

in the formulation increased. All 3DENS fibres were in the submicron size ranging with the average fibre diameter decreasing from 0.22 ηm to 0.05 ηm, from formulations F10 to F50. The addition of chitosan to 3DENS increased the rate of degradation in the scaffolds. Heat was successfully used to crosslink the 3DENS's. Thermally crosslinking chitosan, PVA and PVP 3DENS resulted in a mechanically stronger yet more hydrophilic scaffolds which is an advantage for wound healing applications. Moreover, all chitosan containing 3DENS scaffolds displayed good cell attachment, viability and proliferation. Chitosan containing skin tissue scaffolds would be able to increase retention of the scaffold at the wound site and its porous nature could encourage cell infiltration to deeper layers of the scaffold, enhancing wound healing.

5.5 Limitations

The method used to conduct swelling studies is typically the method used by most researchers in the field (Gu et al. 2009). However, this study design is not capable of measuring the swelling of very delicate 3DENS due to the scaffold breaking into pieces too small to handle. The wet 3DENS also have a tendency to stick to the filter paper during the blotting step for removing excess water. This can affect the final reading in two ways; it can increase the final weight reading due to the wet scaffold picking up fibres from the filter paper or it could reduce the final weight reading due to some of the scaffold staying behind on the filter paper during removal. Better methods need to be established to overcome the handling challenges faced when 3DENS are in wet condition. One possible solution to overcome this challenge is by using transwells which have a mesh like structure at the bottom of the insert well. This removes the need for handling the 3DENS as it can be sieved.

The 3DENS in the current study were difficult to peel from the aluminium foil. One reason for this could be that the 3DENS produced in this study were very light. For removal, the 3DENS was wet first with PBS after which it could be peeled off the aluminium foil easily. As the amount of chitosan increased, the 3DENS became more difficult to handle in wet condition. This is also evident from the images of the 3DENS submerged in PBS in day 7 swelling images. One way to overcome this challenge is to produce thicker scaffolds.

5.6 Future Direction

The results from this study can contribute substantially to the field of dermal tissue engineering and in particular, to encourage the use of physical crosslinking method to stabilise chitosan containing scaffolds instead of using chemical crosslinkers.

The intrinsic antimicrobial strength of chitosan before and after crosslinking need to be investigate using microbiological techniques. Furthermore, longer term degradation needs to be conducted to determine the kinetic degradation profile of the 3DENS from one hundred percent to fully degraded to be able to manipulate formulations and crosslinking strength in order to obtain desired degradation time.

The porous nature of the scaffolds in the current study encouraged cell infiltration into deeper layers. The manipulation of electrospinning parameters to obtain fibres of different morphology (e.g. fibre diameter, pore size, surface texture) for each formulation in order to investigate the cell attachment and proliferation should be investigated. It has also been stated in the literature that interconnected pores result in better angiogenesis. Angiogenesis should be investigated using immunohistological methods.

Crosslinked 3DENS showed excellent water retention capacity which is desirable as it now a well-known fact that moist environments result in better wound healing outcomes. The current study established the suitability of chitosan/PVA/PVP 3DENS for cell viability and growth. However, these results need to be further supported by studies in established burn wound models and with animal studies to determine clinical translation opportunities. In-vivo experiments should also be carried out to investigate effects of 3DENS on growth factor production and cell signals.

While the use of chitosan in wound dressing has been approved by the FDA, it has not yet been approved for drug delivery, despite the numerous amounts of studies showing the positive benefits of chitosan containing scaffolds (Kean and Thanou 2010). Due to this, there are translational challenges that would first need to be addressed to get this product on the market.

6.0 References

Abdull Rasad, M. S. B., A. S. Halim, K. Hashim, A. H. A. Rashid, N. Yusof and S. Shamsuddin (2010). "In vitro evaluation of novel chitosan derivatives sheet and paste cytocompatibility on human dermal fibroblasts." Carbohydrate Polymers **79**(4): 1094-1100.

Alves, M. H., B. E. Jensen, A. A. Smith, and A. N. Zelikin. 2011. "Poly(vinyl alcohol) physical hydrogels: new vista on a long serving biomaterial." *Macromol Biosci* 11 (10):1293-313. doi: 10.1002/mabi.201100145.

Anderson, James M. 2019. "Biocompatibility and bioresponse to biomaterials." In *Principles of Regenerative Medicine*, 675-694. Elsevier.

Aotearoa, Safekids. 2015. "Child unintentional deaths and injuries in New Zealand, and prevention strategies." *Auckland, NZ: Safekids Aotearoa*.

Aytimur, Arda, and İbrahim Uslu. 2014. "Promising materials for wound dressing: PVA/PAA/PVP electrospun nanofibers." *Polymer-Plastics Technology and Engineering* 53 (7):655-660.

Aziz, Z., S. F. Abu, and N. J. Chong. 2012. "A systematic review of silver-containing dressings and topical silver agents (used with dressings) for burn wounds." *Burns* 38 (3):307-318. doi: https://doi.org/10.1016/j.burns.2011.09.020.

Azzopardi, Ernest A, Elayne Azzopardi, Liberato Camilleri, Jorge Villapalos, Dean E Boyce, Peter Dziewulski, William A Dickson, and Iain S Whitaker. 2014. "Gram negative wound infection in hospitalised adult burn patients-systematic review and metanalysis." *PloS one* 9 (4):e95042-e95048.

Bae, Hyun-Su, Adnan Haider, KM Kamruzzaman Selim, Dong-Yoon Kang, Eun-Jin Kim, and Inn-Kyu Kang. 2013. "Fabrication of highly porous PMMA electrospun fibers and their application in the removal of phenol and iodine." *Journal of Polymer Research* 20 (7):158-163.

Banyard, Derek A, Jenna Martin Bourgeois, Alan D Widgerow, and Gregory RD Evans. 2015. "Regenerative biomaterials: a review." *Plastic and reconstructive surgery* 135 (6):1740-1748.

Barbosa, D. B., A. M. Agostinho Hunt, A. Berretta, E. Rodrigues de Camargo, L. F. Gorup, D. R. Monteiro, G. L. Fernandes, R. A. Fernandes, and K. R. Kirker. 2016. "The

importance of preventing and controlling biofilm in wounds: Biofilm models and nanotechnology in antibiofilm approaches." In *Wound Healing Biomaterials*, edited by Magnus S. Ågren, 79-105. Woodhead Publishing.

Bedane, Alemayehu H, Mladen Eić, Madjid Farmahini-Farahani, and Huining Xiao. 2016. "Theoretical modeling of water vapor transport in cellulose-based materials." *Cellulose* 23 (3):1537-1552.

Bellas, Evangelia, Miri Seiberg, Jonathan Garlick, and David L. Kaplan. 2012. "In vitro 3D Full-Thickness Skin-Equivalent Tissue Model Using Silk and Collagen Biomaterials." *Macromolecular Bioscience* 12 (12):1627-1636. doi: 10.1002/mabi.201200262.

Beppu, MM, RS Vieira, CG Aimoli, and CC Santana. 2007. "Crosslinking of chitosan membranes using glutaraldehyde: Effect on ion permeability and water absorption." *Journal of membrane science* 301 (1-2):126-130.

Bercea, Maria, Luiza Madalina Gradinaru, Ioana-Alexandra Plugariu, Mihaela Mandru, and Daniel Laurentiu Tigau. 2020. "Viscoelastic behaviour of self-assembling polyurethane and poly(vinyl alcohol)." *Polymer International* 69 (2):149-155. doi: 10.1002/pi.5928.

Bernstein, EF, CB Underhill, PJ Hahn, DB Brown, and J Uitto. 1996. "Chronic sun exposure alters both the content and distribution of dermal glycosaminoglycans." *British Journal of Dermatology* 135 (2):255-262.

Burke, John F, Ioannis V Yannas, William C Quinby Jr, Conrado C Bondoc, and Walter K Jung. 1981. "Successful use of a physiologically acceptable artificial skin in the treatment of extensive burn injury." *Annals of surgery* 194 (4):413.

Boateng, J., and O. Catanzano. 2015. "Advanced Therapeutic Dressings for Effective Wound HealingA Review." *Journal of Pharmaceutical Sciences* 104 (11):3653-3680. doi: 10.1002/jps.24610.

Cabral, Jaydee D., Marina Roxburgh, Zheng Shi, Liqi Liu, Michelle McConnell, Gail Williams, Natasha Evans, Lyall R. Hanton, Jim Simpson, Stephen C. Moratti, Brian H. Robinson, Peter J. Wormald, and Simon Robinson. 2014. "Synthesis, physiochemical characterization, and biocompatibility of a chitosan/dextran-based hydrogel for postsurgical adhesion prevention." *Journal of Materials Science: Materials in Medicine* 25 (12):2743-2756. doi: 10.1007/s10856-014-5292-3.

Çay, Ahmet, Mohsen Miraftab, and E. Perrin Akçakoca Kumbasar. 2014. "Characterization and swelling performance of physically stabilized electrospun poly(vinyl alcohol)/chitosan nanofibres." *European Polymer Journal* 61:253-262. doi: https://doi.org/10.1016/j.eurpolymj.2014.10.017.

Chong, Ee Jay, Than Thang Phan, Ivor Jinn Lim, YZ Zhang, Boom Huat Bay, Seeram Ramakrishna, and Chwee Teck Lim. 2007. "Evaluation of electrospun PCL/gelatin nanofibrous scaffold for wound healing and layered dermal reconstitution." *Acta biomaterialia* 3 (3):321-330.

Chua, Alvin Wen Choong, Yik Cheong Khoo, Bien Keem Tan, Kok Chai Tan, Chee Liam Foo, and Si Jack Chong. 2016. "Skin tissue engineering advances in severe burns: review and therapeutic applications." *Burns & trauma* 4 (1):3-16.

Costa-Júnior, Ezequiel de Souza , Marivalda M Pereira, and Herman S Mansur. 2009. "Properties and biocompatibility of chitosan films modified by blending with PVA and chemically crosslinked." *Journal of Materials Science: Materials in Medicine* 20 (2):553-561.

Cruz-Maya, Iriczalli, Vincenzo Guarino, Argelia Almaguer-Flores, Marco A Alvarez-Perez, Alessio Varesano, and Claudia Vineis. 2019. "Highly polydisperse keratin rich nanofibers: Scaffold design and in vitro characterization." *Journal of Biomedical Materials Research Part A* 107 (8):1803-1813.

D'Avignon, L. C., B. K. Hogan, C. K. Murray, F. L. Loo, D. R. Hospenthal, L. C. Cancio, S. H. Kim, E. M. Renz, D. Barillo, J. B. Holcomb, C. E. Wade, and S. E. Wolf. 2010. "Contribution of bacterial and viral infections to attributable mortality in patients with severe burns: An autopsy series." *Burns* 36 (6):773-779. doi: 10.1016/j.burns.2009.11.007.

Dantzer, Eric, and Fabienne M Braye. 2001. "Reconstructive surgery using an artificial dermis (Integra): results with 39 grafts." *British journal of plastic surgery* 54 (8):659-664.

Dhariwala, Busaina, Elaine Hunt, and Thomas Boland. 2004. "Rapid prototyping of tissue-engineering constructs, using photopolymerizable hydrogels and stereolithography." *Tissue engineering* 10 (9-10):1316-1322.

Dieckmann, Christina, Regina Renner, Linda Milkova, and Jan C Simon. 2010. "Regenerative medicine in dermatology: biomaterials, tissue engineering, stem cells, gene transfer and beyond." *Experimental dermatology* 19 (8):697-706.

Ding, Jianxun, Jin Zhang, Jiannan Li, Di Li, Chunsheng Xiao, Haihua Xiao, Huanghao Yang, Xiuli Zhuang, and Xuesi Chen. 2019. "Electrospun polymer biomaterials." *Progress in Polymer Science* :1-34.

Fabienne, B, H Daniel, D Odile, M Michel, H Benjamin, and C Hanane. 2007. "Development of a new bilayer dermal matrix, RENOSKIN®: preclinical data." *Burns* 1 (33):S105.

Farroha, A., Q. Frew, N. El-Muttardi, B. Philp, and P. Dziewulski. 2013. "The use of Biobrane® to dress split-thickness skin graft in paediatric burns." *Annals of burns and fire disasters* 26 (2):94-97.

Gandhi, Neha S, and Ricardo L Mancera. 2008. "The structure of glycosaminoglycans and their interactions with proteins." *Chemical biology & drug design* 72 (6):455-482.

Gökmeşe, Faruk, İbrahim Uslu, and Arda Aytimur. 2013. "Preparation and characterization of PVA/PVP nanofibers as promising materials for wound dressing." *Polymer-Plastics Technology and Engineering* 52 (12):1259-1265.

Gu, Shu-Ying, Zhi-Mei Wang, Jie Ren, and Chun-Yan Zhang. 2009. "Electrospinning of gelatin and gelatin/poly (l-lactide) blend and its characteristics for wound dressing." *Materials Science and Engineering: C* 29 (6):1822-1828.

Gurtner, Geoffrey C., Sabine Werner, Yann Barrandon, and Michael T. Longaker. 2008. "Wound repair and regeneration." *Nature* 453 (7193):314-321. doi: 10.1038/nature07039.

Haider, Adnan, Sajjad Haider, and Inn-Kyu Kang. 2018. "A comprehensive review summarizing the effect of electrospinning parameters and potential applications of nanofibers in biomedical and biotechnology." *Arabian Journal of Chemistry* 11 (8):1165-1188.

Haider, Sajjad, Yousef Al-Zeghayer, Fekri A Ahmed Ali, Adnan Haider, Asif Mahmood, Waheed A Al-Masry, Muhammad Imran, and Muhammad Omer Aijaz. 2013. "Highly aligned narrow diameter chitosan electrospun nanofibers." *Journal of Polymer Research* 20 (4):105-112.

Hansbrough, John F, Christine Doré, and Wendy B Hansbrough. 1992. "Clinical trials of a living dermal tissue replacement placed beneath meshed, split-thickness skin grafts on excised burn wounds." *The Journal of burn care & rehabilitation* 13 (5):519-529.

He, Ping, Stanley S Davis, and Lisbeth Illum. 1998. "In vitro evaluation of the mucoadhesive properties of chitosan microspheres." *International journal of pharmaceutics* 166 (1):75-88.

Helander, IM, E-L Nurmiaho-Lassila, Raija Ahvenainen, J Rhoades, and Sibel Roller. 2001. "Chitosan disrupts the barrier properties of the outer membrane of Gram-negative bacteria." *International journal of food microbiology* 71 (2-3):235-244.

Hosseini, Seyed Nejat, Seyed Nouraddin Mousavinasab, and Mojtaba Fallahnezhat. 2007. "Xenoderm dressing in the treatment of second degree burns." *Burns* 33 (6):776-781.

Issler-Fisher, Andrea C, Richard M Fakin, Oliver M Fisher, Genevieve McKew, Riccardo Gazzola, Ann-Kathrin Rauch, Thomas Gottlieb, Peter Haertsch, Merlin Guggenheim, and Pietro Giovanoli. 2016. "Microbiological findings in burn patients treated in a general versus a designated intensive care unit: Effect on length of stay." *Burns* 42 (8):1805-1818.

Jahromi, Mirza Ali Mofazzal, Parham Sahandi Zangabad, Seyed Masoud Moosavi Basri, Keyvan Sahandi Zangabad, Ameneh Ghamarypour, Amir R Aref, Mahdi Karimi, and Michael R Hamblin. 2018. "Nanomedicine and advanced technologies for burns: preventing infection and facilitating wound healing." *Advanced drug delivery reviews* 123:33-64.

Jia, Yong-Tang, Jian Gong, Xiao-Hua Gu, Hark-Yong Kim, Jiong Dong, and Xin-Yuan Shen. 2007. "Fabrication and characterization of poly (vinyl alcohol)/chitosan blend nanofibers produced by electrospinning method." *Carbohydrate polymers* 67 (3):403-409.

Kang, Taek Won, Gopalakrishnan Chandrasekaran, Eu Chang Hwang, Hye Su Kim, and Vinoth-Kumar Lakshmanan. 2018. "Characterization and antibacterial activity of PVA–PVP–CS carvacrol-loaded polymer composite films for urinary catheter." *International Journal of Polymeric Materials and Polymeric Biomaterials* 67 (17):1016-1027. doi: 10.1080/00914037.2017.1417286.

Kean, T., and M. Thanou. 2010. "Biodegradation, biodistribution and toxicity of chitosan." *Advanced Drug Delivery Reviews* 62 (1):3-11. doi: https://doi.org/10.1016/j.addr.2009.09.004.

Keskin, Zalike, Aylin Sendemir Urkmez, and E Esin Hames. 2017. "Novel keratin modified bacterial cellulose nanocomposite production and characterization for skin tissue engineering." *Materials Science and Engineering: C* 75:1144-1153.

Khalil, HPS Abdul, Y Davoudpour, AH Bhat, Enih Rosamah, and Paridah Md Tahir. 2015. "Electrospun cellulose composite nanofibers." In *Handbook of polymer nanocomposites. Processing, performance and application*, 191-227.

Ki, Chang Seok, Doo Hyun Baek, Kyung Don Gang, Ki Hoon Lee, In Chul Um, and Young Hwan Park. 2005. "Characterization of gelatin nanofiber prepared from gelatin–formic acid solution." *Polymer* 46 (14):5094-5102.

Ku, Nam-On, and M Bishr Omary. 2006. "A disease-and phosphorylation-related nonmechanical function for keratin 8." *The Journal of cell biology* 174 (1):115-125.

Lam, Ping K, Eric SY Chan, Edward WH To, Chi H Lau, Siu C Yen, and Walter WK King. 1999. "Development and evaluation of a new composite Laserskin graft." *Journal of Trauma and Acute Care Surgery* 47 (5):918.

Landers, R, A Pfister, U Hübner, H John, R Schmelzeisen, and R Mülhaupt. 2002. "Fabrication of soft tissue engineering scaffolds by means of rapid prototyping techniques." *Journal of materials science* 37 (15):3107-3116.

Laudenslager, Michael J, and Wolfgang M Sigmund. 2012. "Electrospinning." *Encyclopedia of nanotechnology*:769-775.

Lee, Jaehong, Hyukho Kwon, Jungmok Seo, Sera Shin, Ja Hoon Koo, Changhyun Pang, Seungbae Son, Jae Hyung Kim, Yong Hoon Jang, and Dae Eun Kim. 2015. "Conductive fiber-based ultrasensitive textile pressure sensor for wearable electronics." *Advanced materials* 27 (15):2433-2439.

Lee, Kuen Yong, and David J Mooney. 2001. "Hydrogels for tissue engineering." *Chemical reviews* 101 (7):1869-1880.

Li, Jie, Juan Chen, and Robert Kirsner. 2007. "Pathophysiology of acute wound healing." *Clinics in Dermatology* 25 (1):9-18. doi: https://doi.org/10.1016/j.clindermatol.2006.09.007.

Li, Z, and C Wang. 2013. Effects of Working Parameters on Electrospinning, One-Dimensional Nanostructures, One-Dimensional Nanostructures, Chapter 2. Springer, Berlin.

Liu, Haifeng, Yuji Yin, and Kangde Yao. 2007. "Construction of Chitosan—Gelatin—Hyaluronic Acid Artificial Skin In Vitro." *Journal of biomaterials applications* 21 (4):413-430.

Liu, Yunyun, Lie Ma, and Changyou Gao. 2012. "Facile fabrication of the glutaraldehyde cross-linked collagen/chitosan porous scaffold for skin tissue engineering." *Materials Science and Engineering: C* 32 (8):2361-2366. doi: https://doi.org/10.1016/j.msec.2012.07.008.

Liu, Qin, Yaobing Wang, Liming Dai, and Jiannian Yao. 2016. "Scalable Fabrication of Nanoporous Carbon Fiber Films as Bifunctional Catalytic Electrodes for Flexible Zn-Air Batteries." *Advanced Materials* 28 (15):3000-3006.

Lou, Ching-Wen. 2008. "Process technology and properties evaluation of a chitosan-coated Tencel/cotton nonwoven fabric as a wound dressing." *Fibers and Polymers* 9 (3):286-292.

Lou, Ching-Wen, Chun-Hsu Yao, Yueh-Sheng Chen, Tsung-Chih Hsieh, Jia-Horng Lin, and Wen-Hao Hsing. 2008. "Manufacturing and properties of PLA absorbable surgical suture." *Textile Research Journal* 78 (11):958-965.

Ma, Hui, Jiajia Shen, Jianda Cao, Dongsheng Wang, Binbin Yue, Zhiping Mao, Wen Wu, and Huanxia Zhang. 2017. "Fabrication of wool keratin/polyethylene oxide nano-membrane from wool fabric waste." *Journal of Cleaner Production* 161:357-361.

MacLeod, TM, A Cambrey, G Williams, R Sanders, and CJ Green. 2008. "Evaluation of Permacol™ as a cultured skin equivalent." *Burns* 34 (8):1169-1175.

MacNeil, Sheila. 2007. "Progress and opportunities for tissue-engineered skin." *Nature* 445 (7130):874-889.

Mahoney, Christopher, MB McCullough, J Sankar, and N Bhattarai. 2012. "Nanofibrous structure of chitosan for biomedical applications." *Journal of Nanomedicine and Biotherapeutic Discovery* 2 (1):1-9.

Malik, Rafi, Tarun Garg, Amit K Goyal, and Goutam Rath. 2015. "Polymeric nanofibers: targeted gastro-retentive drug delivery systems." *Journal of drug targeting* 23 (2):109-124.

Matabola, KP, and RM Moutloali. 2013. "The influence of electrospinning parameters on the morphology and diameter of poly (vinyledene fluoride) nanofibers-effect of sodium chloride." *Journal of Materials Science* 48 (16):5475-5482.

McKittrick, J, P-Y Chen, SG Bodde, W Yang, EE Novitskaya, and MA Meyers. 2012. "The structure, functions, and mechanical properties of keratin." *Jom* 64 (4):449-468.

Megelski, Silke, Jean S Stephens, D Bruce Chase, and John F Rabolt. 2002. "Micro-and nanostructured surface morphology on electrospun polymer fibers." *Macromolecules* 35 (22):8456-8466.

Mezger, Thomas G. 2006. The rheology handbook: for users of rotational and oscillatory rheometers: Vincentz Network GmbH & Co KG: 29-34.

Mi, Fwu-Long, Yu-Chiun Tan, Hsiang-Fa Liang, and Hsing-Wen Sung. 2002. "In vivo biocompatibility and degradability of a novel injectable-chitosan-based implant." *Biomaterials* 23 (1):181-191. doi: https://doi.org/10.1016/S0142-9612(01)00094-1.

Min, Jang Hwan, In Sik Yun, Dae Hyun Lew, Tai Suk Roh, and Won Jai Lee. 2014. "The use of matriderm and autologous skin graft in the treatment of full thickness skin defects." *Archives of plastic surgery* 41 (4):330-336. doi: 10.5999/aps.2014.41.4.330.

Moghaddam, A. S., A. Raji, J. Movaffagh, A. T. Yazdi, and M. Mahmoudi. 2014. "Effects of autologous keratinocyte cell spray with and without chitosan on third degree burn healing: an animal experiment." *Wounds* 26 (4):109-17.

Nadri, Samad, Fatemeh Nasehi, and Ghasem Barati. 2017. "Effect of parameters on the quality of core-shell fibrous scaffold for retinal differentiation of conjunctiva mesenchymal stem cells." *Journal of Biomedical Materials Research Part A* 105 (1):189-197.

Nathoo, Rajiv, Nicole Howe, and George Cohen. 2014. "Skin substitutes: an overview of the key players in wound management." *The Journal of clinical and aesthetic dermatology* 7 (10):44-48.

Nho, YC, and KR Park. 2002. "Preparation and properties of PVA/PVP hydrogels containing chitosan by radiation." *Journal of Applied Polymer Science* 85 (8):1787-1794.

Noordenbos, John, Christine Doré, and John F Hansbrough. 1999. "Safety and efficacy of TransCyte* for the treatment of partial-thickness burns." *Journal of burn care & rehabilitation* 20 (4):275-281.

Park, Ju-Young, and In-Hwa Lee. 2010. "Relative humidity effect on the preparation of porous electrospun polystyrene fibers." *Journal of nanoscience and nanotechnology* 10 (5):3473-3477.

Park, Mira, Hye Kyoung Shin, Gopal Panthi, Mohammad Mahbub Rabbani, Al-Mahmnur Alam, Jawun Choi, Hea-Jong Chung, Seong-Tshool Hong, and Hak-Yong Kim. 2015.

"Novel preparation and characterization of human hair-based nanofibers using electrospinning process." *International journal of biological macromolecules* 76:45-48.

Pelipenko, Jan, Julijana Kristl, Biljana Janković, Saša Baumgartner, and Petra Kocbek. 2013. "The impact of relative humidity during electrospinning on the morphology and mechanical properties of nanofibers." *International journal of pharmaceutics* 456 (1):125-134.

Peltola, Sanna M., Ferry P. W. Melchels, Dirk W. Grijpma, and Minna Kellomäki. 2008. "A review of rapid prototyping techniques for tissue engineering purposes." *Annals of Medicine* 40 (4):268-280. doi: 10.1080/07853890701881788.

Percival, Nicholas J. 2002. "Classification of wounds and their management." *Surgery (Oxford)* 20 (5):114-117.

Pillay, Viness, Clare Dott, Yahya E Choonara, Charu Tyagi, Lomas Tomar, Pradeep Kumar, Lisa C du Toit, and Valence MK Ndesendo. 2013. "A review of the effect of processing variables on the fabrication of electrospun nanofibers for drug delivery applications." *Journal of Nanomaterials*:1-22 .

Pirayesh, Ali, Henk Hoeksema, Cornelia Richters, Jozef Verbelen, and Stan Monstrey. 2015. "Glyaderm® dermal substitute: Clinical application and long-term results in 55 patients." *Burns* 41 (1):132-144. doi: https://doi.org/10.1016/j.burns.2014.05.013.

Ramakrishna, Seeram, Kazutoshi Fujihara, Wee-Eong Teo, Thomas Yong, Zuwei Ma, and Ramakrishna Ramaseshan. 2006. "Electrospun nanofibers: solving global issues." *Materials today* 9 (3):40-50.

Ranjha, Nazar Mohammad, and Samiullah Khan. 2013. "Chitosan/Poly (vinyl alcohol) based hydrogels for biomedical applications: A review." *Journal of Pharmacy and Alternative Medicine* 2 (1):30-41.

Salbach, Juliane, Tilman D. Rachner, Martina Rauner, Ute Hempel, Ulf Anderegg, Sandra Franz, Jan-Christoph Simon, and Lorenz C. Hofbauer. 2012. "Regenerative potential of glycosaminoglycans for skin and bone." *Journal of Molecular Medicine* 90 (6):625-635. doi: 10.1007/s00109-011-0843-2.

Salmon, J. K., C. A. Armstrong, and J. C. Ansel. 1994. "The skin as an immune organ." *Western Journal of Medicine* 160 (2):146-152.

Schiffman, Jessica D, and Caroline L Schauer. 2007. "Cross-linking chitosan nanofibers." *Biomacromolecules* 8 (2):594-601.

Schindelin, Johannes, Ignacio Arganda-Carreras, Erwin Frise, Verena Kaynig, Mark Longair, Tobias Pietzsch, Stephan Preibisch, Curtis Rueden, Stephan Saalfeld, and Benjamin Schmid. 2012. "Fiji: an open-source platform for biological-image analysis." *Nature methods* 9 (7):676-682.

Schurr, Michael J, Kevin N Foster, John M Centanni, Allen R Comer, April Wicks, Angela L Gibson, Christina L Thomas-Virnig, Sandy J Schlosser, Lee D Faucher, and Mary A Lokuta. 2009. "Phase I/II clinical evaluation of StrataGraft: a consistent, pathogen-free human skin substitute." *The Journal of trauma* 66 (3):866-872.

Schwarze, H., M. Kuntscher, C. Uhlig, H. Hierlemann, L. Prantl, C. Ottomann, and B. Hartmann. 2008. "Suprathel, a new skin substitute, in the management of partial-thickness burn wounds: results of a clinical study." *Annals of Plastic Surgery* 60 (2):181-5. doi: 10.1097/SAP.0b013e318056bbf6.

Shahrokhi, Shahriar, Anna Arno, and Marc G. Jeschke. 2014. "The use of dermal substitutes in burn surgery: acute phase." *Wound repair and regeneration : official publication of the Wound Healing Society [and] the European Tissue Repair Society* 22 (1):14-22. doi: 10.1111/wrr.12119.

Shang, Jing-Ran, Shuang-Ling Zhong, Ye Zhao, Bin Wang, Yu-Shan Gao, Wen-Tao Xiang, and Xue-Jun Cui. 2020. "Preparation of chitosan-modified core–shell SiO2-acidic polymer multiple crosslinked membranes." *Journal of Applied Polymer Science* 137 (13):48494. doi: 10.1002/app.48494.

Shavandi, Amin, Alaa El-Din A Bekhit, Zhifa Sun, Azam Ali, and Maree Gould. 2015. "A novel squid pen chitosan/hydroxyapatite/β-tricalcium phosphate composite for bone tissue engineering." *Materials Science and Engineering: C* 55:373-383.

Shenoy, Suresh L., W. Douglas Bates, Harry L. Frisch, and Gary E. Wnek. 2005. "Role of chain entanglements on fiber formation during electrospinning of polymer solutions: good solvent, non-specific polymer–polymer interaction limit." *Polymer* 46 (10):3372-3384. doi: https://doi.org/10.1016/j.polymer.2005.03.011.

Shevchenko, Rostislav V, Stuart L James, and S Elizabeth James. 2009. "A review of tissue-engineered skin bioconstructs available for skin reconstruction." *Journal of the royal Society Interface* 7 (43):229-258.

Sill, Travis J, and Horst A von Recum. 2008. "Electrospinning: applications in drug delivery and tissue engineering." *Biomaterials* 29 (13):1989-2006.

Smitha, B, S Sridhar, and AA Khan. 2004. "Polyelectrolyte complexes of chitosan and poly (acrylic acid) as proton exchange membranes for fuel cells." *Macromolecules* 37 (6):2233-2239.

Still, Joseph, Paul Glat, Paul Silverstein, John Griswold, and David Mozingo. 2003. "The use of a collagen sponge/living cell composite material to treat donor sites in burn patients." *Burns* 29 (8):837-841.

Strbo, Natasa, Natalie Yin, and Olivera Stojadinovic. 2014. "Innate and adaptive immune responses in wound epithelialization." *Advances in wound care* 3 (7):492-501.

Subramanian, Uma Maheshwari, Samuel Vasanth Kumar, Naveen Nagiah, and Uma Tiruchirapally Sivagnanam. 2014. "Fabrication of polyvinyl alcohol-polyvinylpyrrolidone blend scaffolds via electrospinning for tissue engineering applications." *International Journal of Polymeric Materials and Polymeric Biomaterials* 63 (9):476-485.

Tabilo-Munizaga, Gipsy, and Gustavo V Barbosa-Cánovas. 2005. "Rheology for the food industry." *Journal of food engineering* 67 (1-2):147-156.

Taylor, Geoffrey Ingram. 1969. "Electrically driven jets." Proceedings of the Royal Society of London. A. Mathematical and Physical Sciences 313 (1515):453-475.

Theron, SA, E Zussman, and AL Yarin. 2004. "Experimental investigation of the governing parameters in the electrospinning of polymer solutions." *Polymer* 45 (6):2017-2030.

Topuz, Fuat, and Tamer Uyar. 2017. "Electrospinning of gelatin with tunable fiber morphology from round to flat/ribbon." *Materials Science and Engineering: C* 80:371-378.

Turner, Neill J., and Stephen F. Badylak. 2015. "The Use of Biologic Scaffolds in the Treatment of Chronic Nonhealing Wounds." *Advances in wound care* 4 (8):490-500. doi: 10.1089/wound.2014.0604.

Tysseling-Mattiace, Vicki M, Vibhu Sahni, Krista L Niece, Derin Birch, Catherine Czeisler, Michael G Fehlings, Samuel I Stupp, and John A Kessler. 2008. "Self-assembling nanofibers inhibit glial scar formation and promote axon elongation after spinal cord injury." *Journal of Neuroscience* 28 (14):3814-3823.

Varkey, Mathew, Jie Ding, and Edward E Tredget. 2015. "Advances in skin substitutes—potential of tissue engineered skin for facilitating anti-fibrotic healing." *Journal of functional biomaterials* 6 (3):547-563.

Wang, Shuai, Francesca Taraballi, Lay Poh Tan, and Kee Woei Ng. 2012. "Human keratin hydrogels support fibroblast attachment and proliferation in vitro." *Cell and tissue research* 347 (3):795-802.

Wang, Yiwei, Joanneke Beekman, Jonathan Hew, Stuart Jackson, Andrea C Issler-Fisher, Roxanne Parungao, Sepher S Lajevardi, Zhe Li, and Peter KM Maitz. 2018. "Burn injury: challenges and advances in burn wound healing, infection, pain and scarring." *Advanced drug delivery reviews* 123:3-17.

World Health Organisation (WHO). "Burns." accessed 21 October 2019. https://www.who.int/violence_injury_prevention/other_injury/burns/en/.

Widjaja, Winy, and Peter Maitz. 2016. "The use of dermal regeneration template (Pelnac®) in acute full-thickness wound closure: a case series." *European Journal of Plastic Surgery* 39 (2):125-132.

Woo, Kyung Mi, Victor J Chen, and Peter X Ma. 2003. "Nano-fibrous scaffolding architecture selectively enhances protein adsorption contributing to cell attachment." *Journal of Biomedical Materials Research Part A: An Official Journal of The Society for Biomaterials, The Japanese Society for Biomaterials, and The Australian Society for Biomaterials and the Korean Society for Biomaterials* 67 (2):531-537.

Wood, Fiona M. 2014. "Skin regeneration: The complexities of translation into clinical practise." *The International Journal of Biochemistry & Cell Biology* 56:133-140. doi: https://doi.org/10.1016/j.biocel.2014.10.025.

Wu, Chaoxi, Tian Chen, Yanjiao Xin, Zhen Zhang, Zhe Ren, Jing Lei, Bin Chu, Yifei Wang, and Shunqing Tang. 2016. "Nanofibrous asymmetric membranes self-organized from chemically heterogeneous electrospun mats for skin tissue engineering." *Biomedical Materials* 11 (3):035019.

Yang, Shoufeng, Kah-Fai Leong, Zhaohui Du, and Chee-Kai Chua. 2001. "The design of scaffolds for use in tissue engineering. Part I. Traditional factors." *Tissue engineering* 7 (6):679-689.

Yang, Xiaomin, Qi Liu, Xiliang Chen, Feng Yu, and Zhiyong Zhu. 2008. "Investigation of PVA/ws-chitosan hydrogels prepared by combined γ-irradiation and freeze-thawing." *Carbohydrate Polymers* 73 (3):401-408.

Yeong, Wai-Yee, Chee-Kai Chua, Kah-Fai Leong, and Margam Chandrasekaran. 2004. "Rapid prototyping in tissue engineering: challenges and potential." *TRENDS in Biotechnology* 22 (12):643-652.

Younes, Islem, and Marguerite Rinaudo. 2015. "Chitin and chitosan preparation from marine sources. Structure, properties and applications." *Marine drugs* 13 (3):1133-1174.

Zhang, Chunxue, Xiaoyan Yuan, Lili Wu, Yue Han, and Jing Sheng. 2005. "Study on morphology of electrospun poly (vinyl alcohol) mats." *European polymer journal* 41 (3):423-432.

Zhang, Yin, Jun Feng Li, Ke Hui Qiu, Liang Zhao Zhong, Guan Yu Li, Xue Fei Lai, and Pei Cong Zhang. 2014. "Preparation of a Novel Chitosan-Based Composite Nanofibers by Electrospinning." 850:136-139.